Dissertation
submitted to the
Combined Faculties for the Natural Sciences and for Mathematics
of the Ruperto-Carola University of Heidelberg, Germany
for the degree of
Doctor of Natural Sciences

presented by

Eva-Sophie Wallner, M.Sc.
born in: Vienna, Austria
Oral-examination: 26.11.2018

Early events in phloem formation:
Exploring the molecular network of *SMXL3/4/5*

Referees: Prof. Dr. Thomas Greb

Prof. Dr. Jan Lohmann

Acknowledgements

The following abstract is dedicated to everybody who enabled me to complete this thesis by providing professional and/or mental support.

First of all I would like to express my gratitude to Prof. Dr. Thomas Greb, who provided constant professional guidance, valuable opinions and mental support during both great and tough times. He agreed to have me in his lab since 2013: I originally joined as clueless lab rotation student from the medical field who wanted to “try-out” plant research, later on stayed for my Master’s thesis, worked as lab manager and moved together with the lab to Heidelberg to do my PhD. Now that I am completing my studies, I think it is just fair to say that the Greb lab and especially Thomas were fundamentally shaping my career path and the personal growth of my mid-twentieth. Working in this lab for so long determined my entire future and outlook on life and I do not regret a single day. Thank you for the scientific and humanly upbringing you provided. I am very grateful and will never forget that!

Secondly, I would like to thank my TAC committee members Prof. Dr. Jan Lohmann and Dr. Lazaro Centanin who were providing (together with Thomas) important suggestions and guidance that significantly contributed to the successful completion of my project. Moreover, I would like to thank several collaborators: Thanks to Dr. Gernot Poschet from the Metabolomics Core facility, who performed all sugar measurements. Thanks to Dr. David Ibberson from the Deep Sequencing Core facility for RNAseq service. Thanks to Prof. Dr. Yrjö Helariutta and his lab for great interaction and electron microscopy. And thanks to all those people I met at conferences, who provided interesting ideas and also challenged my project and my approaches from time to time and thereby helped to bring the story to the next level.

Next, I would like to thank several of my colleagues and former colleagues who supported me with their knowledge and who provided a great working environment:
Big thanks especially to Virginie, who taught me all fundamental scientific skills and was a great and inspiring mentor. She also analyzed my RNAseq data (and taught me how to do it myself - thank you!). Many thanks to Ilona for her helping hands during times of big workloads. Thanks to Ivan, who helped me with his philosophical wisdom and who took me on social events. I would also like to thank Vadir for his constant support, his friendliness and our great conversations about both scientific and personal topics. Thanks also to Nina and Theresa for keeping the lab alive and social and thanks to Jiyan for great conversations and good suggestions. And to everybody I did not mention by name: Thank you for creating a great working environment, I really appreciated working with all of you!

Finally, I would like to express my gratitude to several friends and family members (in German): Vielen Dank an meine Eltern, die immer hinter mir stehen, für mich da sind und mich meine Träume leben lassen, egal wie lange wir dadurch auch getrennt sein mögen. Besonderen Dank an meine beste und langjährigste Freundin Kesiban, die sogar an mich geglaubt hat, als

ich es selbst nicht mehr getan habe. Danke an Stefanie für ausgedehnte Spaziergänge, Molchstudien und eine tolle Zeit in diesem „fremden“ Deutschland. Danke an Philip, der mich schon so lange kennt und immer ein offenes Ohr für mich hat. Danke an meinen ehemaligen Kollegen und guten Freund Klaus für die nötige „Entschleunigung“ und die langen, grandiosen Gespräche. Last but not least: Vielen Dank an meinen Freund Tobias, einen großartigen Menschen, den ich leider erst spät hier gefunden habe. Danke dass du an mich glaubst und meine Ziele unterstützt.

Zusammenfassung

Wachstum und Körperform multizellulärer Organismen wird größtenteils durch einen funktionierenden Langstreckentransport von Energiemetaboliten bestimmt, der Stammzellaktivität antreibt. In vaskulären Pflanzen werden Zucker photosynthetisch in Quellen (source) produziert und über das Phloem in Senken (sink) geleitet, wo sie entweder in Speicherorgane gelangen oder für die Aufrechterhaltung von Stammzellnischen, sogenannten Meristemen, genutzt werden. Im Wurzelapikalmeristem (root apical meristem, RAM), welches das Längenwachstum der Wurzeln vorantreibt, wird Zuckerversorgung durch striktes Zusammenspiel zwischen Proto- und Metaphloem aufrechterhalten. Die Ausbildung von Proto- und Metaphloem geht von einer einzelnen Stammzelle aus, deren Tochterzellen sich in einer räumlich- und zeitlich kontrollierten Weise teilen und differenzieren. Protophloem differenziert zuerst innerhalb des RAMs, um Zuckerentladung nahe der Stammzellnische zu ermöglichen. Eine beeinträchtigte oder verzögerte Protophloemausbildung hat schwerwiegende Folgen für Pflanzenwachstum und Vitalität. Es ist daher von zentraler Bedeutung die regulatorischen Mechanismen hinter Protophloementwicklung zu verstehen, um die Zuckertransportleistung in Senken zu erhöhen und somit den Ernteertrag in naher Zukunft zu steigern.

In dieser Studie berichte ich von neuen Schlüsselkomponenten der Phloemregulierung, genannt *SUPPRESSOR OF MAX2 1-LIKE3* (*SMXL3*), *SMXL4* und *SMXL5*. Anders als die meisten *SMXL*-Familienmitglieder, agieren *SMXL3/4/5* unabhängig von Strigolacton- (SL) oder Karrikin (KAR)-Signalwegen als positive Regulatoren der Phloementwicklung. Sie sind die ersten beschriebenen phloemspezifischen Gene, die Promotoraktivität bereits im provaskulären Gewebe des Embryos, in der ersten Phloemstammzelle des RAMs und entlang des gesamten Phloemgewebes in adulten Pflanzen zeigen. *SMXL3/4/5* agieren redundant und dosisabhängig in der zeitlich- und räumlichen Initiierung und Differenzierung von Protophloem. Ein Mangel an *SMXL3/4/5*-Aktivität führt zur kompletten Abwesenheit des Phloemgewebes und Tripelmutanten sind bereits im Keimlingsstadium letal. Doppelmutanten zeigen reduzierten phloemabhängigen Transport und Zuckeransammlung in Blättern. Außerdem spielen *SMXL3/5* eine zusätzliche und *SMXL4*-unabhängige Rolle im radialen Wurzelwachstum, indem sie Zellteilungen des Prokambiums fördern. Interessanterweise ist *SMXL5*-Aktivität ausreichend, um sekundäre Phloemausbildung an der Stammbasis zu initiieren, aber unterdrückt gemeinsam mit *SMXL4* radiales Dickenwachstum. Diese funktionale Spezialisierung deutet darauf hin, dass *SMXL3/4/5* unterschiedliche Rollen in den molekularen Netzwerken der Phloem und/oder (Pro-)Kambium Entwicklung spielen.

Um *SMXL3/4/5* in solch ein molekulares Netzwerk zu integrieren, haben wir nach Protein-Protein-Interaktionspartnern für SMXL5 gesucht. Das *plant homeodomain* (PHD)-finger Protein OBERON 3 (OBE3) ist der erste bestätigte Interaktionspartner, der gemeinsam mit SMXL3/4/5 Phloemausbildung reguliert. Frühere Studien zeigten, dass *OBE* Proteine eine wichtige Rolle in der Aufrechterhaltung von Meristemen und möglicherweise in der Umstrukturierung von

Chromatin spielen. SMXL3/4/5 sind kernlokalisierte, chaperonähnliche Proteine mit konservierter AAA ATPase und *ETHYLENE-RESPONSE FACTOR Amphiphilic Repression* (EAR) Domäne, was sie zu ausgezeichneten Kandidaten für eine transkriptionelle Regulierung von nachgeschalteten Zielgenen macht. Diese Studie und die Charakterisierung von *SMXL3/4/5* und *OBE3* als neuartige und grundlegende Phloemregulatoren ermöglichte tieferere Einblicke in die Phloementwicklung und Zuckerverteilung der Pflanzen.

Abstract

Growth and body shape of complex multicellular organisms is largely determined by a functional long-distance transport of energy metabolites that fuels stem cell activity. In vascular plants, sugars are photosynthetically produced in source tissues and delivered via the phloem to sink tissues for allocation into storage organs or to sustain distinct stem cell niches, called meristems. In the root apical meristem (RAM), which drives longitudinal root growth, sugar supply is ensured by a tight interplay between proto- and metaphloem. Formation of proto- and metaphloem starts with a single stem cell whose daughter cells divide and differentiate in a controlled spatio-temporal manner. Protophloem differentiates first within the RAM to enable sugar unloading close to the stem cell niche. Impaired or delayed protophloem formation has detrimental consequences for plant growth and vitality. Understanding the regulatory mechanisms behind (proto-)phloem formation is an important hub to enhance sink strength and thereby crop yield in the near or further future.

In this study I report novel key-components in phloem regulation called *SUPPRESSOR OF MAX2 1-LIKE3* (*SMXL3*), *SMXL4* and *SMXL5*. Unlike most SMXL family members, *SMXL3/4/5* act independently from strigolactone (SL) or karrikin (KAR) signaling as positive regulators of phloem formation. They are the first described phloem-specific genes that show promoter activity already in provascular tissues of the embryo, the first phloem stem cell in the RAM and along the whole phloem tissue in adult plants. SMXL3/4/5 promote protophloem initiation and differentiation in a dose-dependent manner. Deficiency of all three gene functions results in complete absence of phloem tissue and seedling lethality. In comparison, double mutants show reduced phloem-dependent transport and sugar accumulation in leaves. Moreover, *SMXL3/5* play an additional and *SMXL4*-independent role in radial root growth by promoting procambial cell divisions. Interestingly, *SMXL5* activity is sufficient to induce secondary phloem formation at the stem base, but acts redundantly with *SMXL4* in suppressing radial stem thickening. This functional specialisation suggests that *SMXL3/4/5* play distinct roles in molecular networks of phloem and/or (pro-)cambium formation.

To integrate *SMXL3/4/5* into such molecular networks, I characterized protein-protein interaction partners of SMXL5. The plant homeodomain (PHD)-finger protein OBERON 3 (OBE3) is the first interaction partner that genetically interacts with *SMXL3/4/5* in protophloem formation. Previous studies reported that *OBEs* are important components in meristem maintenance and, potentially, chromatin remodelling. SMXL3/4/5 are nuclear localized, chaperon-like proteins with conserved AAA ATPase and ETHYLENE-RESPONSE FACTOR Amphiphilic Repression (EAR) domain, which makes them perfect candidates to act in transcriptional regulation of downstream targets. This study and the characterization of *SMXL3/4/5* and *OBE3* as novel and fundamental phloem regulators enabled a deeper understanding of phloem development and sugar allocation in plants.

Abbreviations

aa	Amino acid
ABA	Abscisic acid
ACR4	ARABIDOPSIS CRINKLY4
AGO	ARGONAUTE
Agrobacteria	*Agrobacterium tumefaciens*
AM	*Arbuscular mycorrhizal*
Arabidopsis	*Arabidopsis thaliana*
ARF	AUXIN RESPONSE FACTOR
ATHB8	ARABIDOPSIS THALIANA HOMEOBOX GENE 8
BAH	Bromo-associated homology domain
BAM3	BARELY ANY MERISTEM 3
bp	Base pair
BRX	BREVIS RADIX
CALS7	CALLOSE SYNTHASE 7
CC	Companion cell
CCD	Carotenoid cleavage deoxigenase (CCD)
CDF4	CYCLING DOF FACTOR 4
CDS	Coding sequence
CDT	Cambium-derived tissue
CHD	Chromodomain
ChIP	Chromatin immunoprecipitation
CLE	CLAVATA3/ESP-RELATED (CLE)
CLV	CLAVATA
CRN	CORYNE
CTLH	C-Terminal to Lissencephaly Homology
CVL1	CVP2-LIKE1
CVP2	COTYLEDON VASCULAR PATTERN 2
CZ	Central zone
D14	DWARF14
D27	DWARF 27
D3	DWARF3 (MAX2)
D53	DWARF 53
D6PK	D6 PROTEIN KINASE
DCL	DICER-LIKE
DLK2	DWARF14-LIKE2
DNA	Deoxyribonucleic acid
Ds	Double stranded
E1	Ubiquitin activating enzyme
E2	Ubiquitin conjugating enzyme
E3	Ubiquitin ligase
EAR	ETHYLENE RESPONSE FACTOR ASSOCIATED-AMPHIPFATIC REPRESSION

EDTA	Ethylenediaminetetraacetic acid
ER	Endoplasmic reticulum
Escherichia coli	*E. coli*
ETT	ETTIN (ARF3)
G	Guanine
GFP	Green fluorescent protein
GLS7	Glucan Synthase-Like7
GRXS	GLUTAREDOXIN
GSK3	Glycogen synthase kinase 3
HDAC	Histone deacetylase
HD-ZIP III	Class III HOMEODOMAIN LEUCINE ZIPPER
HSP101	HEAT SHOCK PROTEIN 101
IAA	Auxin indole-3-acetic-acid
IC	Interfascicular cambium
IP	Immunoprecipitation
JUL	JULGI
KAI2	KARRIKIN INSENSITIVE 2
KAR	Karrikin
kDa	Kilo Dalton
LRR-RLK	Leucine-rich repeat receptor like kinase
M	Molar
MAX3	MORE AXILLARY GROWTH 1-4 (D3)
MEP	Methylerythritol phosphate
min	minutes
miRNA	micro ribonucleic acid
MOL1	MORE LATERAL GROWTH 1
MP	MONOPTEROS (ARF5)
mRNA	messenger ribonucleic acid (mRNA)
MSE	Metaphloem sieve elements
NAC	NO APICAL MERISTEM
NEN	NAC45/86-DEPENDENT EXONUCLESE-DOMAIN PROTEIN1 -4
NLS	Nuclear localization signal
Nicotiana	*Nicotiana benthamiana*
Nt	Nucleotide
OBE	OBERON
OPS	OCTOPUS
PAX	PROTEIN KINASE ASSOCIATED WITH BRX
PBS	Phosphate-buffered saline
PCR	Polymerase chain reaction
PD	Plasmodesmata
PEAR	PHLOEM EARLY DOF
PFA	Paraformaldehyde

PHD	Plant homeodomain
PI	Propidium iodide
PID	PINOID
PIN	PIN-FORMED
PM	Plasma membrane
PMSF	Phenylmethane sulfonyl fluoride
PPP	Phloem pole pericycle
PSE	Protophloem sieve element
PXY	PHLOEM INTERCALATED WITH XYLEM
PZ	Peripheral zone
QC	Quiescent centre
RAM	Root apical meristem
RDR	RNA-DEPENDENT RNA POLYMERASE
RISC	RNA-induced silencing complex
RNA	ribonucleic acid
ROS	Reactive oxygen species
RZ	Rib zone
SAM	Shoot apical meristem
SCF	(SUPPRESSOR OF KINETOCHORE PROTEIN1 (SKP1), Cullin (CUL1), F-box)
SDS-PAGE	Sodium dodecyl sulfate - polyacrylamide gel electrophoresis
SE	Sieve element
SGS	SUPPRESSOR OF GENE SILENCING
SID	Selected interacting domain
siRNA	Small interfering ribonucleic acid
SL	Strigolactone
SMAX1	SUPPRESSOR OF MAX2 1
SMXL	SUPPRESSOR OF MAX2 1-LIKE
ta-siRNA	Trans-acting small interfering ribonucleic acid
T-DNA	Transfer DNA
TE	Tracheary element
TIR1	TRANSPORT INHIBITOR RESPONSE 1
TPL	TOPLESS
TPR	TPL-RELATED
UTR	Untranslated region
VISUAL	Vascular Cell Induction Culture System Using Arabidopsis Leaves
WOX	WUSCHEL RELATED HOMEOBOX
WT	Wild type
WUS	WUSCHEL
w/v	Weight per volume
YFP	Yellow fluorescent protein

Table of contents

1. Introduction

1.1 Plants as systems to study the spatio-temporal regulation of cell fate

Our planet is inhabited by a vast variety of life forms. Their appearance ranges from rather simple unicellular organisms to large and complex multicellular bodies with an impressive repertoire of distinct morphologies. The emergence of multicellular organisms was a major step in evolution that required a completely new set of cellular traits and regulatory mechanisms. One of the most striking advantages of multicellularity is the ability to divide labour among specialized sub-sets of cells that assemble in specific body parts to form new tissue layers and organs exhibiting particular functions (Somorjai et al. 2012). Although the same main principles of cell specification and compartmentation evolved independently in multicellular organisms of all three kingdoms of life, mechanisms during ontogeny and in acquiring a certain morphology can differ (Gaillochet and Lohmann 2015).

To ensure an organized coordination of tissue formation and interaction, a tight spatio-temporal control of cell fate specification is essential. While ontogeny within the animal kingdom relies on several events of cell migration and movement, plant cells are immobile (Fowler and Quatrano 1997; Dupuy et al. 2010). They are contained within a certain cellular context by semi-rigid primary or rigid secondary cell walls (Alberts 2002). The cell wall gives plant cells shape, withstands turgor pressure, provides mechanical support and acts as a signalling compartment (Wolf et al. 2012; Voxeur and Hofte 2016; Alberts 2002). Consequently, position and timing of cell division, cell expansion and differentiation as well as the orientation of division planes are key aspects of plant development that determine both morphology and fitness (Wendrich and Weijers 2013; De Rybel et al. 2014).

Model plants, such as *Arabidopsis thaliana* (*Arabidopsis*), can serve as great systems to study the spatio-temporal regulation of cell fate. Due to the lack of plant cell mobility, cell lineages can be traced from the first stem cell to fully differentiated cells in a rather easy manner (Scheres 2007). This allows a precise investigation of cell identity changes and their underlying regulatory mechanisms.

1.2 Plant meristems maintain life-long growth

Unlike animals, plants are sessile organisms and constantly exposed to ever changing environmental cues. Thus, plants developed an amazing set of traits and mechanisms to adapt. Seeds can outlast many years while waiting for the best environmental conditions to germinate (Bentsink and Koornneef 2008). In the vegetative state plants maintain continuous growth and morphological plasticity to overcome and withstand environmental hardship for thousands of

years (Tonn and Greb 2017). The plants infinite capacity to grow post-embryonically is achieved by distinct stem cell niches (Scheres 2007).

Stem cell niches are specialized, stem cell-protecting microenvironments that contain a pool of pluripotent stem cells (Scheres 2007; Miyashima et al. 2013). Despite the independent evolution of animals and plants, the niche concept proved effective and is common in multicellular organisms of both kingdoms (Scheres 2007). Stem cells allow multicellular organisms to continuously renew tissues and organs and to regenerate cells after e.g. an injury (Aichinger et al. 2012). They have the capacity to undergo asymmetric divisions to form a differentiating daughter cell and a self-renewed stem cell (Wendrich and Weijers 2013). Each stem cell niche displays layers of cells with different degrees of potency and identity. At the core usually resides an organizing centre that forms a strictly controlled pool of rarely dividing cells. The organizer maintains the niche by inhibiting differentiation of the adjacent stem cells through cell-to-cell signalling. Those stem cells are located next to the organizing centre and their asymmetric divisions lead to their self-renewal and the production of daughter cell. This third layer of daughter cells is highly proliferative (De Rybel et al. 2014; Wendrich and Weijers 2013; Scheres 2007). Cell lineages produced by daughter cells will eventually differentiate into a certain tissue type. In plants, those highly organized stem cell areas are called meristems (Miyashima et al. 2013).

1.2.1 Primary meristems drive initial longitudinal growth

The root apical meristem (RAM) and shoot apical meristem (SAM) are primary plant meristems that are located at the apical positions of root and shoot tips, respectively (Aichinger et al. 2012; Scheres 2007). The origin of RAM and SAM dates back to the first tracheophytes (vascular plants) that evolved after plants started to colonize the land (Seago and Fernando 2013; Kenrick and Crane 1997; Imaichi and Hiratsuka 2007). The SAM evolved to enable longitudinal growth of stems in vascular plants that were still partially growing in or nearby water reservoirs (Imaichi and Hiratsuka 2007; Seago and Fernando 2013; Greb and Lohmann 2016). As plants conquered drier environments, the establishment of an elongated root system for water uptake gained importance and so the RAM emerged (Bennett and Scheres 2010; Seago and Fernando 2013; Matsunaga and Tomescu 2016). It is suggested that seed plants, lycophytes and ferns developed SAMs and RAMs independently and consequently show differences in structural organization and development (Imaichi and Hiratsuka 2007; Seago and Fernando 2013). Thus, RAM and SAM development cannot be generalized but will be discussed on the basis of our herbaceous angiosperm model organism *Arabidopsis*.

Although RAM activity is first initiated during germination (Masubelele et al. 2005), primary meristems are already established during embryogenesis (Peris et al. 2010; ten Hove et al. 2015). In the first step of embryogenesis the zygote elongates and asymmetrically divides into an apical cell and a bigger basal cell (Lau and Bergmann 2012; Ueda et al. 2011). The

apical cell undergoes several rounds of highly organized divisions with specific changes in the division plane to specify the initial plant tissues (Ueda et al. 2011). The basal cell divides symmetrically into the suspensor that connects the embryo to the maternal seed coat (Kawashima and Goldberg 2010). In the globular stage embryo the most important tissue types, such as vascular precursor cells, are specified and the shoot and root identities are established at the apical and basal ends, respectively (Wendrich and Weijers 2013; ten Hove et al. 2015).

1.2.2 The root apical meristem (RAM)

The RAM is derived from the most apical suspensor cell which develops at the globular stage into the hypophysis, which in turn divides asymmetrically and forms the root organizer (Wendrich and Weijers 2013; ten Hove et al. 2015; Perilli et al. 2012). During transition from globular to heart stage, the root organizer develops into the quiescent centre (QC) and the columella stem cells (Hamann et al. 1999; Schlereth et al. 2010). The QC is the largely mitotically arrested organizing centre of the RAM (Dolan et al. 1993). It consists of four cells that are surrounded by different types of stem cells or so-called initials: Columella initials, epidermis initials, cortex/endodermis initials and stele initials (Figure 1.1) (Sozzani and Iyer-Pascuzzi 2014; Scheres 2007). Cell fate among those cells remains quite plastic and the QC or single initials can be rapidly restored after laser ablation (van den Berg et al. 1995). One important factor involved in stem cell maintenance is the homeodomain transcription factor *WUSCHEL RELATED HOMEOBOX 5 (WOX5)* (Sarkar et al. 2007). *WOX5* activity marks the QC but the WOX5 protein can move into adjacent columella initials to suppress their differentiation by repressing the differentiation promoting transcription factor *CYCLING DOF FACTOR 4* (*CDF4*) (Pi et al. 2015). In turn, *WOX5* expression is negatively regulated and positioned to the QC by receptor-like kinase ARABIDOPSIS CRINKLY4 (ACR4) (De Smet et al. 2008; Stahl et al. 2009). *CLAVATA3/ESP-RELATED 40* (*CLE40*) is expressed in differentiated vascular cells of the stele and in columella cells and promotes expression of *ACR4* in RAM initials. *WOX5* expression thereby remains restricted to the QC where *ACR4* activity is absent (De Smet et al. 2008; Stahl et al. 2009). Thus, the QC maintains stem cell properties of the contacting initials (van den Berg et al. 1997). Each initial divides asymmetrically into a stem cell and a proliferating daughter cell, which are also known as transit-amplifying cells (Scheres 2007). Daughter cells lose contact with the QC and thus start to expand and differentiate post-germination after about four rounds of divisions (Sozzani and Iyer-Pascuzzi 2014; Scheres 2007). At the same time, the outermost layer of columella and root cap cells is shed. Consequently, the root grows forward while the RAM remains at the apical position (Figure 1.1) (Scheres 2007).

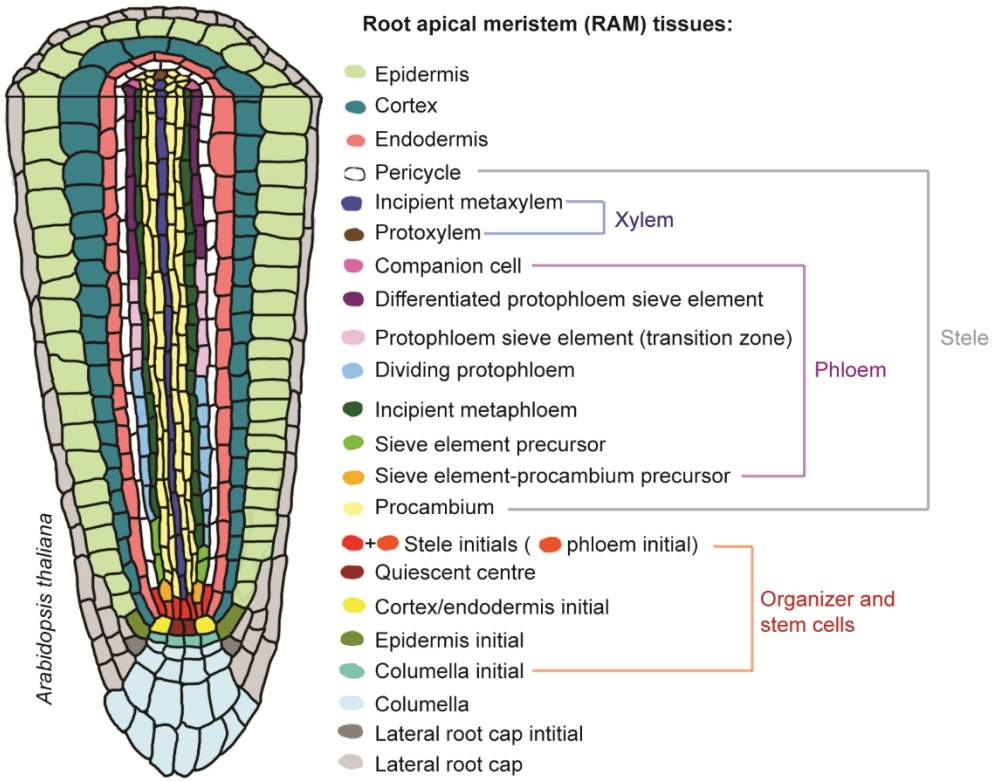

Figure 1.1: Tissues of the root apical meristem (RAM)
A schematic representation of a root apical meristem (RAM) from *Arabidopsis* is shown. Important tissues are colour-coded according to the legend. The quiescent centre (QC) is the stem-cell maintaining organizer at the root tip. Vascular (or stele) initials produce the vascular tissues phloem and xylem that are surrounded by the pericycle. Together those tissues form the cylindrical core of the root, which is called stele. The figure is based on information found in Lee et al. 2013; Rodriguez-Villalon et al. 2015; Bonke et al. 2003 and Miyashima et al. 2013.

1.2.3 The shoot apical meristem (SAM)

The SAM is established at the apical position in the globular embryo and stem cells are specified between the premature cotyledons at the heart stage (Wendrich and Weijers 2013; ten Hove et al. 2015). After germination, the SAM drives the formation of all above-ground tissues (Gaillochet et al. 2015). The dome-like structure of the SAM is organized in three cell layers that are clonally distinct and exhibit different cell division planes (Reddy et al. 2004). The SAM can be further categorized into three functional domains: A slowly dividing central zone (CZ) that harbours the stem cells, a fast dividing peripheral zone (PZ) that gives rise to leaf and flower primordia and the rib zone (RZ) that establishes the primary stem (Reddy and Meyerowitz 2005; Aichinger et al. 2012). An organizing centre sits basally of the CZ and is marked by the expression of the homeodomain transcription factor *WUSCHEL* (*WUS*) (Schoof et al. 2000). Similar to WOX5 in the root, cell-to-cell movement of WUS to the CZ is required for stem cell maintenance (Daum et al. 2014). The *WUS* expression domain is restricted by CLAVATA3 (CLV3) signalling. *CLV3* is expressed in the CZ and encodes a small peptide that signals through binding to the

leucine-rich repeat receptor like kinases (LRR-RLK) CLAVATA1 (CLV1), CLAVATA2 (CLV2) and CORYNE (CRN) (Brand et al. 2000; Müller et al. 2008; Gaillochet et al. 2015).

By presenting the key players in RAM and SAM formation, I aimed to highlight similarities and conserved principles of meristem regulation. Importantly, those networks also include other genes, hormonal pathways and feedback loops not discussed here (Gaillochet et al. 2015; Aichinger et al. 2012; Scheres 2007). Moreover, new shoot and root meristems are also formed post-embryonically during shoot branching and lateral root formation, respectively (De Smet et al. 2006). Lateral shoot primordia are established from axillary meristems that derive from the SAM, whereas lateral root primordia emerge from de-differentiating pericycle cells within the differentiation zone of the RAM (Leyser 2009; Dastidar et al. 2012; Steeve and Sussex 1989; Sussex 1989). This high plasticity in cell fate is one driving force behind plant morphogenesis.

1.2.4 A secondary meristem drives radial plant growth

One of the best examples highlighting morphological and cell fate plasticity of vascular plants is the post-embryonic establishment of the cambium. The cambium is a secondary meristem that is formed de-novo in stems, hypocotyls and roots (Elo et al. 2009; Sanchez et al. 2012). Cambium formation generates a closed cylinder of cambial stem cells with presumably different degrees of potency that enables plants to grow radially (Brackmann and Greb 2014; Sanchez et al. 2012). Although earliest indications for radial growth were found in fossils of extinct euphyllophytes, cambium formation is nowadays mostly restricted to gymnosperms and angiosperms, where it was partially lost and re-invented during evolution (Ragni and Greb 2017). While still present in dicots, monocots lost radial growth and re-established a new radial meristem in arborescent monocots, such as Dracaena or Yucca species (Jura-Morawiec et al. 2015). In all cases, radial growth is the driving force behind biomass production on our planet. It enables woody-plants to establish and maintain big body structures that survive and withstand environmental changes for millennia (Tonn and Greb 2017). Although the results of radial growth might be most obvious in trees, also herbaceous species, such as *Arabidopsis*, grow radially to a certain extent and can therefore serve as great models to study the dynamics and regulatory principles of cambium formation (Elo et al. 2009).

In the primary stem, which derives from the RZ of the SAM, procambial stem cells are restricted to vascular bundles and located between the vascular tissues of primary xylem and phloem (Figure 1.2) (Sanchez et al. 2012). In adult *Arabidopsis* stems, interfascicular cambium (IC) is initiated de-novo in interfascicular regions at the stem base. Those new cambial stem cells are supposedly derived from dividing starch sheath cells (Sehr et al. 2010; Altamura et al. 2001). The IC connects the cambium of the vascular bundles to form a closed ring of stem cells (Figure 1.2). This secondary meristem produces phloem distally (towards the starch sheath) and

xylem proximally (towards the pith), which in turn leads to thickening of the stem and to an increase in transport capacity and stability (Figure 1.2) (Nieminen et al. 2015). The vasculature as long distance transport system and the vascular tissues xylem and phloem will be discussed in chapter 1.3.

Unlike for the SAM and RAM, a dormant organizing centre has not been determined for the cambium and an in-depth understanding of different cambium domains and cell identities is still lacking (Ragni and Greb 2017). Although many of these gaps of knowledge are subject of ongoing studies, cambium research is challenging since the tissue of interest is difficult to access and new methods that allow real-life imaging are still pending. Nevertheless, several genes and hormonal signalling pathways have been identified to shape and regulate cambium activity (Brackmann and Greb 2014; Brackmann et al. 2018). The transcription factor *WUSCHEL-RELATED HOMEOBOX4 (WOX4)* and the LRR-RLK PHLOEM INTERCALATED WITH XYLEM *(PXY)* are two of the best studied and most specific cambium markers (Etchells and Turner 2010; Hirakawa et al. 2010; Suer et al. 2011). *WOX4* maintains cambial stem cell activity (Suer et al. 2011; Dolzblasz et al. 2016; Etchells et al. 2013). It is transcriptionally activated by PXY-dependent intracellular signalling (Hirakawa et al. 2010; Etchells et al. 2016). PXY additionally suppresses xylem differentiation upon binding its ligand CLAVATA3/ESP-RELATED 41 (CLE41) (Ito et al. 2006; Fisher and Turner 2007; Etchells et al. 2016). Although *WOX4* and *PXY* expression domains overlap in cambium stem cells, especially *PXY* promoter activity is clearly located towards the proximal cambium side (Gursanscky et al. 2016; Brackmann et al. 2018). The LRR-RLK MORE LATERAL GROWTH 1 (MOL1) counteracts PXY in regulating cambium homeostasis. Unlike *PXY*, *MOL1* was the first identified gene expressed in cambium stem cells expressed towards the distal cambium side (Gursanscky et al. 2016). Of note, *PXY* and *MOL1* activities do not overlap, which could hint towards the presence of two distinct cambium stem cell types. Moreover, cambium activity is stimulated and/or balanced by many important hormonal signalling pathways, such as auxin, cytokinin, gibberellin, brassinosteroid, ethylene, jasmonic acid and strigolactone signalling (reviewed in Brackmann and Greb 2014). Auxin (indole-3-acetic-acid, IAA) is probably the most famous plant hormone and a key regulator of plant development in numerous stages and aspects (Sauer et al. 2013). Recent studies in our lab showed that distinct *AUXIN RESPONSE FACTORS* (*ARFs*) play an essential role in modulating cambium activity (Brackmann et al. 2018). *ARF* genes encode auxin-dependent transcription factors that are activated when auxin signalling is high (Hagen 2015). While *ARF3* and *ARF4* generally promote cambium activity, *ARF5*, which is also known as *MONOPTEROS* (*MP*), is directly attenuating *WOX4* activity to maintain a defined stem cell pool, similar to mechanisms in the SAM and RAM (Brackmann et al. 2018).

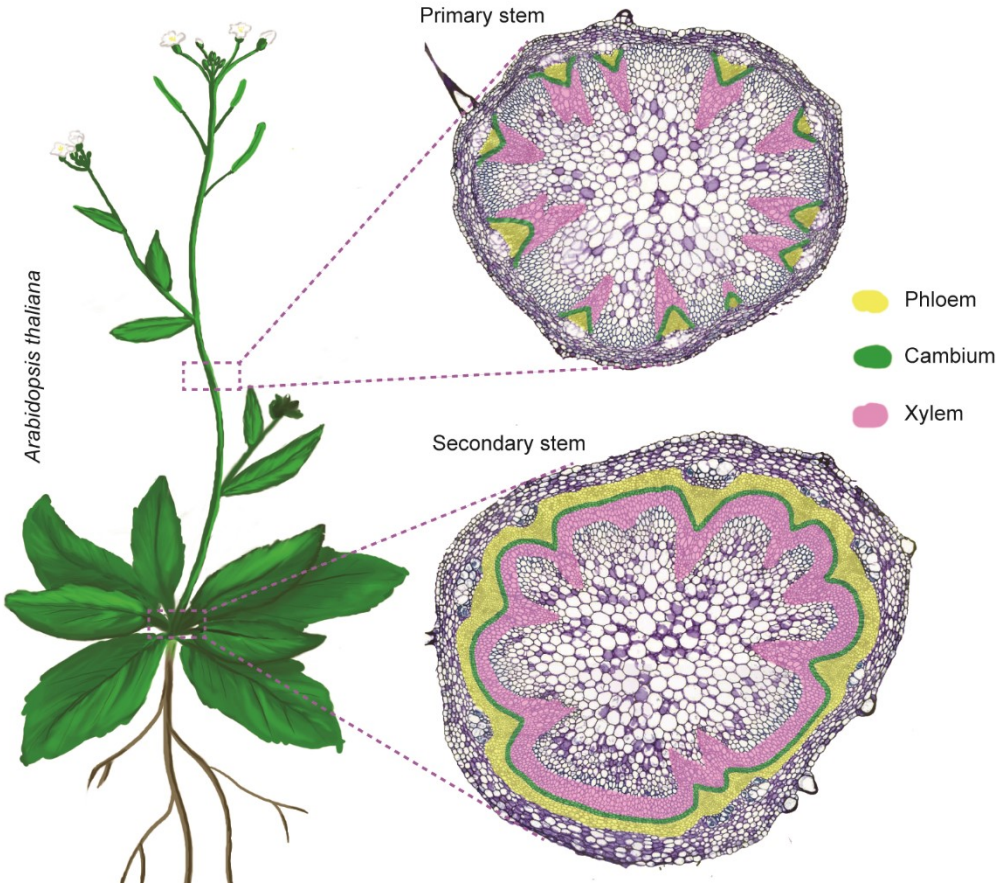

Figure 1.2: The cambium is a stem cell niche that enables radial growth
A schematic *Arabidopsis* plant with stem cross sections representing primary and secondary growth configuration is shown. In the primary configuration, which can be found in upper stem positions, cambium is restricted to vascular bundles. The secondary configuration can be found close to the stem base. IC is formed de-novo between vascular bundles and connects the vascular cambium to form a closed ring that gives rise to phloem and xylem. Cambium, phloem and xylem are colour-coded as indicated in the legend. The figure is based on information found in Sanchez et al. 2012 and Suer et al. 2011.

1.3 The plant vasculature as long distance transport system

Having distinct stem cell niches to direct body growth is just one side of the coin when it comes to establishing complex multicellular organisms. The second key component is a functioning long-distance transport system that distributes water, nutrients, energy metabolites and other signalling components, such as peptides, RNA and hormones throughout the body (Oparka and Turgeon 1999). In early land plants the evolutionary pressure for a long-distance transport system was high. As photoautotrophs, carbon dioxide uptake and fixation is more efficient for plants growing outside of the water. Yet, photosynthesis requires water and the produced sugars have to be allocated from source to sink tissues. Cell-to-cell transport via plasmodesmata (PD) alone is not sufficient to provide transport across long distances (Lucas et al. 2013). Thus, plants invented a symplastic transport system that is driven by hydrostatic pressure

only and therefore differs quite fundamentally from the circulatory system found in many animals (Lucas et al. 2013; Furuta et al. 2014b). The plant vasculature is generally comprised out of water-conducting xylem and sugar-allocating phloem (Lucas et al. 2013).

1.3.1 Xylem and the cohesion-tension theory

Mature xylem contains tracheary elements (TEs) which passively transport water and mineral nutrients from soil via roots to shoots and leaves (Ye et al. 2002). In eudicots, such as *Arabidopsis*, differentiated TEs are interconnected and form xylem vessels (Ruzicka et al. 2015). Primary xylem can be separated into two different vessel-types: Protoxylem and metaxylem (Figure 1.1). Protoxylem differentiates earlier and is later on functionally replaced by metaxylem (Kubo et al. 2005). Other xylem cell types include fibres for mechanical support and xylem parenchyma, which function as location of storage and contribute to lignification of vessels (Smith et al. 2013; Ruzicka et al. 2015). Differentiation of vessels includes programmed cell death and secondary cell wall thickening, which is also known as impregnation (Fukuda 2000). While primary cell walls still allow cell expansion, secondary cell walls are stiff and rich in lignin, cellulose and hemicellulose (Turner et al. 2007; Ruzicka et al. 2015). Lignification provides mechanical support for vessels as they are subjected to negative hydraulic pressure and the hydrophobic properties of lignin might even positively affect the water flow (Wang and Dixon 2012). Water “transport” via xylem vessels happens solely passively via transpiration and forces of cohesion. Water can enter the apoplast of the root by osmosis. To prevent uncontrolled loading of water and nutrients into xylem, the vascular cylinder (stele) is protected by a hydrophobic barrier of lignin that connects endodermis cells. This barrier is known as casparian strip and forces water and nutrients to enter the stele symplastically by shuttling trough the endodermis cells (Purves 2007; Geldner 2013). After entering xylem vessels, water is sucked shootwards by capillary forces and constant transpiration of water through stomata, which are located in the epidermis of leaves to regulate gas exchange and transpiration (Steudle 2001; Purves 2007; Bergmann and Sack 2007). The constant evaporation at leaves creates a negative pressure (vacuum) that pulls water shootwards. This physical principle creating tension combined with the cohesion properties of water are the driving forces described in the cohesion-tension theory. Although intensively debated and questioned from time to time, this more than 100 year-old theory established by Böhm is still the most widely accepted one when it comes to explaining the mechanisms of water uptake and transport within plants (Steudle 2001; Brown 2013).

1.3.2 Phloem and the pressure-flow hypothesis

Phloem holds the crucial function of allocating photosynthates and other organic molecules, such as hormones, proteins and RNAs throughout the plant body (Figure 1.3) (Oparka

and Turgeon 1999; Blob et al. 2018; Otero and Helariutta 2017). It is basically comprised out of sieve elements (SEs) and companion cells (CCs) (Dettmer et al. 2014).

Long-distance transport of the phloem sap occurs via differentiated SEs (Dettmer et al. 2014; Lucas et al. 2013). Upon differentiation, SEs enter a highly selective program of autolysis that degrades most organelles, including the nucleus, vacuole, golgi, and the rough endoplasmic reticulum (ER) (Lucas et al. 2013; Oparka and Turgeon 1999). The cells thereby enter an intermediate state between life and death, but keep mitochondria, an altered version of the smooth ER, the plasma membrane and a degenerated cytoplasm, which means that they are limited to few - but not deprived of all - cellular processes (Evert and Eichhorn 2006; Lucas et al. 2013; Anne and Hardtke 2017). Transport through SEs is facilitated by sieve plates that connect SEs to form sieve tubes (Purves 2007). Sieve plates are formed from anticlinal cell walls and exhibit a vast number of enlarged PD that are known as sieve pores (Dettmer et al. 2014). Those pores enable passive movement of the phloem sap, including larger molecules, between SEs (Knoblauch et al. 2015). Their formation and diameter is tightly regulated by CALLOSE SYNTHASE 7 (CALS7), which is also known as GLUCAN SYNTHASE-LIKE 7 (GLS7) (Froelich et al. 2011; Barratt et al. 2011; Xie et al. 2011; Vaten et al. 2011). CALS7 and its family member CALS3/GSL12 have been shown to deposit callose at sieve plates, which is on the one hand important for pore formation and increase of pore diameter but can on the other hand completely block the pores if the vasculature is subjected to stress by e.g. wounding (Xie et al. 2011; Vaten et al. 2011). Thus, callose deposition is an important hub to modulate pore size and consequently phloem conductivity (Dettmer et al. 2014).

Unlike xylem vessels, SEs stay alive and are metabolically sustained by CCs (Oparka and Turgeon 1999; Otero and Helariutta 2017). CCs have large nuclei, a lot of small vacuoles, a dense cytoplasm and are tightly connected to SEs by PDs (Evert and Eichhorn 2006; Lucas et al. 2013; Otero and Helariutta 2017; Oparka and Turgeon 1999). Moreover, CCs play an essential role in sieve tube loading with sugars from source tissues (Otero and Helariutta 2017; Slewinski et al. 2013). Source tissues are sugar-producing, photosynthetically active tissues, such as leaf mesophyll cells (Lemoine et al. 2013). Three different mechanisms of SE-loading are known: Apoplastic loading, polymer trapping and passive loading. Depending on the plant species, one or the other loading mechanism is usually preferred. *Arabidopsis* mostly relies on apoplastic loading. This means that sucrose, which is the main sugar transport form in plants, is released by mesophyll cells into the apoplast and special CCs, called transfer cells, actively import sucrose into the symplast. In polymer trapping, CCs convert sucrose into bigger sugar polymers that cannot escape, while passive loading works solely by osmosis and via PD between mesophyll cells and CCs (Otero and Helariutta 2017; Slewinski et al. 2013).

After phloem loading, sucrose is allocated into sink tissues (Knoblauch et al. 2016). Sink tissues simply describe places where sugars are transported to. Those include mitotically active

regions that require sugars as energy metabolites, flowers and storage organs, such as fruits. The terms “source” and “sink” are thereby not describing a special tissue type, but the state of either sugar-producing or sugar-requiring. A growing leaf can be, for instance, first a sink that later on becomes a source of sugars (Lemoine et al. 2013; Purves 2007). Similar to the water transport in xylem, the mechanism behind allocation of sugars from source to sink remained speculative for a long time. In 1930 Ernst Münch postulated the pressure-flow hypothesis that is solely based on the principle of osmosis: The high concentration of sugars in SEs surrounded by source cells draws water from the xylem into the phloem sap. This increases the hydraulic pressure in the sieve tube and pushes the phloem sap over long distances along the concentration gradient to sink tissues with significantly lower sugar concentration. In sinks sugar is either consumed by meristems, secreted into flowers or stored in fruits and therefore detracted from the system. Consequently, the differences in osmotic pressure between sources and sinks are maintained which keeps the phloem sap moving into sinks (Knoblauch et al. 2016). Although already postulated almost 90 years ago, the pressure-flow hypothesis was just recently experimentally proven by Knoblauch et al. 2016.

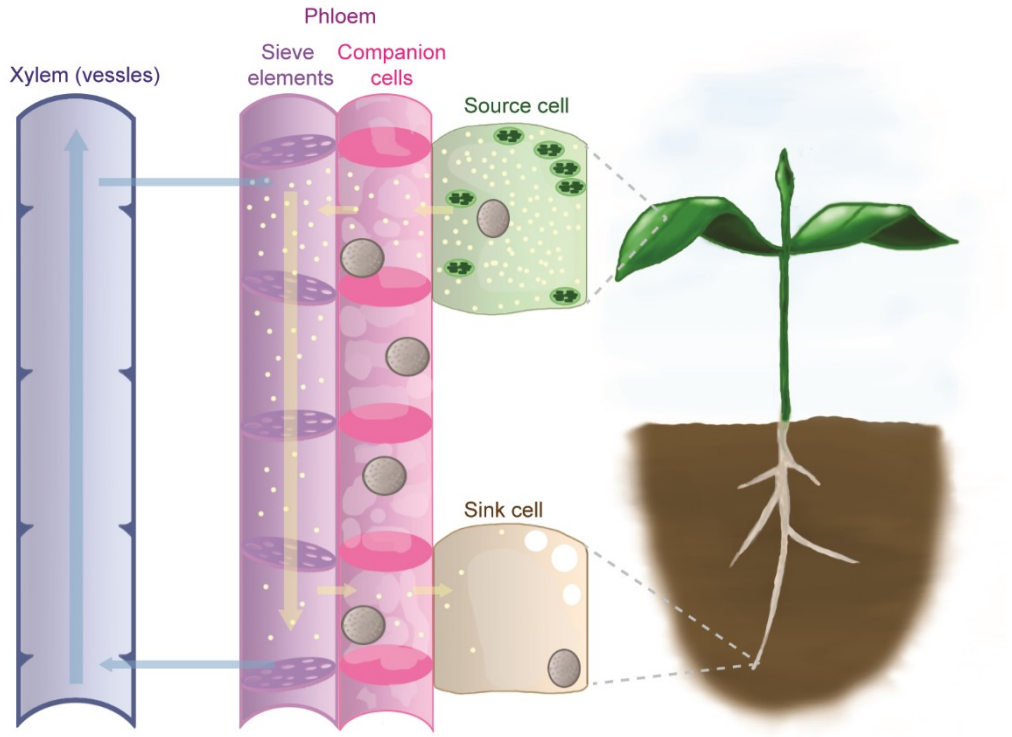

Figure 1.3: The vascular long-distance transport system
A scheme depicting the vascular transport system of a plant: Xylem vessels transport water from roots to shoots to hydrate source cells (blue arrows). The phloem allocates photosynthetically produced sugars (yellow dots and arrows) from source cells via sieve tube elements into sink cells for storage (e.g. in starch granules shown as white dots) and to fuel stem cell niches. The figure is based on information found in Oparka and Turgeon 1999; Froelich et al. 2011; Knoblauch et al. 2016; Purves 2007 and Campbell et al. 2016.

1.3.2.1 Phloem unloading: An interplay of proto- and metaphloem

As sucrose and other organic compounds of the phloem sap reach sink organs, they finally have to be unloaded from the SEs. Unlike in phloem loading, apoplastic unloading is relatively rare (Zhang et al. 2004; Patrick 1997). Phloem unloading is predominantly symplastic and sugars pass through PD of SE-CC-complexes into adjacent sink tissues (Imlau et al. 1999; Haupt et al. 2001). Successful unloading into mitotically active regions requires an interplay between two different phloem types, namely protophloem and metaphloem (Ross-Elliott et al. 2017; Lalonde et al. 2003). Both proto- and metaphloem are comprised out of a SE-CC-complex each, but exhibit critical differences in their spatio-temporal differentiation. Protophloem is the first cell type to differentiate. In the RAM, the first mature protophloem sieve elements (PSEs) are established within the meristematic zone (Lucas et al. 2013) (Figure 1.4). Since fully differentiated SEs are enucleated, they are unable to divide together with their still immature surrounding cells. Thus, PSEs and their accompanying CCs are forced to elongate until torn apart and physically crushed (Figure 1.4) (Ross-Elliott et al. 2017; Esau 1950). PSEs are therefore short-lived and eventually replaced by differentiated metaphloem (Lucas et al. 2013; Ross-Elliott et al. 2017). Consequently, metaphloem facilitates sugar unloading into storage sinks, while the sole purpose of protophloem is to fuel mitotically active regions, such as the RAM (reviewed in Lalonde et al. 2001). In root tips, proto-and metaphloem can be found adjacent to each other in both phloem poles (Figure 1.4). Organic cargo is first transferred from meta- into protophloem (Stadler et al. 2005) and translocated by mature, elongating PSEs until it enters the differentiating PSEs (Ross-Elliott et al. 2017). Differentiating PSEs are cells with newly established sieve plates and nuclear membranes that just started to degenerate. They are the only cells involved in unloading of sugars and bigger macromolecules. Small cargo, sugars and amino acids exit the differentiating PSEs through PD into adjacent tissues at a constant rate and diffuse freely within the symplast of the root tip. Macromolecules and larger cargo that could impede the sugar unloading process are unloaded through special funnel PD with bigger pore size into the phloem pole pericycle (PPP) (Figure 1.4). Unloading of large molecules happens in pulses and is called batch unloading. Small proteins, such as free GFP, can still move within the entire root tip, while larger proteins are trapped in the PPP. Notably, unloading occurs solely between PSEs and PPP and does not involve CCs. If PD connecting PSEs and PPP are clogged by callose deposition, unloading is effectively inhibited (Ross-Elliott et al. 2017).

Impaired unloading and/or defects in protophloem have immediate and severe effects on the RAM (Ross-Elliott et al. 2017; Depuydt et al. 2013). The RAM is a meristem of high stem cell activity and most distant from source tissues. It highly depends on a constant supply of energy metabolites provided by the protophloem (Depuydt et al. 2013; Anne and Hardtke 2017). Deficiencies in sugar abundance due to protophloem defects result in meristem death and thus termination of root growth (Depuydt et al. 2013).

1.3.3 Phloem: From formation to differentiation

The first provascular cells are already established in the early globular stage of embryogenesis, before shoot and root organizers are initiated (Zhang and Laux 2011; De Rybel et al. 2016). Directed, periclinal divisions of four procambium precursor cells lead to the formation of ground tissue and provascular cells (Scheres et al. 1994; Yoshida et al. 2014; De Rybel et al. 2016). At the final stages of embryo development, those provascular cells have established the initial - but still undifferentiated - root vasculature that is organized in a specific diarch pattern: Two phloem poles are flanking one xylem axis (Figure 1.4) (Lucas et al. 2013; Miyashima et al. 2011; Furuta et al. 2014a). This initial organization of the root vasculature is RAM-independent (De Rybel et al. 2016). After germination, primary root growth still follows this pre-determined pattern and phloem and xylem start to differentiate (Bauby et al. 2007; De Rybel et al. 2016).

1.3.3.1 Phloem formation in the RAM

During vegetative growth, roots grow approximately 100-150 µm per hour (Ross-Elliott et al. 2017). That speed requires an accurate spatio-temporal organization of cell division, division plane orientation, cell elongation and differentiation (Anne and Hardtke 2017). Protophloem is the first cell type that differentiates already within the RAM to ensure sugar supply of the stem cell niche (Ross-Elliott et al. 2017; Lucas et al. 2013). Delays and/or disruption of protophloem has therefore detrimental consequences for root growth (Depuydt et al. 2013; Rodriguez-Villalon et al. 2014). Despite its fundamental function for root growth and consequently plant fitness, the molecular processes regulating protophloem formation are still largely obscure. Only in recent years, a few genes have been described to evidentially and specifically regulate certain aspects of (proto-)phloem formation (Depuydt et al. 2013; Rodriguez-Villalon et al. 2014; Blob et al. 2018; Rodriguez-Villalon et al. 2015). Those genes are predominantly expressed during late stages of protophloem formation and knowledge about their interactions within a molecular network is still incomplete (reviewed in Blob et al. 2018).

The phloem cell lineage is initiated by the SE-procambium stem cell, or phloem initial, that divides asymmetrically and anticlinally to produce the SE-procambium precursor (Figure 1.4) (Rodriguez-Villalon et al. 2014). One of the earliest protophloem regulators already expressed in this first daughter cell is *OCTOPUS (OPS)* (Rodriguez-Villalon et al. 2014; Truernit et al. 2012). Five OPS-like proteins can be found in the proteome of higher plants that display, apart from a domain of unknown function, no specific protein motifs (Truernit et al. 2012). Although already expressed in provascular cells of heart-stage embryos, *OPS* expression is later on very specific for the phloem cell lineage and the protein localizes polarly to the shootward (apical) PM (Rodriguez-Villalon et al. 2014; Truernit et al. 2012). Of note, recent results showed that OPS activity rather depends on the presence of a positive charge on phosphosite S318 than on its polar localization (Breda et al. 2017). OPS plays a role in timing of protophloem differentiation

and patterning as the *ops* mutant shows discontinuous PSE differentiation (Truernit et al. 2012). This means that some, but not all, differentiating PSEs fail to enucleate and differentiate into mature PSEs. Those so-called “gap cells” disrupt the protophloem continuity and transport capacity, which results in short rooted *ops* seedlings (Rodriguez-Villalon et al. 2014; Truernit et al. 2012). The family member *OPS-LIKE2 (OPL2)* is broadly expressed throughout the root tip, but acts redundantly with *OPS* in both proto- and metaphloem differentiation. Double mutants *ops opl2* have shorter roots than *ops* single mutants and even show gap cells in the differentiated metaphloem (MSEs) (Ruiz Sola et al. 2017).

In the next step the SE-procambium precursor divides tangentially to initiate the procambium cell lineage and the SE precursor cells (Rodriguez-Villalon et al. 2014). After a few rounds of anticlinal divisions, the apical SE precursor cell divides a second time tangentially to initiate undifferentiated proto- and metaphloem cell lineages (Figure 1.4). The SE precursor cells are the first to express a number of phloem regulators, including the auxin-responsive *BREVIS RADIX* (*BRX*) (Scacchi et al. 2009) and the phosphoinositide 5-phosphatases encoding *COTYLEDON VASCULAR PATTERN 2 (CVP2*) gene (Rodriguez-Villalon et al. 2015). Similar to OPS, the BRX protein localizes polarly to the PM, but on the rootward (basal) side and only if auxin levels are low (Scacchi et al. 2009; Scacchi et al. 2010). Upon auxin treatment, BRX is translocated into the nucleus and subjected to proteosomal degradation (Scacchi et al. 2009). *CVP2* and its redundantly acting partner *CVP2-LIKE1 (CVL1)* balance phosphatidylinositol-4,5-biphosphate levels, which is one important aspect of PSEs differentiation (Rodriguez-Villalon et al. 2015). Phenotypically, *ops*, *brx* and *cvp2;cvl1* mutants show the exact same protophloem defects (Rodriguez-Villalon et al. 2015; Truernit et al. 2012; Scacchi et al. 2009). However, *brx* and *cvp2;cvl1* defects can be overcome by additional *OPS* expression (Rodriguez-Villalon et al. 2014). Likewise, another pair of phloem regulators first expressed in SE procambium precursors are the peptide CLE45 and its receptor, the LRR-RLK BARELY ANY MERISTEM 3 (BAM3). The CLE45-BAM3 interaction is effective in repressing protophloem initiation and differentiation (Rodriguez-Villalon et al. 2014; Depuydt et al. 2013). Upon CLE45 treatments, the second tangential division is either absent or delayed and protophloem fails to differentiate (Depuydt et al. 2013). The same delay or absence of the second tangential division can be observed in *ops* and *brx* mutants (Hernandez-Leon et al. 2014). Contrariwise, *bam3* mutants are CLE45 insensitive (Depuydt et al. 2013). Crossing an *ops* or *brx* mutant into a *bam3* background was effective in restoring protophloem continuity and root length to wild type levels (Rodriguez-Villalon et al. 2014). This, on the one hand, indicates a molecular interplay between OPS/BRX and BAM3-CLE45 in balancing protophloem formation, but on the other hand also shows that none of those factors is required to obtain protophloem cell identity and proper differentiation in the first place (Rodriguez-Villalon et al. 2014; Depuydt et al. 2013; Rodriguez-Villalon 2016).

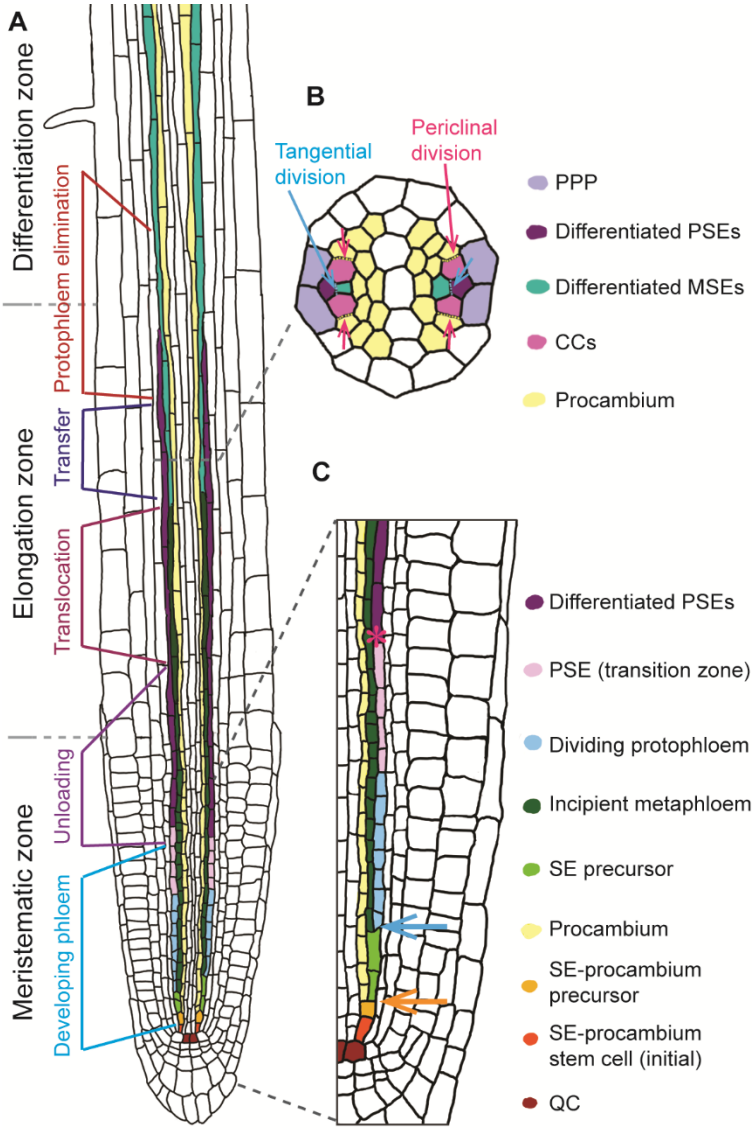

Figure 1.4: Phloem formation in the root

A A schematic representation of a longitudinal root section is shown. Phloem tissue types originating from the initial are coloured accordingly. Proto-phloem-mediated transport and unloading is shown by colour-coded zones.

B A schematic cross section of the stele at the transfer zone depicts the diarch pattern of two primary phloem poles. Pink arrows point to periclinal divisions of procambium that initiate CCs. Blue arrows point to tangential cell divisions that initiate proto- and metaphloem SEs.

C A schematic close-up of one developing phloem pole within the meristematic zone. Two tangential cell divisions (orange and blue arrows) lead to the initiation of SE precursors and proto- and metaphloem cell lineages, respectively. The pink asterisk marks the first differentiated PSE.

The figure is based on information found in Rodriguez-Villalon et al. 2014; Bonke et al. 2003 and Ross-Elliott et al. 2017.

Amongst later phloem marker genes are *ALTERED PHLOEM DEVELOPMENT (APL)* and *NAC45/86* (Bonke et al. 2003; Furuta et al. 2014b). The MYB coiled-coil-type transcription factor APL is famous for its fundamental role of repressing xylem and promoting both SE and CC differentiation (Bonke et al. 2003). Unlike mutants of the previously discussed phloem regulators, *apl* roots initially display wild type-like stele patterning and continuous PSE differentiation during the first two days after germination. However, already at the third day of vegetative growth, phloem identity is lost and cells that should differentiate into SEs and CCs, differentiate into TEs instead (Truernit et al. 2008). Older seedlings also frequently show absence or a delay of the tangential cell divisions that initiate phloem cell lineages (Figure 1.4) (Bonke et al. 2003). Those defects indicate that, although a correct tissue template was established during embryogenesis, *apl* mutant seedlings eventually fail to uphold the acquisition of phloem cell identity, which is crucial for plant vitality (Bonke et al. 2003; Truernit et al. 2008). Consequently, root growth is terminated and *apl* seedlings are lethal (Bonke et al. 2003). The two *NO APICAL*

MERISTEM (*NAC*)-type transcription factors, *NAC45* and *NAC86* were identified to act downstream of *APL*. They directly promote enucleation and cytoplasmic rearrangement during SE differentiation and are expressed alongside *APL* in developing SEs and the PPP. *nac45;nac86* double mutants fail to complete the enucleation process during SEs differentiation and are - just like *apl* - seedling lethal. Interestingly, certain traits associated with SE differentiation, such as changes in cell wall composition and sieve plate formation, still occur in *nac45;nac86* (Furuta et al. 2014b). Consequently, *NAC45/86* specifically regulate enucleation during SE differentiation which they do by modulating the expression of the downstream targets *NAC45/86-DEPENDENT EXONUCLESE-DOMAIN PROTEIN1 -4* (*NEN1, NEN2, NEN3* and *NEN4*) (Furuta et al. 2014b; Blob et al. 2018).

1.3.3.2 Phloem formation in above-ground organs

Although primary phloem formation is preferentially studied in root tips, proto- and metaphloem are abundant and important throughout the whole plant body (Evert and Eichhorn 2006). In fact, protophloem precursors established during embryogenesis start to differentiate within the midvein of cotyledons already 24 hours after germination, while protophloem differentiation in the RAM starts only after 48 hours (Bauby et al. 2007). During vegetative and generative growth, new leaves, stems and flowers are continuously generated by leaf, axillary and flower primordia, respectively. All vascular cells in above-ground tissues originate from procambial cells (Scarpella and Helariutta 2010). In leaves, procambial cells are formed de-novo from ground tissues in leaf primordia (Furuta et al. 2014a; Scarpella et al. 2004; Mattsson et al. 2003). ARF5/*MP* and HD-ZIP III genes, such as *ARABIDOPSIS THALIANA HOMEOBOX GENE 8* (*ATHB8*), are early vascular markers and important, universal regulators of procambium formation (Kang and Dengler 2002; Furuta et al. 2014a). The first specified procambium is formed at the midvein of the developing leaf and expands into higher order veins as the leaf expands (Scarpella et al. 2004). Venation follows certain patterns in an auxin-dependent manner (Sieburth 1999; Scarpella and Helariutta 2010; Mattsson et al. 2003). The newly formed veins have to be connected to the vasculature in stems, which itself has to form a continuum with the vasculature of hypocotyl and roots. This crucial vascular continuity is dependent on auxin-flux (Sachs 1981; Furuta et al. 2014a).

1.4 Signalling pathways in plant development

The modulation of transcription and/or translation by signalling pathways is the central regulatory force behind development across species (Basson 2012; McCarty and Chory 2000; Becraft 2002). The stimuli that trigger such a cascade of molecular events can be either of exogenous or endogenous nature. Exogenous stimuli include plant interactions with biotic factors

(other organisms) and abiotic factors, such as temperature, light, mechanical forces, water availability or chemical properties of soil and air (Atkinson and Urwin 2012; Suzuki et al. 2014). Endogenous signals involve peptides (Kucukoglu and Nilsson 2015), proteins (Zhang et al. 2015), RNA (Muraro et al. 2014; Parent et al. 2012), phytohormones (Davies 2010) or metabolites, such as sugars (Xiong et al. 2013). In the previous chapters I already briefly touched upon CLE-peptide mediated signalling and mentioned several famous plant phytohormones, such as auxin.

Two recently discovered mediators of plant development are the exogenous signalling molecule karrikin (KAR) and the endogenous hormone strigolactone (SL) (Brewer et al. 2013; Stanga et al. 2013). Although both pathways integrate the same or evolutionary very similar signalling components, they regulate quite distinct growth processes (Stanga et al. 2013; Gomez-Roldan et al. 2008).

1.4.1 Karrikins

KARs are compounds present in smoke produced through wildfires. The compounds are well known for their promoting role of post-fire germination in numerous species (Waters et al. 2014; Flematti et al. 2004; Flematti et al. 2010). Six different KARs are known, with KAR1 being the most common and active member (Waters et al. 2014). KARs are small and rigid molecules of a bicyclic structure with a pyran and butenolide ring (Figure 1.5) (Zwanenburg et al. 2016; Waters et al. 2014). The butenolide ring is generated during the combustion of carbohydrates found in plant material, like cellulose, and is essential for its function as germination stimulant (Flematti et al. 2004; Flematti et al. 2010). Studies in *Arabidopsis* showed that KARs induce light signal transduction and photomorphogenesis during germination (Nelson et al. 2010). Most interestingly, KARs are not only stimulating light and various phytohormone responses, but themselves signal via a KAR-specific signalling cascade to regulate germination, leaf expansion and hypocotyl elongation (Figure 1.6) (Nelson et al. 2010; Stanga et al. 2016; Stanga et al. 2013; Meng et al. 2016).

1.4.2 Strigolactones

SLs are ancient phytohormones whose origin probably dates back to the first land plants that colonized the earth (de Saint Germain et al. 2013). They can be already found in basal, non-vascular plants, such as the green algae *Chara corallina*, the liverwort *Marchantia spp*. and the moss *Physcomitrella patens*. There is experimental evidence that SLs promote rhizoid elongation in those species, which hints towards a primitive role of SL as endogenous hormones promoting land colonization (Delaux et al. 2012). Among those first land plants, SL started to serve another, indispensable function: Low amounts of the natural SL 5-deoxystrigol (Figure 1.5) are secreted from roots into the rhizosphere and attract symbiosis with arbuscular mycorrhizal (AM) fungi (Delaux et al. 2012; Akiyama et al. 2005; Xie and Yoneyama 2010). Upon

secretion from the root, SLs are unstable and therefore induce hyphal branching of AM fungi only in close proximity to the host root (Xie and Yoneyama 2010). AM fungi rely on sugar supply from a host plant and, in return, enable the host to take up more nutrients from the soil through their extended mycelium (Bouwmeester et al. 2007). Nowadays also vascular plants rely on AM fungi symbiosis that is efficiently triggered by SLs (Russell and Bulman 2005; Awad et al. 2006; Yoneyama et al. 2008). Parasitic plants of the *Orobanchaceae* family take advantage of this host-symbiont communication and use host-derived SLs as germination stimulus (Xie and Yoneyama 2010). Angiospermatous root parasites, such as *Striga lutea*, are a threat to agriculture and the identification of their unwelcome trigger was a long-sought goal. In 1966 the potent germination stimulus was first isolated from cotton root exudates and identified as SL (Cook et al. 1966).

1.4.2.1 Strigolactone structure and biosynthesis

Up to date more than 20 natural SLs have been identified (Xie 2016). They all share a tricyclic lactone, also known as ABC scaffold, which is linked to a butenolide ring D via an enol ether bridge (Figure 1.5) (Zwanenburg and Pospisil 2013; Alder et al. 2012). Of note, the CD ring structure is the most important part to ensure bioactivity (Zwanenburg et al. 2016). The stereochemistry at the B and C ring junction determines whether the SL belongs into the strigol or orobanchol class (Zwanenburg et al. 2015; Scaffidi et al. 2014). Both naturally occurring classes are biochemically active (reviewed in Wallner et al. 2016). The synthetically produced and widely used SL analogue *rac*-GR24 is - if not specially purified - a racemic mixture. The isoform GR24$^{5\text{ - deoxystrigol (5DS)}}$ acts as an analogue to the natural SL 5-deoxystrigol, whereas its enantiomer GR24$^{ent\text{-}5DS}$ has been shown to trigger KAR responses (Scaffidi et al. 2014; Conn et al. 2015; Umehara et al. 2015; Waters et al. 2014).

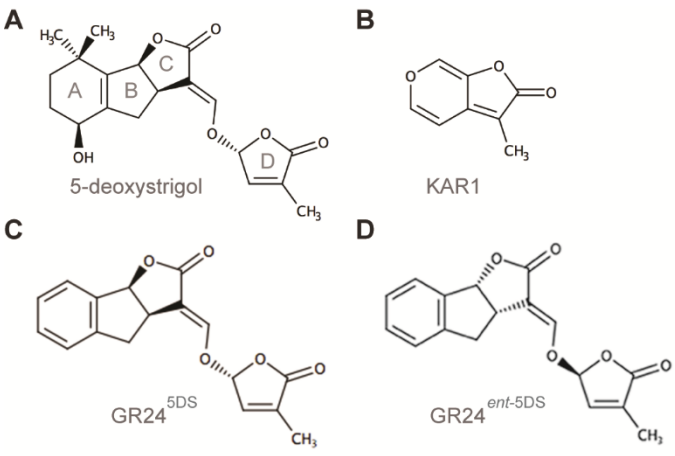

Figure 1.5: Molecular structures of strigolactone (SL) and karrikin (KAR)
A SLs share an ABC scaffold that is bound to a butenolide (ring D) by a flexible enol ether bridge.
B Karrikins (KAR) are of small and rigid bicyclic structure, but also possess a butenolide ring.
C - D The synthetically produced GR24^{5DS} is a potent SL analog, but its enantiomer GR24$^{ent\text{-}5DS}$ triggers KAR responses.
The figure was created using Marvin version 15.11.23, 2015, ChemAxon (http://www.chemaxon.com) and is based on information found in Zwanenburg et al. 2016 and Waters et al. 2014.

The biosynthetic pathway of SLs involves the enzymatic activities of at least four enzymes and starts from a C_{40} carotenoid precursor that is itself derived from the methylerythritol phosphate (MEP) pathway (Alder et al. 2012). In the first reaction the DWARF 27 (D27) isomerase converts all-trans-β-carotene to 9-cis-β-carotene (Alder et al. 2012; de Saint Germain et al. 2013). The CAROTENOID CLEAVAGE DEOXIGENASE 7 (CCD7), which is also known as MORE AXILLARY GROWTH 3 (MAX3) cleaves 9-cis-β-carotene into 9-cis-β-apo-19'-carotenal, which is converted by CCD8/MAX4 into the SL precursor carlactone (Alder et al. 2012; Waters et al. 2017). Those enzymatic reactions are much conserved across SL-producing species (Beveridge and Kyozuka 2010). The final conversion to SL is catalysed by the cryptochrome P450 monooxygenase MAX1 (Booker et al. 2005; Yoneyama et al. 2018). Depending on the plant species, MAX1 catalyses one to three different reactions: In *Arabidopsis* and *Nicotiana benthamiana* MAX1 only converts carlactone into carlactonic acid, which can be methylated by a so far unknown methyltransferase into methyl carlactononate (Abe et al. 2014; Zhang et al. 2014b). In *Arabidopsis* the oxidoreductase-like enzyme LATERAL BRANCHING OXIDOREDUCTASE (LBO) acts downstream of MAX1 and converts methyl carlactononate into an SL-like compound of yet unidentified chemistry (Brewer et al. 2016). In rice, different MAX1 homologues convert carlactonic acid into 4-Deoxyorobranchol and further into orobranchol (Zhang et al. 2014b; Yoneyama et al. 2018). The enzymes which catalyse the last steps into the broad variety of different SLs are still unknown and whether species, such as *Arabidopsis* truly generate canonical SLs, such as 5-deoxystrigol, is still a controversial topic (Waters et al. 2017).

1.4.2.2 Strigolactones in plant development

Only in the last years SLs gained considerable attention as plant hormones that orchestrate many developmental processes (Brewer et al. 2013; Rasmussen et al. 2013; Gomez-Roldan et al. 2008; Agustí et al. 2011a). In the root, SL biosynthesis is increased upon phosphate starvation to optimize root architecture (Kumar et al. 2015). SLs for instance promote primary and adventitious root growth, increase the meristematic cell number in the RAM and restrict lateral root formation (Sun et al. 2016; Rasmussen et al. 2013; Kumar et al. 2015). In the stem, SLs induce cambium formation in an auxin-dependent manner (Agustí et al. 2011a). SLs were additionally found to play a role in leaf expansion and senescence (Ueda and Kusaba 2015), are potentially involved in light signalling pathways and stress responses to draught and salinity (Ha et al. 2014; Waldie et al. 2014). However, their most famous role is the regulation of branching (Gomez-Roldan et al. 2008). SLs are transported against the auxin flux from roots to shoots to mediate apical dominance by increasing the competition between branches (Gomez-Roldan et al. 2008; Umehara et al. 2008; Crawford et al. 2010). Several hypotheses have been brought forward on how an interplay of SL, auxin and cytokinin regulates branching and the

research in this direction is still ongoing (Bennett et al. 2006; Dun et al. 2012; Brewer et al. 2009; Waldie et al. 2014; Hayward et al. 2009; Brewer et al. 2015).

1.4.3 Strigolactone and karrikin signalling pathways

The evolution of SL- and KAR-signalling is closely related and both pathways utilize similar signalling components and conserved mechanisms (Waters et al. 2017; Waters and Smith 2013).

1.4.3.1 SL and KAR are perceived by enzymatically active receptors

SL and KAR are perceived by two specific homologous receptors called DWARF14 (D14) and KARRIKIN INSENSITIVE 2 (KAI2), respectively (Guo et al. 2013; Kagiyama et al. 2013; Bennett and Leyser 2014; Scaffidi et al. 2014). The KAI2-like family is structurally highly conserved and already present in non-vascular plants, whereas D14 is unique to angiosperms and potentially derived from early KAI2 receptors that sensed SL in parasitic plants (Toh et al. 2015; Conn et al. 2015; Bythell-Douglas et al. 2017). Both KAI2 and D14 are α/β-hydrolases that possess a binding pocket with a catalytic triade consisting of a serine (Ser/S) at position 147, histidine (His/H) at position 297 and aspartic acid (Asp/D) at position 268 (Fig 1.6) (Kagiyama et al. 2013; Zhao et al. 2015). Upon SL binding to the catalytic binding pocket of D14, the enol ether bridge connecting the ABC scaffold to ring D is hydrolysed by a nucleophilic attack of Ser147 (Fig 1.5 and 1.6) (Zhao et al. 2015; Wallner et al. 2016). The hydrolysis of SL induces a conformational change in the lid domain of D14 (Zhao et al. 2015; Nakamura et al. 2013). This conformational switch stabilizes the interaction between D14 and the SL-signalling component DWARF3 (D3), also known as MAX2 in *Arabidopsis* (Zhao et al. 2015; Waters et al. 2017; Yao et al. 2018). Of note, the binding pocket of KAI2 is smaller and densely packed, which prevents its ability to hydrolyse SL (Kagiyama et al. 2013). Interestingly, exogenous KAR induces a change of KAI2 conformation by binding the pocket distally to the catalytic triade (Guo et al. 2013; Conn and Nelson 2015; Zhao et al. 2015). Just like for D14, the conformational change of KAI2 enables a stable interaction with the F-box protein MAX2/D3 (Guo et al. 2013; Waters et al. 2017). At the same time, D14 and KAI2 are themselves destabilized upon ligand binding. D14 is subsequently degraded in a MAX2-dependent manner, whereas KAI2 levels drop due to a yet unknown, but MAX2-independent degradation mechanism (Chevalier et al. 2014; Waters et al. 2014). Of note, *kai2* mutants are insensitive to KARs and display several *MAX2*-like phenotypes that are not found in *d14*, including reduced light-responsiveness and germination (Waters et al. 2012). A point mutation leading to an amino acid substitution of alanine (Ala) to valine (Val) at position 219 within the KAI2 ligand binding pocket compromises both binding capacity and flexibility of the receptor. Interestingly, this point mutation is sufficient to induce

typical *kai2* phenotypes (Lee et al. 2018). Thus, the existence of an endogenous KAI2 ligand has been proposed (Waters et al. 2013).

1.4.3.2 Signal transduction by SCF^{MAX2}-mediated ubiquitination

MAX2/D3 encodes an F-box protein that builds a key component of the SCF (SUPPRESSOR OF KINETOCHORE PROTEIN1 (SKP1), Cullin (CUL1), RING BOX1 (RBX1), F-box) E3 ubiquitin ligase (Nelson et al. 2011; Stirnberg et al. 2002; Hamiaux et al. 2012; Somers and Fujiwara 2009). SCF complexes are important machineries of post-translational regulation across eukaryotes (Sun et al. 2009). They enable target-specific protein modification by polyubiquitination, which results in degradation by the 26S proteasome (Somers and Fujiwara 2009). The ubiquitination process involves three different enzymes: The ubiquitin activating enzyme (E1) utilizes adenosine triphosphate (ATP) to transfer activated ubiquitin to the ubiquitin conjugating enzyme (E2). E2 covalently attaches ubiquitin to a target protein, which is specified by the F-box protein of the E3 ligase/SCF complex (Figure 1.6) (Hershko and Ciechanover 1998). Of note, SCF-mediated proteolysis of downstream targets is a common form of signal transduction among plants. Besides SL/KAR, many other hormones, such as auxin, gibberellin and jasmonate signal via SCF complexes (Waters et al. 2017; Morffy et al. 2016). While the auxin and jasmonate receptors are themselves F-box proteins that determine target specificity upon hormone binding (Tan et al. 2007; Sheard et al. 2010), the targets of gibberellin, SL and KAR are determined by the F-box-receptor complex (Wallner et al. 2016; Morffy et al. 2016).

1.4.3.3 SUPPRESSOR of MORE AXILLARY GROWTH 2 1-LIKE (SMXL) proteins are targets of proteolysis

Recent studies identified distinct members of the SUPPRESSOR OF MAX2 1-LIKE (SMXL) protein family as targets of either SL or KAR signalling (Wang et al. 2015; Soundappan et al. 2015; Stanga et al. 2013). The *Arabidopsis* SMXL family consists of eight members that can be divided into four sub-clades according to their phylogeny and function (Moturu et al. 2018). Their name reflects their role as genetic suppressors of several SL- and KAR-dependent *max2* mutant phenotypes (Soundappan et al. 2015; Stanga et al. 2013). Genetically, the *max2* phenotype is a beautiful combination of both *kai2* and *d14* defects, which therefore can be easily separated (Waters et al. 2012; Waters and Smith 2013).

The founding member and eponym of the family, SUPPRESSOR OF MAX2 1 (SMAX1) and its most closely related family member SMXL2 have convincingly been shown to be proteolytic targets of KAR signalling. The double mutant *smax1;max2* and the triple mutant *smax1 smxl2;max2* efficiently suppress KAR-dependent *max2* mutant defects, such as impaired germination, enhanced hypocotyl elongation and reduced leaf expansion (Figure 1.6) (Soundappan

et al. 2015; Stanga et al. 2016). The other well-studied members are SMXL6/7/8, which belong to sub-clade 4 (Liang et al. 2016; Moturu et al. 2018). The SMXL6/7/8 proteins have been shown to be protein targets of the SL-dependent MAX2-D14 complex. They physically interact with both MAX2 and D14 and are ubiquitinated and degraded upon *rac*-GR24 treatments (Soundappan et al. 2015; Wang et al. 2015). In genetic terms, *smxl6/7/8;max2* quadruple mutants are able to suppress the *max2* branching phenotype and are therefore important regulators of branching within the SL-signalling pathway (Figure 1.6) (Liang et al. 2016; Soundappan et al. 2015; Wang et al. 2015). Their function is conserved across species and the SL-dependent SMXL orthologue in rice, DWARF 53 (D53), has been subject of in-depth studies that helped to elucidate the molecular mechanisms in SL signalling (Jiang et al. 2013; Zhou et al. 2013). The breakthrough came with the investigation of the rice mutant *d53* that grows an extensive number of short tillers. This mutant carries a base pair change and a 15 base pair deletion within the coding sequence of *D53*, which results in a deletion of eight amino acids (RGKTGI) (Figure 1.7). It was shown that D53 acts as a repressor of SL-signalling that is rapidly degraded upon *rac*-GR24 treatments in a MAX2/D3-D14 dependent manner (Zhou et al. 2013). The mutated d53 version still interacts with both MAX2 and D14, but is no longer ubiquitinated and therefore remains constitutively active (Jiang et al. 2013; Zhou et al. 2013).

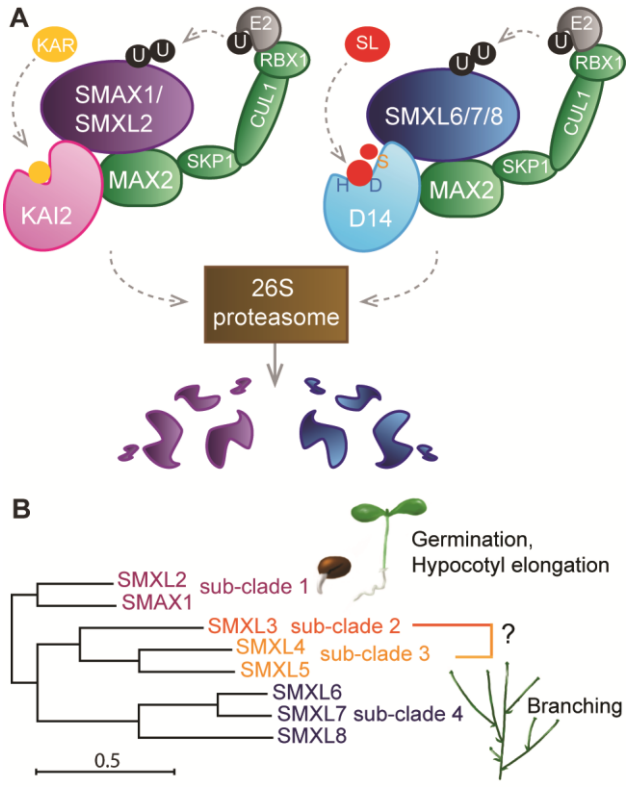

Figure 1.6: SUPPRESSOR OF MAX2 1-LIKE (SMXL) proteins are repressors of KAR- and SL-signalling
A Schematic representation of KAR-signalling (left) and SL-signalling (right) that leads to ubiquitination and subsequent degradation of SMAX1/ SMXL2 and SMXL6/7/8, respectively.
B The maximum likelihood phylogenetic tree represents an amino acid sequence alignment of all eight SMXL family members and was performed using CLC Main Workbench Version 7.6.1 (CLC Bio Qiagen, Aarhus, Denmark). SMXLs are grouped into four subclades: The KAR-dependent sub-clade 1 regulates germination and hypocotyl elongation, whereas the SL-dependent sub-clade 4 regulates branching. The function of subclades 2 and 3 were unknown. The scale bar represents a branch length of 0.5 amino acid substitutions per site.
The figure is based on information found in Waters et al. 2017; Soundappan et al. 2015; Stanga et al. 2016; Stanga et al. 2013; Liang et al. 2016 and Wallner et al. 2016.

1.4.3.4 The regulation of SMXL3/4/5

Interestingly, the eight amino acids that are essential for MAX2-receptor-dependent ubiquitination of SMXL/D53 are also conserved in SMXL sub clade 1 and 4. Strikingly, the so far unexplored SMXL family members SMXL3/4/5 show quite dramatic changes in this particular amino acid sequence (Figure 1.7) (Wallner et al. 2016; Soundappan et al. 2015). Their function as mediators of either KAR- or SL- signalling is therefore highly questionable. So far, our lab identified SMXL5 of sub-clade 3 as early and highly specific cambium marker during IC initiation in *Arabidopsis* stems (Agustí et al. 2011b).

Of note, the expression patterns of all SMXL family members and SL- and KAR- signalling components, such as MAX2, D14 and KAI2 are to a certain extent associated with vascular tissues (Chevalier et al. 2014; Shen et al. 2007; Liang et al. 2016). Although still underexplored, the role of SL-signalling in cambium regulation supports this notion (Agustí et al. 2011a). However, the function of SMXL3/4/5 and their molecular network remained unknown.

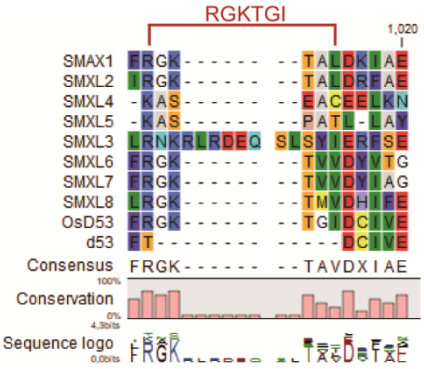

Figure 1.7: The motif important for MAX2-dependent ubiquitination is changed in SMXL3/4/5
Shown is an amino acid sequence alignment of all SMXL family members and the rice orthologue D53. Eight amino acids (RGKTGI) are conserved in all SMXLs and D53 except for SMXL3/4/5 and the *d53* mutant. The alignment was done in CLC Main Workbench Version 7.6.1 (CLC Bio Qiagen, Aarhus, Denmark) (Wallner et al. 2016).

1.4.4 SMXL protein function and downstream action

To truly understand the signalling mechanics that lead to a certain morphology, the molecular role of all signalling components has to be uncovered. So far, there is a clear genetic link between certain SMXL family members and SL/KAR-dependent phenotypic traits and yet, whether SMXLs regulate transcription or translation of certain downstream targets is still unknown (Liang et al. 2016; Soundappan et al. 2015). For SL-dependent branching regulation it was shown that signalling via SMXL7 happens in the nucleus (Liang et al. 2016). MAX2, D14 and all so far investigated SMXL proteins, including the rice orthologue D53 localize to the nucleus (Liang et al. 2016; Soundappan et al. 2015; Jiang et al. 2013; Zhou et al. 2013). SMXLs are chaperon-like proteins and most closely related to HEAT SHOCK PROTEIN 101 (HSP101) (Soundappan et al. 2015; Stanga et al. 2013). They are AAA ATPases with a conserved Clp-N motive, one to three conserved ETHYLENE RESPONSE FACTOR ASSOCIATED-AMPHIPFATIC REPRESSION (EAR) domains and a coiled-coil domain (Ma et al. 2017).

1.4.4.1 SMXL interaction with TOPLESS (TPL)

The EAR3 domain of SMXL6/7/8 and D53 interacts with the transcriptional regulator TOPLESS (TPL) (Liang et al. 2016; Smith and Li 2014; Ma et al. 2017). TPL and TPL-RELATED (TPR) proteins act as transcriptional co-repressors that interact with EAR domains of transcriptional repressors via a C-Terminal to Lissencephaly Homology (CTLH) domain (Szemenyei et al. 2008). Moreover, they are known scaffolds to recruit chromatin-modifying complexes and histone deacetylases (HDAC) (Ma et al. 2017; Krogan and Long 2009). Consequently, TPL/TPR proteins are involved in chromatin remodelling and transcriptional regulation of downstream targets (Szemenyei et al. 2008; Krogan and Long 2009). Recent findings indicated that D53 stabilizes a tetramer of TPL proteins and their interaction with nucleosomes as well as histones H3 and H4 (Ma et al. 2017). Despite this apparent interaction, the regulation of branching via SMXL7 was found to be mostly TPL-independent (Liang et al. 2016). The actual relevance of the SMXL/D53-TPL interaction thus remains largely obscure.

1.4.4.2 The diverse roles of OBERONs (OBEs)

In 2011, two years before the role of the first *SMXL* family member (*SMAX1*) was published, our lab started a Yeast Two-Hybrid screen with SMXL5 that was performed by Hybrigenics SA (Paris, France). Our aim was to understand the molecular network and role of this back then “unknown protein” AT5G57130 in the cambium (Agustí et al. 2011b). Based on our screen, we identified several potential protein-protein interaction partners of SMXL5 (data unpublished). Among those we also identified the OBERONs (OBEs).

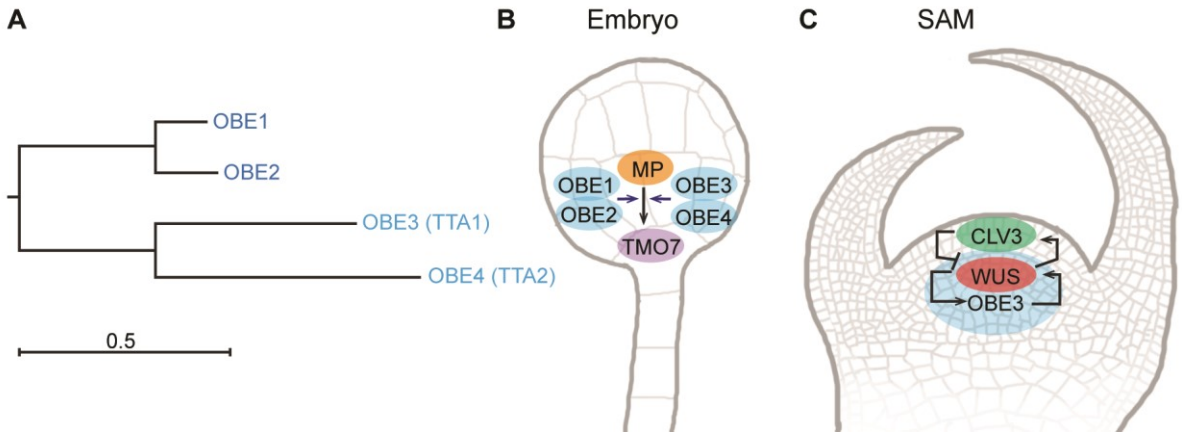

Figure 1.8: OBEs regulate RAM and SAM maintenance

A The maximum likelihood phylogenetic tree shows an amino acid sequence alignment of the four OBE family members and was performed using the CLC Main Workbench Version 7.6.1 (CLC Bio Qiagen, Aarhus, Denmark). The scale bar represents a branch length of 0.5 amino acid substitutions per site.

B *OBE1/2* and *OBE3/4* act redundantly in embryonic root initiation, supposedly by enabling binding of the transcription factor *ARF5/MP* to *TMO5* and *TMO7* promoters (Saiga et al. 2012). **C** *OBE3* interacts with *WUS* in stem cell maintenance of the SAM, potentially by enhancing WUS expression in a positive feedback loop (Lin et al. 2016).

OBEs build a family of four proteins (Figure 1.8 A) that hold a highly conserved plant homeodomain (PHD)-finger and a coiled coil domain (Saiga et al. 2008; Saiga et al. 2012). PHD-finger domains are known to specifically bind di- and trimethylated histone H3 to recruit nucleosome-associated protein complexes and transcription factors to chromatin (Wysocka et al. 2006; Li et al. 2006; Saiga et al. 2012). OBEs are ubiquitously expressed, nuclear localized proteins that also have predicted DNA binding and proposed chromatin remodelling properties (Saiga et al. 2008; Saiga et al. 2012). They form homo- and heterodimers and pair into two groups of OBE1/2 and OBE3/4 to act redundantly in *ARF5/MP*-dependent embryonic RAM initiation during early stages of embryogenesis (Saiga et al. 2008; Saiga et al. 2012; Thomas et al. 2009). Double mutants *obe1;obe2* and *obe3;obe4* are rootless and lethal due to embryonic defects in the establishment of the hypophysis (Figure 1.8 B) (Saiga et al. 2008; Saiga et al. 2012). *OBE1/2* have been additionally shown to act in auxin-mediated development and vascular patterning (Thomas et al. 2009). New data also showed that *OBE3* interacts with the transcription factor *WUSCHEL (WUS)* in SAM regulation (Figure 1.8 C), which indicates that certain *OBE* family members exhibit unique roles in stem cell regulation and meristem maintenance (Lin et al. 2016; Saiga et al. 2008).

1.5 Aim

My PhD project was centred around three main goals:

1) Characterizing the role of *SMXL3/4/5* in plant development

Since *SMXL3/4/5* were so-far underexplored SMXL family members whose function was obscure, I aimed for determining their role and significance in plant development. Initial experiments during my Master's thesis indicated that *smxl4;smxl5* double mutants are short rooted and show altered stem morphologies and increased cambium-derived tissue (CDT) production, which hints towards a fundamental role in development (Wallner 2014). Thus, I aimed to conduct an in-depth study to investigate the functional redundancies and differences of *SMXL3/4/5* during RAM and IC formation on a cellular and molecular level.

2) Investigating a potential contribution of SMXL3/4/5 to SL- or KAR-signalling

Unlike all other SMXL family members that are either involved in SL- or KAR-signalling, SMXL3/4/5 show differences in an amino acid motif that proved essential for MAX2-dependent ubiquitination and subsequent proteosomal degradation (Liang et al. 2016; Zhou et al. 2013; Wallner et al. 2016). It was therefore questionable whether SMXL3/4/5 are proteolytic targets of SL/KAR-signalling. To investigate their contribution to SL/KAR-signalling, I therefore aimed to test their genetic interaction with *MAX2* and to determine their protein stability in the presence of the SL/KAR-analogue *rac*-GR24.

3) Elucidating the functional relevance of the SMXL5-OBE interaction

To integrate *SMXL3/4/5* into a broader molecular network, we performed a Yeast Two-Hybrid screen with SMXL5 as a bait and obtained a list of potential protein-protein interaction partners, including OBE2/3/4 (by Hybrigenics SA (Paris, France), data unpublished). *OBEs* are especially interesting candidates because they hold diverse roles in meristem maintenance and encode nuclear localized proteins with proposed chromatin remodelling abilities (Saiga et al. 2012). To determine the biological relevance of the SMXL5-OBE interaction and to understand the molecular action of SMXL proteins in general, I aimed for testing the protein-protein interaction between SMXL5 and OBE *in planta* and to investigate a potential genetic interaction between *OBE1/2/3/4* and *SMXL3/4/5* in plant development.

2. Material

2.1 Organisms

2.1.1 Plants

2.1.1.1 *Arabidopsis thaliana*

The plant species *Arabidopsis thaliana* (L.) Heynh. of the ecotype Columbia (Col) was primarily used in this study. In Table 1 the plant lines used and their origins are listed. Double and triple mutants were obtained by crossing these lines.

Genotype	Gene locus	Construct	Origin	Reference
smxl5-1	*AT5G57130*	*SALK_018522*	NASC (N518522)	Stanga, et al., 2013
smxl4-1	*AT4G29920*	*SALK_037136*	NASC (N537136)	Stanga, et al., 2013
smxl3-1	*AT3G52490*	*SALK_024706*	NASC (N524706)	Stanga, et al., 2013
max2-1	*AT2G42620*	tilling (point mutation), *DR5::GUS*	Ottoline Leyser	Stirnberg, et al., 2002
obe1-1	*AT3G07780*	*SALK_075710*	Dolf Weijers	Saiga, et al., 2008
obe2-1	*AT5G48160*	*KG16805*	Dolf Weijers	Saiga, et al., 2008
obe3-2 (tta1-2)	*AT1G14740*	*SALK_042597*	Dolf Weijers	Saiga, et al., 2012
obe4-1 (tta2-1)	*AT3G63500*	*SALK_082338*	Dolf Weijers	Saiga, et al., 2012
WT	-	-	Gudrun Böhmdorfer	
WT	-	*OBE1:OBE1-GFP*	Dolf Weijers	Saiga, et al., 2008
WT	-	*OBE2:OBE2-GFP*	Dolf Weijers	Saiga, et al., 2008
WT	-	*OBE3:OBE3-GFP*	Dolf Weijers	Saiga, et al., 2012
WT	-	*OBE4:OBE4-GFP*	Dolf Weijers	Saiga, et al., 2012
WT	**-**	*SMXL5:YFP-ER* (pJA24)	Javir Agusti	Wallner, et al., 2017
WT	**-**	*SMXL4:YFP-ER* (pIL46)	Ivan Lebovka	Wallner, et al., 2017
WT	**-**	*SMXL3:YFP-ER* (pEW18)	this study	Wallner, et al., 2017
smxl4-1 smxl5-1	*AT4G29920, AT5G57130*	*SMAX1:YFP-ER* (pKG64)	Karin Grünwald	Wallner, et al., 2017
smxl4-1 smxl5-1	*AT4G29920, AT5G57130*	*SALK_037136, SALK_018522, SMXL5:SMXL5-YFP* (pKG52)	Karin Grünwald	Wallner, et al., 2017

smxl4-1 smxl5-1	*AT4G29920, AT5G57130*	*SALK_037136, SALK_018522, SMXL5:SMAX1-YFP* (pKG62)	Karin Grünwald	Wallner, et al., 2017
smxl4-1 smxl5-1	*AT4G29920, AT5G57130*	*SALK_037136, SALK_018522, SMXL4:SMXL4-YFP* (pEW23)	this study	Wallner, et al., 2017
smxl3-1 smxl5-1	*AT3G52490, AT5G57130*	*SALK_024706, SALK_018522, SMXL3:SMXL3-YFP* (pEW20)	this study	Wallner, et al., 2017
smxl5-1 obe3-2	*AT5G57130, AT1G14740*	*SALK_018522, SALK_042597, SMXL5:OBE3-turquoise* (pEW72)	this study	unpublished
smxl5-1	*AT5G57130*	*SALK_018522, SMXL5:obe3-miRNA1* (pEW65)	this study	unpublished
smxl5-1	*AT5G57130*	*SALK_018522, SMXL5:obe3-miRNA2* (pEW66)	this study	unpublished

Table 2.1: *Arabidopsis* lines used in this study.

2.1.1.2 *Nicotiana benthamiana*

Nicotiana benthamiana (*Nicotiana*) plants were provided by the laboratory of Prof. Dr. Karin Schumacher and grown in the greenhouse at the Centre for Organismal Studies (COS, Heidelberg, Germany).

2.1.2 Nematodes

Sciaridae infestation of soil was counteracted by regular treatment (each second week) with nematodes of the species *Steinernema feltiae*. This beneficial organism was purchased as nemaplus® (e-nema, Schwentinental, Germany).

2.1.3 Bacterial strains

2.1.3.1 *Escherichia coli*

The *Escherichia coli* (*E. coli*) genotype DH5α (Hanahan, 1983) was used for molecular cloning and plasmid amplification.

DH5α F-, end A1, hsdR17 (rk^-, mk^+), gyrA96, relA1, supE44, L^-, recA1, 80dlacZM15, Δ(lacZYA-argF)U196

2.1.3.2 *Agrobacterium tumefaciens*

The *Agrobacterium tumefaciens* (*Agrobacteria*) genotypes C58C1: RifR with pSoup plasmid (TetR) or ASE: KanR, CamR with pSoup+ plasmid (TetR) were used (Ashby 1988, Fraley 1985, Hellens 2000).

2.2 Plasmids

2.2.1 Vectors

Name	Description	Resistance for bacteria	Resistance for plants	Origin	Reference
pGreen0179	Binary vector	Kanamycin	Hygromycin	Klaus Theres	Hellens, et al., 2000
pGreen0229:35S	Binary vector with 35S promoter	Kanamycin	BASTA	Thomas Greb	Based on Hellens, et al., 2000
pGreen0229	Binary vector	Kanamycin	BASTA	Klaus Theres	Hellens, et al., 2000
pGGZ003	GreenGate destination vector	Spectinomycin	Sulfadiazine	Jan Lohmann	Lampropoulos, et al., 2013
pGGA000	GreenGate entry Module A	Ampicillin	-	Jan Lohmann	Lampropoulos, et al., 2013
pGGB000	GreenGate entry Module B	Ampicillin	-	Jan Lohmann	Lampropoulos, et al., 2013
pGGC000	GreenGate entry Module C	Ampicillin	-	Jan Lohmann	Lampropoulos, et al., 2013
pGGD000	GreenGate entry Module D	Ampicillin	-	Jan Lohmann	Lampropoulos, et al., 2013
pGGE000	GreenGate entry Module E	Ampicillin	-	Jan Lohmann	Lampropoulos, et al., 2013
pGGF000	GreenGate entry Module F	Ampicillin	-	Jan Lohmann	Lampropoulos, et al., 2013
pGGI000	GreenGate entry Module I	Ampicillin	-	Jan Lohmann	Lampropoulos, et al., 2013

Table 2.2: Vectors used in this study.

2.2.2 Constructs

All constructs generated in this study were either cloned by standard methods using the vectors *pGreen0179* or *pGreen0229* (Hellens, et al., 2000) or by Green Gate cloning using the Green Gate modules *pGGA000-pGGI000* and the destination vector *pGGZ003* (Lampropoulos et al. 2013). Some constructs were based on plasmids from Karin Grünwald (*pKG*), Ivan Lebovka (*pIL*) or Vadir López-Salmerón (*pVL*), which are described in the Thomas Greb lab plasmid database (COS, Heidelberg, Germany).

Name	Vector	Description	Used for	Reference
pEW16	*pGreen0179*	*SMXL3* 3' promoter (amplified from gDNA, digest with HindIII and XhoI)	Cloning of *pEW17*	Wallner, et al., 2017
pEW17	*pEW16*	*SMXL3* 5' promoter (amplified from gDNA, digest with SacII and Cfr9I)	Cloning of *pEW18*	Wallner, et al., 2017
pEW18	*pEW17*	*SMXL3:ER-YFP* (*ER-YFP* amplified from *pKG64*, digest with Cfr9I)	Transformation into WT (*Arabidopsis*)	Wallner, et al., 2017
pEW19	*pEW17*	*SMXL3:SMXL3* (*SMXL3* exon amplified from *pEW15*, digestion with Cfr9I and EcoRI)	Cloning of *pEW20*	Wallner, et al., 2017
pEW20	*pEW19*	*SMXL3:SMXL3-YFP* (YFP-linker amplified from *pEW15*, digestion with EcoRI and EcoRV)	Transformation into *smxl3;smxl5*	Wallner, et al., 2017
pEW21	*pGreen0229*	*SMXL4* 5' promoter (amplified from *pIL46*, digestion with BamHI and XbaI)	Cloning of *pEW22*	Wallner, et al., 2017
pEW22	*pEW21*	*SMXL4:SMXL4-YFP* (exon + YFP amplified from *pEW13*)	Cloning of *pEW23*	Wallner, et al., 2017
pEW23	*pEW22*	*SMXL4:SMXL4-YFP* (+ 3' *SMXL4* terminator)	Transformation into *smxl4;smxl5*	Wallner, et al., 2017
pEW31	*pGreen0229-35S*	*35S:3xHA* (without stop codon)	Cloning of *pEW32* and *pEW33*	unpublished
pEW32	*pEW31*	*35S:3xHA-MAX2*	Transient expression in *Nicotiana*	unpublished
pEW33	*pKG33*	*35S:SMXL5-3xHA*	Transient expression in *Nicotiana*	unpublished
pEW45	*pGGI000*	*OBE3 miRNA 3* (see primer list) in GreenGate entry Module I	Cloning of *pEW65*	unplublished
pEW46	*pGGI000*	*OBE3 miRNA 4* (see primer list) in GreenGate entry Module I	Cloning of *pEW66*	unpublished
pEW65	*pGGZ003*	*SMXL5:OBE3-miRNA3* (GreenGate reaction with *pVL28, pEW45, pVL66, pVL53*)	Transformation in *smxl5*	unpublished
pEW66	*pGGZ003*	*SMXL5:OBE3-miRNA4* (GreenGate reaction with *pVL28, pEW46, pVL66, pVL53*)	Transformation in *smxl5*	unpublished
pEW72	*pGGZ003*	*SMXL5:OBE3-turquoise* (GreenGate with *pVL28, pVL50, pVL85, pVL101, pVL20, pVL53*)	Transformation of *smxl5 obe3*	unpublished
pEW75	*pGGB000*	*6x-Myc* taq (no stop) in Module B (amplified from *pTGM61*)	Cloning of *pEW78*	unpublished
pEW78	*pGGZ003*	*35S:6xc-Myc-OBE3* (GreenGate with *pDS34, pEW75, pVL85, pVL51, pVL66, pVL53*)	Transient expression in *Nicotiana*	unpublished

Table 2.3: Self-generated constructs used in this study.

Some constructs were received as *Agrobacteria* glycerol stocks:

Name	Vector	Description	*Agrobacteria* strain	Used for	Received by
pVL127	*pGGZ003*	35S*:OBE3-mGFP*	C58C1: RifR, pSoup+ (TetR)	Transient expression in *Nicotiana*	Vadir Lopez-Salmeron
pVL122	*pGGZ003*	*35S:SMXL5-mCherry*	C58C1: RifR, pSoup+ (TetR)	Transient expression in *Nicotiana*	Vadir Lopez-Salmeron
pMG103	*pGGZ003*	*35S:mCherry-NLS*	ASE: KanR, CamR, pSoup+ (TetR)	Transient expression in *Nicotiana*	Michael Gebert
pCW194	*pGGZ003*	*UBI10:mGFP-mCherry-NLS*	ASE: KanR, CamR, pSoup+ (TetR)	Transient expression in *Nicotiana*	Christian Wenzl
p19	*pBin61*	*35S:p19* (Voinnet et al. 2003)	C58C1: RifR	Transient expression in *Nicotiana*	Rainer Waadt

Table 2.4: Received glycerol stocks used in this study.

2.3 Primers

The primers used for the described experiments were designed using CLC Main Work-bench 7 (CLC Bio Qiagen, Aarhus, Denmark) and purchased from Sigma-Aldrich (St. Louis, USA). For Open Reading Frame (ORF) amplification from cDNA, “ACTA” sequences were added to the 5’ prime end to allow restriction of PCR products by DNA restriction enzymes at added recognition sites.

	Used for	Primer name	Primer sequence (5' → 3')
Genotyping	*smax1-2*	*SALK_128579-LP*	GTGGCAACTGTTTAGGCTGAG
		SALK_128579-RP	AAGCTAGCTTTTCAAGTCCCG
	smax2-1	*SAIL_596_E08-LP*	GCTCCCAAGCCTAATCAAAAC
		SAIL_596_E08-RP	CCACTTCAGTGTCGAGCTCTC
	smxl3-1	*SALK_024706_LP*	CCCTACACAGCTCTTCACGAG
		SALK_024706_RP	TGCCTCTCTCACAAGAAAAGC
	smxl4-1	*SALK_037136-LP*	TTGAAGCCATGGAAGAATCTG
		SALK_037136-RP	ACAAAGAACAATGCGGTCAAG
	smxl5-1	*SALK_018522-LP*	TGTCTCATTGAAGCCAAAACC
		SALK_018522-RP	AATGGTGCAAGAATTCTGACG
	smxl6-4	*SALK_050363-LP*	AGCCAGAGAAAGACTCGAACC
		SALK_050363-RP	TCCGAAATTAAGCTCGATGTG
	smxl7-3	*WiscDsLox339C04_LP*	GATCAAGAAACGAACGCTGAG
		WIscDsLox339C04_RP	CGTATTAGCCTCTCGGATTCC
	smxl8-1	*SALK_025338_LP*	GAATCACAAATTCTGCATGGC
		SALK_025338_RP	CTGACGAAGCTCCACTTTCAC
	obe1-1	*SALK_075710_LP*	ATTCGACTCAAACGTTGAACG
		SALK_075710_RP	CTCGTCTGGACAAACTTCTGC
	obe2-1	*obe2-1_RP*	CTTCAAGATCAAGGTATTGACCTAAATTACC
		obe2-1_LP	CATTTGGTGAGGATGATTCGAACC
		obe2-1_Insertion	GATCAGATTGTCGTTTCCCGCC
	obe3-1	*SALK_042597_LP*	TTCCAACAACAAAGGCTTTTG

		SALK_042597_RP	TTTCCCACAAAACGAAACAAG
	obe4-1	*SALK_082338_LP*	TGCTTATTGACACCTGACTGC
		SALK_082338_RP	AAGAAAAGCGAGGAGGAAGTG
	WiscDsLox_ insertion	*WiscDsLox-LB-p745*	AACGTCCGCAATGTGTTATTAAGTTGTC
	SAIL_insert	*SAIL_LB3*	TAGCATCTGAATTTCATAACCAATCTCGATACAC
	SALK_insert	*SALK_LBa1*	TGGTTCACGTAGTGGGCCATCG
	max2-1	*max2-1 dCAPS F*	TGTCCGAATTTGGAAGAGATTAGG
		max2-1 dCAPS R	CAAGAAGAATCTTTCCCATAAACTCGAAT
RT-PCR	*smxl3-1*	*SMXL3_p2*	CACCTTCCATATAGACGCCG
		smxl3_cDNA	AAGCTACGTTGAAGCAGAGC
	smxl4-1	*SMXL4_p3*	TGTTGGGTAGACAAGTTCCC
		SMXL4_p1	GAAACCGGAATATGATGCTG
	smxl5-1	*SMXL5_p3*	GCTGATTCGGCTTCAAACCT
		CEB1for20	TGTGGGCACTTCATCCTGTC
	ACT2 (Ref)	*qACT2f*	GCCATCCAAGCTGTTCTCTC
		qACT2r	ACCCTCGTAGATTGGCACAG
Molecular cloning	*pEW16*	*p3SMXL3rev*	ACTAAAGCTTCACTAACAGCATGCACGTATG
		p3SMXL3for	ACTACTCGAGACCGTTGGTTCAATCCAATG
	pEW17	*p5SMXL3rev*	ACTACCCGGGAGTGACAAAACACCCTAAAATAACAC
		p5SMXL3for2	ACTACCGCGGGCAAGTGGGCTTGAGAGATGGGTTG
	pEW18	*ERYFPfor*	ACTACCCGGGATGAATAAGACTAATCTTTTTCTC
		ERYFPrev2	ACTACCCGGGTTAGAGTTCGTCGTGCTTGTACAGC
	pEW19	SMXL3for	ACTAGAATTCTGTTGATGAACACTTGAAATGAAAC
		SMXL3rev2	ACTACCCGGGATGAGAGCTGGAGGCTGCACGGTG
	pEW20	YFPrev4	ACTAGATATCTCACTTGTACAGCTCGTCCATGCC
		YFPrev5	ACTAGAATTCGGAGGAAGTGGAGTGAGCAAGGGC
	pEW21	p5SMXL4rev	ACTAGGATCCCACAAAACCACCCACCTTAAATCC
		p5SMXL4for	ACTATCTAGAACCATGTCGAACCCTCCAATTG
	pEW22	EYFPfor	ACTAGAATTCTCACTTGTACAGCTCGTCCATGCC
		SMXL4rev	ACTAGGATCCATGCGTACAGGGGCTTATACCGTG
	pEW23	p3SMXL4for	ACTAGGGCCCCTTCGGCTTTTATTTCTGTTC
		p3SMXL4rev	ACTAGGTACCCATTCACTCAAAATAATCAGTTG
	pEW31	3xHA_for	ACTAGGATCCTCCGCTTCCTCCTGCGTAGTCCGG-GACATCATAC
		3xHA_rev	ACTAAAGCTTATGTATCCTTATGATGTACCTGAT-TATG
	pEW32	MAX2_for	ACTAGGATCCGCTTCCACTACTCTCTCCGAC
		MAX2rev4	ACTACCCGGGTCAGTCAATGATGTTGCGGCTGTTC
	pEW33	3xHA_SMXL5_for	ACTAGGATCCAGGAGGAAGTGGAG-GAAGTTATCCTTATGATGTACCTG
		3xHA_SMXL5_rev	ACTACCCGGGTCATGCGTAGTCCGGGACATC
	miRNA PCRs for *pEW45/46*	P-0950 Oligo A	AACAGGTCTCAAACACTGCAGCCCCAAACACACGC
		P-0951 Oligo B	AACAGGTCTCTGCAGCCCCATGGCGATGCC
	pEW45	I_miRNAsOBE3_3	GATAATTTCTGGTATTGACTCAGTCTCTCTTTT-GTATTCC
		II_miRNAaOBE3_3	GACTGAGTCAATACCAGAAATTATCAAAGA-GAATCAATGA
		III_miRNA*sOBE3_3	GACTAAGTCAATACCTGAAATTTTCACAGGTCGTGA-TATG
		IV_miRNA*aOBE3_3	GAAAATTTCAGGTATTGACTTAGTCTACAT-ATATATTCCT
	pEW46	I_miRNAsOBE3_4	GATAATTTCTGGTATTGACTCATTCTCTCTTTT-GTATTCC
		II_miRNAaOBE3_4	GAATGAGTCAATACCAGAAATTATCAAAGA-GAATCAATGA
		III_miRNA*sOBE3_4	GAATAAGTCAATACCTGAAATTTTCACAGGTCGTGA-TATG

		IV_miRNA*aOBE3_4	GAAAATTTCAGGTATTGACTTATTCTACAT-ATATATTCCT
	pEW75	cMyc_ModulB_for	AACAGGTCTCAAACAATGGAGCAAAAGCTC
		cMyc_ModulB_rev	AACAGGTCTCAAGCCCAAGTCCTCTTCAGA
Sequencing	*SMXL7* exon	SMXL7_rev4	GTCAAAGAATCCATCAAACTC
		SMXL7_rev5	GAAACAACCACGTAGCAACC
		SMXL7_rev6	GAGGAAAGAGTTCTCAATGCC
	SMXL7 5'promoter	pSMXL7_seq_1	GAAGGCTCTTCTACTGTGCATC
		pSMXL7_seq_2	GCAAATCAATTCATTTTAAC
		pSMXL7_seq_3	GAATAAAGCTAACAGAAGTTG
	SMXL4 5' promoter	5'SMXL4_for	CCACAGACTTTTGATCATTC
		5'SMXL4_for2	TATCGGAAATATGGGACTTG
		5'SMXL4_for3	ATTGAGGTGGTGTCACTGTC
		5'SMXL4_for4	GTAGAGATATTTAGGTGTAC
		5'SMXL4_for5	GTTTGATCATGTGTAGTGATC
		5'SMXL4_for6	TGAATAGTAAGGCAGCTTTC
		5'SMXL4_rev1	CTAAGTTTACTTCCACCATTAC
	SMXL4 exon	smxl4_rev1	GTGAACCCGAATCTCTCTTC
		smxl4_rev2	CGAGGATGTTCATGAACTGAG
		smxl4_for1	GCAGCTTGTTGTGTCGATTC
		smxl4_rev3	GTCCAGCTTCTCTCATCAC
	SMXL3 exon	smxl3_for1	GAGTAGAGTGATGAGAGAAGC
		smxl3_for2	GTGGAGCATATGATAATG
		smxl3_for3	CTTCAATCAGTACTCTTCATC
		smxl3_for4	CTCGTGTTTGGATCGCAAGAC
	SMXL3 5' promoter	smxl3 prom_for	AGTGAATGATGATTTGCATC
		smxl3 prom_for2	CAAAGACCAAGCTAGTGATCC
		smxl3 prom_for3	GATTTAAGTGGCATCTGCATC
		smxl3 prom_for4	CTGTTGCAGAGAATAGTGGC
		smxl3 prom_for5	TAGACAGCGAGGACGAAACAG
		smxl3 prom_for6	CACTTCTGAGTATTAGTAC
	MAX2 exon	MAX2_for2	CTTAACCCAAACTCTGGCTC
		MAX2_for3	CAGCCTCACTAGTTTCCACT
	OBE3 exon	Obe3_F2	TTTCCCCTCTTGATGCTT
		Obe3_R2	GCTCTTCTTCTTTTGATCCT
		OBE3dM4_For	TTCGTTCATAGGGATTCTG
	YFP	YFP/CFPrev11	GCTGAACTTGTGGCCGTTT
		YFP/CFPrev10	GCTTCTCGTTGGGGTCTT
	GreenGate Module D insert	D-dummy_seq_1	GGGAATGAAGGTAAAGGT
		D-dummy_seq_2	TAACCTTTACCTTCATTCCC
	SulfR	SulfR_GGF	CCTACACGCCGAAATAAAC
	p35S	35S	CCTTCGCAAGACCCTTCCTC

Table 2.5: Primers used in this study.

2.4 Chemicals

Standard chemicals were shared between the research groups of Prof. Dr. Jan Lohmann and Prof. Dr. Thomas Greb and are listed in our common and officially accessible Dangerous Materials Registry Information System (DaMaRIS) that is provided by the University of Heidelberg, Germany.

2.4.1 Antibiotics

1000x stocks:

100 mg/ml Ampicillin (Sigma-Aldrich; St. Louis, USA)

25 mg/ml Chloramphenicol in ethanol (Roth; Karlsruhe, Germany)

50 mg/ml Kanamycin (Roth; Karlsruhe, Germany)

100 mg/ml Spectinomycin (Sigma-Aldrich; St. Louis, USA)

100 mg/ml Sulfadiazine (Sigma-Aldrich; St. Louis, USA)

2000x stocks:

10 mg/ml Tetracyclin in ethanol (Sigma-Aldrich; St. Louis, USA)

100 mg/ml Rifampicin (Sigma-Aldrich; St. Louis, USA)

50 mg/ml Hygromycine B (Roche; Basel, Switzerland)

2.4.2 Dyes

DirectRed 23 #212490 (Sigma-Aldrich; St. Louis, USA)

FM® 4-64 #T3166 (Thermo-Scientific; Waltham, USA)

Propidium iodide #81845 (Sigma-Aldrich; St. Louis, USA)

Methyl blue #95290 (Sigma-Aldrich; St. Louis, USA)

Toluidine blue #52040 (AppliChem, Darmstadt, Germany)

Ethidium bromide solution 0,025 % in dropper bottle (Roth; Karlsruhe, Germany)

2.4.3 Herbicides

10 µg/ml Glufosinate: Basta ® (Bayer; Leverkusen, Germany)

2.4.4 Hormones

The synthetic strigolactone-analogue *rac*-GR24 was ordered from Chiralix B. V., Nijmegen, Netherlands and a stock solution of 10 mM in acetone was stored at -20 °C.

2.5 Antibodies

Anti-HA-Peroxidase High Affinity (3F10), rat monoclonal (Roche; Basel, Switzerland)

c-Myc Antibody (9E10) sc-40 HRP, mouse monoclonal (Santa Cruz Biotechnology, Santa Cruz, USA)

2.6 Media, buffers and solutions

2.6.1 Growth media

E. coli

Lysogeny broth (LB) medium

1 % NaCl
1 % Peptone
0.5 % Yeast extract
1.5 % Bacto agar (for LB-agar plates)
pH 7, autoclaved

Agrobacteria

YEB medium

5 % Meat extract
5 % Peptone
1 % Yeast Extract
5 % NaCl
5 % Sucrose
2 mM $MgSO_4$
1 % Bacto agar (for YEB-agar plates)
autoclaved

Arabidopsis

Murashige and Skoog (MS)-medium (100 ml)

0.43 g Murashinge-Skoog salt
1 g Sucrose
0.05 g MES hydrat
0.8 g Phyto Agar (for MS-plates)
pH 5.8, autoclaved

Autoclaved growth media were cooled down to approximately 55 °C before antibiotics or herbicides were added.

2.6.2 Standard buffers and solutions

2.6.2.1 Seed sterilization

Sterilization solution

70 % Ethanol with 0.2 % Tween

2.6.2.2 Rough extraction of gDNA from *Arabidopsis* for genotyping

Extraction buffer

200 mM Tris (pH 7.5)
250 mM NaCl
0.5 % SDS
25 mM EDTA

10xTE buffer

100 mM Tris (pH 8)
10 mM EDTA (pH 8)

2.6.2.3 RNA extraction for cDNA synthesis and sequencing

Extraction buffer

0.1 M NaCl
2 % SDS
50 mM Tris/HCl (pH 9)
10 mM EDTA
20 mM β-mercaptoethanol (added freshly)

2.6.2.4 Gel electrophoresis

50x TAE (1 L)

242 g TRIS
100 ml EDTA (0.5 M)
57.1 ml Acetic acid
pH 7.6

Loading dye

0.25 % Xylene cyanole
0.25 % Bromophenol blue
50 % Glycerol
10 mM Tris (pH 8)
1 mM EDTA (pH 8)

DNA Ladder

(Thermo-Scientific; Waltham, USA) GeneRuler 1 kb DNA Ladder #SM0311

MassRuler Low Range DNA Ladder #SM0383

2.6.2.5 Transformation of *Arabidopsis*

Infiltration medium

5 % Sucrose

0.015 % Silwet L-77

2.6.2.6 Infiltration of *Nicotiana* leaves

Induction buffer

10 mM MES pH 5.5

10 mM $MgSO_4$

150 µM Acetosyringone

2.6.2.7 Embryo extraction of *Arabidopsis*

Embryo extraction buffer

(Raissig et al. 2013) ½ liquid MS (see *Arabidopsis* growth media)

1 M Glycine

2.6.2.8 Protein extraction, IP and Western blotting

Protein extraction buffer

50 nM Na_3PO_4

150 mM NaCl

10 % Glycerol

5 mM EDTA

10 µM β-mercaptoethanol

0.1 % Triton X-100

2 mM $NaVO_4$

2 mM NaF

cOmplete tablet (1/2 tablet per 20ml)

20 µM MG132

1 mM PMSF

Wash buffer I	
	50 nM Na_3PO_4 150 mM NaCl 10 % Glycerol 5 mM EDTA 0.1 % triton X-100 2 mM $NaVO_4$ 2 mM NaF cOmplete tablet (1/2 tablet per 20ml) 20 µM MG132 1 mM PMSF
Wash buffer II	
	50 nM Na_3PO_4 150 mM NaCl 10 % Glycerol 5 mM EDTA
4x Resolving buffer	
	1.5 M Tris-HCl pH 8.8
4x Stacking gel buffer	
	0.5 M Tris-HCl pH 6.8
Laemmli	
	Sample Buffer, Laemmli 2x Concentrate #S3401 (Sigma-Aldrich; St. Louis, USA)
Protein ladder	
	PageRuler™ Plus Prestained Protein Ladder, 10 to 250 kDa # 26619 (Thermo-Scientific; Waltham, USA)
10x Running buffer	
	250 mM Tris 1.92 M Glycine

10x Transfer buffer	
	0.48 M Tris
	0.39 M Glycin
	0.375 % SDS (20% stock)
1x Transfer buffer + methanol	
	10 ml 10x Transfer buffer
	20 ml Methanol (freshly added)
	filled to 100 ml with H_2O
5x TBS	
	125 mM Tris
	625 mM NaCl
	pH 8
1x TBS-T working solution	
	5x TBS (1:10)
	0.1 % Tween added
Blocking solution	
	1x TBS-T
	5 % powdered milk (Roth; Karlsruhe, Germany)

2.7 Kits

2.7.1 DNA extraction

QIAprep Spin Miniprep Kit (QIAGEN, Venlo, Netherlands)
QIAquick PCR Purification Kit (QIAGEN, Venlo, Netherlands)
Wizard® SV Gel and PCR Clean-Up System (Promega, Madison, USA)

2.7.2 Enzymes

Polymerases

JumpStart™REDTaq® ReadyMix™ (Sigma-Aldrich; St. Louis, USA)
Taq DNA Polymerase, recombinant (5 U/µL) (Thermo-Scientific; Waltham, USA)
Phusion High-Fidelity DNA Polymerase (2 U/µL) (Thermo-Scientific; Waltham, USA)

Phosphatase

Antarctic Phosphatase (NEB, Frankfurt am Main, Germany)

Restriction enzymes

For molecular cloning restriction enzymes and their reaction buffers were ordered from Thermo Fisher Scientific (Thermo-Scientific; Waltham, USA) or New England Biolabs (NEB, Frankfurt am Main, Germany) and used as recommended by the manufacturers. Green Gate cloning (Lampropoulos et al. 2013) required the FastDigest Eco31I restriction enzyme (Thermo-Scientific; Waltham, USA).

Ligase

T4 DNA Ligase (5 U/µL) #EL0014 (Thermo-Scientific; Waltham, USA)

DNase and reverse transcriptase

DNase I, RNase-free (supplied with MnCl2) (1 U/µL)

RevertAid First Strand cDNA Synthesis Kit (Thermo-Scientific; Waltham, USA)

2.8 Immunoprecipitation and Western blotting

Anti-HA MicroBeads #130-094-255 (Miltenyi Biotec, Bergisch Gladbach, Germany)

µ Columns #130-042-701 (Miltenyi Biotec, Bergisch Gladbach, Germany)

MACS MultiStand (Miltenyi Biotec, Bergisch Gladbach, Germany)

cOmplete™ Protease Inhibitor Cocktail (Roche; Basel, Switzerland)

Immun-Blot® PVDF Membrane #1620177 (Bio-Rad Laboratories; Hercules, USA)

Whatman Paper (Thick Blot Paper) 7.5 x 10 cm (Bio-Rad Laboratories; Hercules, USA)

Bio-Rad Protein Assay Dye Reagent Concentrate (Bio-Rad Laboratories; Hercules, USA)

Protein Standard II #5000007 (Bio-Rad Laboratories; Hercules, USA)

SuperSignal™ West Femto Maximum Sensitivity Substrate (Thermo-Scientific; Waltham, USA)

SuperSignal™ West Pico Chemiluminescent Substrate (Thermo-Scientific; Waltham, USA)

2.9 Software and technical equipment

2.9.1 Websites as resources and for processing data

National Center for Biotechnology Information (NCBI, Bethesda, USA)

Arabidopsis Information Resource (TAIR) (Huala, et al., 2001)

InterPro (EMBL-EBI, Cambridgeshire, UK)

VirtualPlant 1.3 (Katari et al. 2010)

VENNY (Oliveros 2007)

WMD3 - Web MicroRNA Designer Version 3 (Max Planck Institute for Developmental Biology, Tübingen. http://www.weigelworld.org)
cNLS Mapper (Kosugi et al. 2009)

2.9.2 Software

CLC Main Workbench 7.6.1 (CLC Bio Qiagen, Aarhus, Denmark)
CaseViewer 2.2 (3DHistech, Budapest, Hungary)
ImageJ 1.51h (National Institute of Health, Bethesda, USA)
Microsoft Office 2016 (Excel, Word and PowerPoint) (Microsoft, Redmond, USA)
Adobe Creative Suite CS6 (Photoshop, Illustrator) (Adobe, San Jose, USA)
SPSS V. 25 (IBM, Armonk, USA)
GraphPad Prism version 6.01 (GraphPad Software, La Jolla, USA)
Marvin 15.11.23, 2015, ChemAxon (http://www.chemaxon.com)
R (https://cran.r-project.org/)
R Studio (https://www.rstudio.com/)
Fast QC (http://www.bioinformatics.babraham.ac.uk/projects/fastqc)
TopHat2 v2.0.14 (Kim et al. 2013)
DESeq2 package from the R/Bioconductor software (Love et al. 2014)

2.9.3 Technical equipment

2.9.3.1 Microscopes

Confocal microscope TCS SP5 (Leica Microsystems; Mannheim, Germany)
provided by Prof. Dr. Joachim Wittbrodt
Confocal microscope TCS SP8 (Leica Microsystems; Mannheim, Germany)
provided by Prof. Dr. Annika Guse
Microscope Axio Imager.M1 (Carl Zeiss; Oberkochen, Germany)
provided by Prof. Dr. Ingrid Lohmann
Stereomicroscope (Nikon Corporation; Tokyo, Japan)
provided by Prof. Dr. Jan Lohmann

2.9.3.2 Laboratory equipment

The following equipment was shared between laboratories of Prof. Dr. Thomas Greb and Prof. Dr. Jan Lohmann:
Microtome RM2235 (Leica Microsystems; Mannheim, Germany)

Paraffin embedding center EG1160 (Leica Microsystems; Mannheim, Germany)
Leica ASP 200S (Leica Microsystems; Mannheim, Germany)
Leica EG1160 Embedding Centre (Leica Microsystems; Mannheim, Germany)
Leica HI1220 Flattening table for clinical histopathology (Leica Microsystems; Mannheim, Germany)
Stereo microscope Stemi 2000-C (Carl Zeiss; Oberkochen, Germany)
ActivFlo Routine I Lids Cassettes (Leica Microsystems; Mannheim, Germany)
Tissue-Tek® Mega-Cassette Base Mold #4166 (Sakura Finetek Europe B.V., Alphen aan den Rijn, Netherlands)
Superfrost™ Microscope Slides (Thermo-Scientific; Waltham, USA)
Micromount Mounting Media (Leica Microsystems; Mannheim, Germany)
Pannoramic SCAN II (3DHistech, Budapest, Hungary)
Refrigerated centrifuge Eppendorf 5430R (Eppendorf; Hamburg, Germany)
Precision balance (Kern & Sohn; Balingen, Germany)
Heating block neoBlock Duo (neoLab Migge Laborbedarf; Heidelberg, Germany)
Power Pac HC (Bio-Rad Laboratories; Hercules, USA)
Trans-Blot® SD Semi-Dry Transfer Cell (Bio-Rad Laboratories; Hercules, USA)
Mini-PROTEAN® Tetra Cell #1658001EDU (Bio-Rad Laboratories; Hercules, USA)
Nanodrop ND-1000 (Nanodrop, Wilmington, USA)
Thermocycler Biometra TRIO (Analytik Jena, Jena, Germany)
Microwave (Sharp, Osaka, Japan)
Basic pH meter PB-11 (Sartorius, Göttingen, Germany)
Advanced Fluorescence and ECL Imager (Intas Science Imaging Instruments, Göttingen, Germany)*
Spark Multimode reader (TECAN, Männedorf, Switzerland)*
TissueLyser II (Retsch®, Haan, Germany)*
Ice machine (Ziegra Eismaschinen, Isernhagen, Germany)*
Sorvall RC-5C Plus Superspeed Centrifuge (Sorvall®, Newtown, USA)*
*provided by Prof. Dr. Karin Schumacher

2.9.3.3 Other equipment

Wacom Intuos3 graphic tablet (Wacom®, Kazo, Japan)
HP EliteDesk 800 G1 DM Business PC (Hewlett Packard Inc., Palo Alto, USA)
HP Z24i monitor (Hewlett Packard Inc., Palo Alto, USA)

3 Methods

Every method not precisely described, can be found in *Arabidopsis: A Laboratory manual* by Weigel & Glazebrook, 2002.

3.1 Seed sterilization and stratification

Arabidopsis seeds were sterilized by sterilization solution for 15 min, washed twice with 100 % ethanol and air dried under sterile conditions. To break seed dormancy, seeds were stratified in microcentrifuge tubes containing dH_2O at 4 °C in the dark for 3 days.

3.2 Plant growth conditions and maintenance

Arabidopsis plants were grown in plastic pots on standard soil (Einheitserde Klassik, Einheitserdewerke Patzer Gebr. Patzer GmbH & Co. KG, Sinntal-Altengronau, Germany) mixed 1:4 with perlite (Perligran extra, Knauf, Iphofen, Germany) and soaked in nematode solution for pest control.

Plants dedicated for histology sectioning were first grown in short day (SD) conditions (8 h light and 16 h dark) with 65 % humidity and 23 °C for 3 weeks and then transferred to long day (LD) conditions (16 h light and 8 h dark) at 23 °C and 65 % humidity. The plants were watered by soaking the pots with water for 20 min twice a week. For seed collection and crossings, plants were solely grown in LD conditions.

Seedlings grown on MS-plates were either kept in LD or SD conditions (depending on the experiment) for 2, 5, 7 or 10 days.

3.3 *E. coli* growth conditions

E. coli of the strain DH5α were grown at 37 °C over night in liquid LB medium on a shaker (180 rpm to an OD_{600} > 1) or plated on LB-plates in an incubator. Depending on the transformed plasmid, antibiotics were added to the medium to select transformed colonies.

3.4 *Agrobacteria* growth conditions

Agrobacteria strains were grown at 28 °C over night in liquid YEB medium on a shaker (180 rpm to an OD_{600} > 1) or plated on YEB-plates in an incubator. Depending on the transformed plasmid and the used strain, antibiotics were added to the medium to select transformed colonies.

3.5 Tissue staining

3.5.1 Direct Red staining

To preserve fluorescent signals in roots, seedlings were fixed in a vacuum chamber for 1 h by 4 % (w/v) PFA dissolved in PBS. The tissue was washed twice by PBS and cleared with ClearSee solution for 7 days according to (Kurihara et al. 2015). Cleared seedlings were stained by 0.01 % (w/v) Direct Red 23 in ClearSee solution for 2 h. Excess staining was removed by clearing once again in pure ClearSee solution for 1 h. Stained seedlings were analysed by confocal microscopy with an excitement of 561 nm (DPSS laser) and detecting wavelengths >660 nm.

3.5.2 FM4-64 staining of roots

The cell membrane dye FM® 4-64 Dye was used for visualizing cell membranes in seedling roots. The dye was diluted 1:2000 in sterile tap water and seedlings incubated for 30 sec. Afterwards seedlings were transferred to H_2O without dye and incubated for 10-15 min before analysed by confocal microscopy with an excitement of 561 nm (DPSS laser) and detecting wavelengths >660 nm.

3.5.3 Propidium iodide (PI) staining of stem sections

The cell wall dye propidium iodide (PI) was applied to fresh stem cross sections to visualize lignified secondary cell walls by confocal microscopy. Prior to imaging, fresh stem sections were counterstained by for 5 min by 5 µg/ml PI dissolved in sterile tap water. PI-stained tissues were excited at 561 nm (DPSS laser) and detected at 590-690 nm.

3.5.4 mPS-PI staining of roots

The mPS-PI staining of roots was carried out as described before (Truernit et al. 2008). PI-stained tissues were excited at 561 nm (DPSS laser) and detected at 590-690 nm.

3.5.5 Aniline staining of callose

Aniline staining was performed as described in (Schenk and Schikora 2015). Stained stem sections were analysed at the epifluorescent microscope Zeiss Axio Imager.M1 by exciting Fluorescence of aniline was excited by the UV lamp and emission was collected using the DAPI filter.

3.6 Grafting of *Arabidopsis* seedlings

Grafting was performed on 5 day-old seedlings grown in SD as previously described (Melnyk and Meyerowitz 2015).

3.7 Sugar measurements

Grafted seedlings were grown on soil for 3 weeks to the rosette stage. Three fully developed leaves from individual plant were pooled into one sample. Five samples (biological replicates) were collected per grafted combination. Tissue samples were immediately frozen in liquid nitrogen and ground using a porcelain mortar prior to analysis. Soluble sugars were extracted and determined by the Metabolomics Core facility (EMBL Heidelberg, Germany) as described before (Poschet et al. 2011).

3.8 Histology

1-cm stem fragments just above the uppermost rosette leaf were harvested from 15 – 20 cm tall plants, transferred into embedding cassettes and infiltrated by 70 % ethanol for at least 3 days at 4 °C. Samples were processed by the Leica ASP 200S tissue processing machine. Fixed samples were embedded into paraffin using metal molds and the paraffin embedding centre EG1160 (Leica Microsystems; Mannheim, Germany). Using the microtome RM2235 (Leica Microsystems; Mannheim, Germany) 10 µm sections were produced and placed onto Superfrost™ Microscope Slides (Thermo-Scientific; Waltham, USA) covered with hot water to stretch the tissue. Samples were dried over night at 42 °C on a heating plate. Dry samples were deparaffinised and stained as follows:

Dewaxing		Toluidin blue staining (see chapter 2.5.1.2)	
Histo-Clear™	10 min	0.05 % Toluidin blue	4 min
Histo-Clear™	10 min	H_2O	washing
100 % ethanol	1 min	H_2O	1 min
100 % ethanol	1 min	85 % ethanol	30 sec
95 % ethanol	1 min	95 % ethanol	30 sec
85 % ethanol	1 min	100 % ethanol	30 sec
50 % ethanol	1 min	100 % ethanol	30 sec
30 % ethanol	1 min		
H_2O	5 min		

Stained samples were air-dried and embedded in Micromount Mounting Media (Leica Microsystems; Mannheim, Germany). Slides were scanned using the slide scanner Pannoramic SCAN II (3DHistech, Budapest, Hungary) and analysed using the software CaseViewer 2.2 (3DHistech, Budapest, Hungary) by measuring the CDT production. Data processing was done in Microsoft Excel (Microsoft, Redmond, USA) and SPSS (IBM, Armonk, USA).

3.9 Extraction of torpedo-stage embryos

Embryos of mid-torpedo stage were extracted by sticking the first full-length silique of a mature *Arabidopsis* plant onto a double-sided tape fixed on an objective slide. The silique was opened with a micro-scalpel using a stereomicroscope. Ovules were removed and transferred into microcentrifuge tubes with approximately 50 µl embryo isolation buffer (Raissig et al. 2013). The ovules were opened by slightly squeezing them with a small plastic mortar without destroying the embryo. The liquid was transferred onto an objective slide and embryos were collected and separated from the debris by a 10 µl pipet tip attached to a plastic pasteur pipette. Images were taken by confocal microscopy.

3.10 Rough DNA extraction and genotyping of *Arabidopsis*

3.10.1 DNA extraction

This quick DNA extraction method was adapted from Dr. Nial Gursanscky and used for genotyping 3 - 4 week old mutant plants. A middle-sized leaf was supplied with 200 µl extraction buffer and ground manually with a drill. After adding additional 200 µl extraction buffer, the solution was centrifuged at 14,000 g at RT for 5 min. The supernatant was transferred into a new microcentrifuge tube and incubated with 350 µl isopropanol for 10 min. The sample was centrifuged again (14000 g, 5 min), the supernatant discarded and the pellet washed with 70 % ethanol. The pellet was dried and dissolved in 50 µl 1xTE buffer prior to use.

3.10.2 Genotyping

Genotyping of *Arabidopsis* was performed using 1 µl of DNA solution (obtained as described in 3.8.1) and the Taq DNA Polymerase, recombinant (5 U/µL) kit (Thermo-Scientific; Waltham, USA). Genotyping PCRs and thermocycler settings were set up as recommended by the manufacturer.

3.11 RNA extraction from *Arabidopsis*

The RNA extraction procedure was adapted from (Mallory and Vaucheret 2010). Plant material was frozen in liquid nitrogen and pulverized in a 2 ml microcentrifuge tube with 2 glass beads using the mixer mill MM 400 (Retsch, Haan, Germany). The pulverized tissue was mixed with 500 µl RNA extraction buffer. 500 µl phenol and 500 µl chloroform were added and the mixture centrifuged at 13,000 g, 4 °C for 10 min. The aqueous phase was recovered and the phenol/chloroform extraction step repeated. 1 ml chloroform was added to the aqueous phase to remove residual phenols and again centrifuged at 13,000 g, 4 °C or 10 min. The aqueous

phase was recovered and RNA precipitated for 1 h at -80°C with 1/10 V 3 M NaAc pH 5.2 and 3 V cold 100 % ethanol. Samples were centrifuged at 13,000 g, 4°C for 30 min and the RNA pellets were washed 3x with cold 70 % ethanol before air dried and resuspended in 30 µl ddH_2O (RNAse free). The RNA concentration was measured using a NanoDrop ND-1000 (ThermoScientific; Waltham, USA).

3.11.1 cDNA synthesis

Extracted RNA was treated with DNAse to remove residual genomic DNA according to the protocol of DNAse I, RNAse free (ThermoScientific; Waltham, USA). cDNA synthesis was performed following the instructions of the Thermo Revert Aid Kit (ThermoScientific; Waltham, USA).

3.11.2 RNA sequencing

RNA was extracted from 1-cm stem segments including the stem base. Three stem segments were pooled into one biological replicate. Tree biological replicates were collected per genotype. Extracted RNA was treated with DNAse to remove residual genomic DNA according to the protocol of DNAse I, RNAse free (ThermoScientific; Waltham, USA). Library preparation and next-generation-sequencing was performed at the Deep Sequencing Core Facility provided by the Exzellenzkluster CellNetworks at the University of Heidelberg (http://www.cellnetworks.uni-hd.de/483065/Deep_Sequencing_Core_Facility). Single reads of 50 nucleotides in length were sequenced using HiSeqV4 SR50. Reads were aligned to the *Arabidopsis* genome (TAIR10) using TopHat2 v2.0.14 (Kim et al. 2013) and the statistical analysis was done by Dr. Virginie Jouannet using the DESeq2 package from the R/Bioconductor software (Love et al. 2014). Mutant genotypes were compared to wild type by applying a stringency of adjusted p-value < 0.01. Data processing included the use of VENNY (Oliveros 2007) and alignment to The Arabidopsis Information Resource (TAIR)-databases Huala et al. 2001) by VirtualPlant 1.3 (Katari et al. 2010). RNA sequencing data can be accessed in “Supplementary file 1” that is published online together with an electronic version of this thesis (heiDOK, Universitätsbibliothek Heidelberg, http://archiv.ub.uni-heidelberg.de/volltextserver/view/divisions/140001/).

3.12 Agarose gel electrophoresis

Agarose was melted in 1xTAE using a microwave and cooled down to approximately 40 °C. To visualize DNA bands, 1 drop ethidium bromide solution 0.025 % in dropper bottle (Roth; Karlsruhe, Germany) per 20 ml agarose solution was added and the gel was solidified in

a gel tray with an appropriate comb. The percentage of agarose ranged between 1 - 4 % depending on the experiment and expected DNA fragment size. The electrophoresis was run in 1xTAE at 100 V for 30 min-90 min and DNA bands were visualized using UV light of a transilluminator.

3.13 Molecular cloning

3.13.1 Standard cloning procedure

3.13.1.1 Amplifying DNA sequences

For exon amplification out of cDNA or for promoter amplification out of genomic DNA dedicated for molecular cloning, Phusion High-Fidelity DNA Polymerase (2 U/µL) (Thermo-Scientific; Waltham, USA) was used following the user manual specifications. The Phusion HF PCR product was purified using the QIAquick PCR Purification Kit (QIAGEN, Venlo, Netherlands) and DNA was eluted in dH_2O.

3.13.1.2 Designing miRNAs

miRNA-constructs were designed by following the instructions of WMD3 - Web MicroRNA Designer Version 3 (Max Planck Institute for Developmental Biology, Tübingen. http://www.weigelworld.org; Ossowski Stephan, Fitz Joffrey, Schwab Rebecca, Riester Markus and Weigel Detlef, personal communication).

3.13.1.3 Restriction enzyme treatment

The purified PCR product (DNA insert) and 500-1000 ng vector DNA were digested using the same restriction enzymes and buffer at 37 °C for >2 h according to the user manuals New England Biolabs (NEB, Frankfurt am Main, Germany), respectively. After digestion, the vector and the DNA insert were purified using the QIAquick PCR Purification Kit (QIAGEN, Venlo, Netherlands) and the vector was dephosphorylated by the Antarctic Phosphatase (NEB, United Kingdom) for 1 h at 37 °C and purified again.

3.13.1.4 Ligation

10-20 ng of the digested, dephosphorylated and purified vector were mixed with 50-100 ng digested and purified insert and ligations were performed at 16 °C over night using the T4 DNA Ligase (5 U/µL) (Thermo-Scientific; Waltham, USA) according to the user manual.

3.13.1.5 *E. coli* heat-shock transformation

500 µl of competent DH5α cells were incubated for 20 min on ice supplemented with 10 µl of the ligation reaction. Afterwards a heat shock was performed for 90 sec at 42 °C to introduce plasmid DNA into the cells, before putting them back on ice for 1 min. 500 µl LB medium was added to the bacterial solution and incubated at 37 °C, 180 rpm for 45 min. 100 µl of transformed bacteria were plated on LB-plates supplied with appropriate antibiotics for selection of transformed cells. The plates were incubated over night at 37 °C until colonies appeared.

3.13.1.6 Colony PCR

The growing bacteria colonies were tested for the presence of the correctly ligated plasmid by colony PCR. Several colonies were picked from the plate and each colony was dissolved in 10 µl H_2O. Afterwards a standard PCR was performed with primers targeting the cloned gene by using the JumpStart™REDTaq ® ReadyMix™ (Sigma-Aldrich; St. Louis, USA) according to the user manual.

3.13.1.7 DNA extraction and sequencing

Positive clones were grown in 2 ml LB supplied with the appropriate antibiotic. Plasmid DNA was isolated using the QIAprep Spin Miniprep Kit (QIAGEN, Venlo, Netherlands) and sequenced with appropriate sequencing primers at Eurofins Genomics (Eurofins Scientific, Luxemburg, Luxemburg). The obtained sequences were aligned to the designed vector sequence using the program CLC Main Workbench 7 (CLC Bio Qiagen, Aarhus, Denmark).

3.13.2 Green Gate cloning

Green Gate cloning was performed as described in (Lampropoulos et al. 2013)

3.14 Transformation using *Agrobacteria*

3.14.1 Transformation and glycerol stocks of *Agrobacteria*

To transform the *Agrobacteria* strain C58C1: RifR with pSoup+ plasmid (TetR) 500 ng plasmid were added to 500 µl frozen bacteria. The mixture was incubated for 5 min on ice, for 5 min in liquid nitrogen and heat shocked for 5 min at 37 °C. 800 µl LB-medium were added and the sample was incubated for 1 h at 28 °C moderately shaking. 200 µl of the bacterial solution were spread on a YEB-agar plate supplemented with rifampicine and tetracycline (1:2000 each)

and the respective antibiotic for plasmid selection (1:1000). Bacterial clones were grown at 28 °C for 2-3 days until colonies appeared.

To generate glycerol stocks, one clonal *Argobacteria* colony was picked and grown in liquid culture (see chapter 3.4). 250 µl densely grown culture was mixed 1:3 with sterile glycerol, frozen in liquid nitrogen and stored at -80 °C.

The *Agrobacteria* strain ASE: KanR, CamR with pSoup+ plasmid (TetR) was solely received as glycerol stock from the research group of Prof. Dr. Jan Lohmann at the Centre for Organismal Studies (COS).

3.14.2 Stable transformation of *Arabidopsis*

To generate transgenic lines of *Arabidopsis*, T-DNA constructs were introduced using *Agrobacteria* and the floral dip method (Steven 1998, plant journal). *Agrobacteria* of the strain C58C1: RifR, pSoup+ (TetR) harbouring the construct of interest were cultured in 200 ml YEB supplemented with the respective antibiotics. The densely grown culture was centrifuged at 4000 rpm for 15 min and the pellet was washed by 10 ml infiltration medium (without SILWET) and resuspended in 150 ml infiltration medium with SILWET. Flowering *Arabidopsis* plants were dipped into the bacterial solution for 5 min and subsequently incubated in the dark over night before transferred back into a LD chamber. The seeds were harvested two weeks post-transformation and T1 transformants were selected on MS-plates containing the respective antibiotic or herbicide.

3.14.3 Transient gene expression in *Nicotiana* leaves

Agrobacteria containing T-DNA constructs with coding sequences expressed under the control of a Cauliflower Mosaic Virus (CaMV) *35S* promoter were used to infiltrate *Nicotiana* leaves.

Transformed *Agrobacteria* were stored as glycerol stocks and grown in a 10 ml YEB liquid culture prior to use. The densely grown culture was centrifuged at 4000 rpm for 5 min at RT. The SN was removed and the pellet was washed with 5 ml induction buffer and re-suspended in 10 ml induction buffer. Culture densities were adjusted to an OD_{600} of 1. Prior to infiltration, these bacterial solutions were mixed with *Agrobacteria* expressing *35S:P19* in a ratio 1:2 and incubated in the dark for 2-3 h. *P19* codes for a protein of the Tomato bushy stunt virus (TBSV) that efficiently suppresses gene-silencing (Scholthof 2006; Voinnet et al. 2003).

Healthy and approximately 4 week-old *Nicotiana* leaves were infiltrated with the mixtures using a 1 ml syringe (Becton Dickinson S.A., Madrid, Span). To detect transient gene expression, leaves were harvested 3 days after infiltration.

3.15 Protein extraction, IP and Western blot

3.15.1 Protein extraction from *Nicotiana* leaves

Infiltrated *Nicotiana* leaves dedicated for protein extraction, were frozen in liquid nitrogen three days after infiltration and ground into a fine powder using a pre-cooled porcelain mortar. 500 µl leaf powder were mixed with 500 µl extraction buffer and vigorously mixed using a pre-cooled metal drill. Each sample was vortexed for 10 sec and centrifuged at 13000 rpm for 10 min at 4 °C. The protein extract was retrieved by sieving it through a nylon mesh.

3.15.2 Immunoprecipitation

Five protein extracts (5x 500 µl) were pooled per sample and 100 µl were transferred to a new microcentrifuge tube as “Input” sample and stored at 4 °C. To immunoprecipitate fusion proteins with HA-tag, the remaining protein extract was mixed with 50 µl Anti-HA MicroBeads (Miltenyi Biotec, Bergisch Gladbach, Germany) and incubated for 2.5 h at 4 °C while slowly rotating. µ Columns (Miltenyi Biotec, Bergisch Gladbach, Germany) were equilibrated with 200 µl extraction buffer and placed on a magnetic stand (MACS MultiStand, Miltenyi Biotec, Bergisch Gladbach, Germany). The processed protein extract was loaded to the column and the flow-through was collected as fraction “Unbound”. The beads remained bound to the column by magnetic forces and were washed 3x by 200 µl Wash buffer I and 2x by 200 µl Wash buffer II. Immunoprecipitated proteins were eluted from the beads by incubating with 20 µl hot (95 °C) 2x Laemmli. After 5 min incubation, 50 µl additional 2xLaemmli were added and the flow-through was collected as “IP”.

3.15.3 Bradford

Protein concentrations of the processed “Input” samples were measured using a 96-well plate and protein standards generated out of bovine serum albumin (BSA) (Protein Standard II, Bio-Rad Laboratories; Hercules, USA). The Bradford assay was performed according to the manual provided with the Bio-Rad Protein Assay Dye Reagent Concentrate (Bio-Rad Laboratories; Hercules, USA) and the OD_{595} was determined using a microplate reader (Spark Multimode reader, TECAN, Männedorf, Switzerland). Calculation of the standard curve and protein quantities was done in Microsoft Excel (Microsoft, Redmond, USA).

3.15.4 Western blotting and detection

To denaturate proteins, “Input” and “Unbound” fractions were mixed with 2x Laemmli in a ratio 1:1 and boiled together with the “IP” fraction for 5 min at 95 °C. Approximately 35 µg protein (depending on the experiment) of “Input”, an equal volume of “Unbound” and half of the “IP” fraction were run by a SDS-PAGE at 20 V until the bromophenol blue left the gel. SDS poly-acrylamid gels were prepared as follows:

Stacking gel (6 %)		Running gel (10 %)	
AA-Bis (40 %)	1 ml	AA-Bis	3.3 ml
Stacking buffer 4x	1.24 ml	Resolving buffer 4x	2.5 ml
SDS (20 %)	25 µl	SDS (20 %)	50 µl
		Glycerol (100 %)	99,6 µl
H2O	2.68 ml	H2O	3.94 ml
TEMED	5 µl	TEMED	10 µl
APS (10 %)	50 µl	APS (10 %)	100 µl

Size-separated proteins were transferred from the gel onto a methanol-activated PVDF membrane at 20 V for 90 min using a Semi-dry blotting machine. Four thick blotting papers (Bio-Rad Laboratories; Hercules, USA) soaked in 1x transfer buffer were used at bottom and on top of membrane and gel. After blotting, the membranes were washed by 1x TBS-T and blocked for 1 h in blocking solution. For specific detection of blotted HA- or Myc-fusion proteins, the membranes were incubated over night at 4 °C in blocking solution supplemented with 1:500 dilutions of the antibody Anti-HA-Peroxidase High Affinity (3F10), rat monoclonal (Roche; Basel, Switzerland) or the c-Myc Antibody (9E10) sc-40 HRP, mouse monoclonal (Santa Cruz Biotechnology, Santa Cruz, USA), respectively. Prior to detection, the antibody solutions were removed and the blots were washed four times by 1x TBS-T. Antibody-specific bands were revealed by mixing the chemiluminescence agents SuperSignal™ West Femto Maximum Sensitivity Substrate (Thermo-Scientific; Waltham, USA) and SuperSignal™ West Pico Chemiluminescent Substrate (Thermo-Scientific; Waltham, USA) in a ratio 1:3. The kits were otherwise used as recommended by the manufacturers and bands were revealed using an Advanced Fluorescence and ECL Imager (Intas Science Imaging Instruments, Göttingen, Germany).

3.16 Confocal microscopy and analysis

Confocal microscopy was carried out on a Leica TCS SP5 II or Leica TCS SP8 II (Leica Microsystems; Mannheim, Germany) equipped with a 10x air objective, 20x multi-immersion objective, 40x or 63x water objective or 63x glycerol immersion objective. To visualize fluorescence an argon laser or a DPSS diode was used with either PMT or HyD detectors. YFP (yellow

fluorescent protein) was excited by an argon laser at 514 nm and the emission detected in a range of 520-540 nm. GFP (green fluorescent protein) was excited by an argon laser at 488 nm, collecting the emission between 500-575 nm. Cherry was excited by a DPSS diode laser at 561 nm, collecting the emission between 600-640 nm. Turquoise was excited by an argon laser at 458 nm, collecting the emission between 470-490 nm. Staining was detected as described in chapter 3.5. To prevent cross-talk, a sequential scan was used if two or more fluorescent signals were present in one sample.

GFP-intensities of confocal root pictures were measured using ImageJ and as described in (Burgess et al. 2010).

3.17 Statistical analysis

Statistical analyses were performed using IBM SPSS Statistics for Windows, Version 23.0 (IBM Corp, Armonk, USA). Means were calculated from measurements with sample sizes as indicated in the respective figure legends. Error bars represent ± standard deviation. Prior to analysis, all datasets were tested for homogeneity of variances by the Levene statistic. Statistically different groups were determined by a One-way ANOVA with a confidence interval (CI) of 95 %. If variances were homogeneous (equal), a post-hoc Bonferroni test was applied for datasets $n < 5$ and a post-hoc Tukey HSD test was applied for datasets with $n > 4$. If variances were not homogeneous (unequal), a post-hoc Tamhane-T2 test was applied. For comparison of two datasets a Student's t-test (for equal variances) or a Welch's t-test (for unequal variances) was performed. Graphs were generated in GraphPad Prism version 6.01 (GraphPad Software, La Jolla, USA) or in Excel (Microsoft, Redmond, USA).

3.18 Figure creation and data assembly

All data presented in this study was assembled into figures using Adobe Illustrator CS6 (Adobe, San Jose, USA). Schemes and drawings depicted in Figures 1.1, 1.2, 1.3, 1.4, 1.6, 1.8, 4.5, 4.6, 4.10 and 5.1 were created using a Wacom Intuos3 graphic tablet (Wacom®, Kazo, Japan) and Adobe Photoshop CS6 (Adobe®, San Jose, USA).

4 Results

4.1 The role of *SMXL3/4/5* in early seedling stages

The *SMXL* family members fulfil diverse regulatory roles ranging from early processes, such as germination and hypocotyl elongation (Stanga et al. 2016; Stanga et al. 2013), to late developmental processes, such as branching (Soundappan et al. 2015; Liang et al. 2016). To gain insights into the roles of the so far unexplored SMXL sub-clades 2 and 3 (Fig 1.6), I first determined tissue specificity and mutant phenotypes at the seedling stage.

4.1.1 Promoter activities of *SMXL3/4/5* are specific for the phloem

To establish first hypotheses about a potential *SMXL3/4/5* function, I investigated the spatial pattern of their promoter activities in young seedlings (Figure 4.1). I generated transgenic lines expressing an endoplasmic reticulum (ER)-localized YELLOW FLUORESCENT PROTEIN (YFP) reporter under the control of the *SMXL3* (Figure 4.1 A and A'), *SMXL4* (Figure 4.1 B and B'), *SMXL5* (Figure 4.1 C and C') and the less closely related *SMAX1* (Figure 4.1 D and D') promoter. By comparing the promoter activities of *SMXL3/4/5* to *SMAX1* I aimed to investigate differences in tissue specificities among the *SMXL* family. I visualized the respective YFP signals in seven day-old root tips that I counterstained by the membrane dye FM4-64 (Figure 4.1). Interestingly, the promoter activities of *SMXL3/4/5* showed a strong specificity for phloem and/or procambium related tissues: *SMXL3* was active in developing proto- and metaphloem, the procambium and the PPP (Figure 4.1 A and A'). *SMXL4* activity showed the strongest spatial specificity and was restricted to immature and developing proto- and metaphloem (Figure 4.1 B and B'). The *SMXL5* YFP-reporter activity was localized to developing proto- and metaphloem as well as the procambium (Figure 4.1 C and C'). Of note, the activity patterns of *SMXL4* and *SMXL5* were fully overlapping

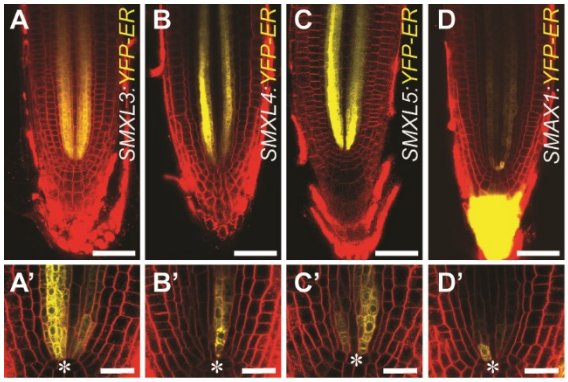

Figure 4.1: *SMLXL3/4/5* promoter activities are specific for phloem and procambium
A-D Shown are 7 day-old root tips expressing ER-localized YFP reporters (yellow) under the *SMXL3* (A), *SMXL4* (B), *SMXL5* (C) and *SMAX1* (D) promoter. Cell membranes are counterstained by FM4-64. Scale bars represent 50 µm.
A'-D' Close-ups of the promoter-reporter lines depicted in A-D show that all tested *SMXL* promoters are already active next to the QC (marked by white asterisks) in phloem initials. Scale bars represent 20 µm.

throughout the plant vasculature, whereas the *SMXL3* promoter activity was mostly restricted to the root vasculature (Wallner et al. 2017). As can be seen in Figure 4.1 D and D', the promoter activity of *SMAX1* was less specific. The strongest YFP signal was detected in columella and root cap cells and a weak signal could be detected in phloem tissues (Figure 4.1 D). Strikingly, all four promoters were already active in the SE-procambium stem cell, which is also known as phloem initial (Figure 4.1 A'-D' compare with Figure 1.4). This was a unique finding which was not reported for any phloem-specific gene before.

4.1.2 *SMXL3/4/5* promote root length

To characterize the function of the *SMXL3/4/5* genes I started a reverse genetic approach and selected loss of function mutants that had a T-DNA inserted into the respective coding regions (Figure 4.2). Sanger sequencing of genomic DNA revealed the localization of all three T-DNAs: Line *SALK_024706* (*smxl3-1*) had the T-DNA inserted 140 bp after the ATG, line *SALK_037136* (*smxl4*-1) had the T-DNA inserted 3180 bp after the ATG and line *SALK_018522* (*smxl5-1*) had the T-DNA inserted 2219 bp after the ATG (Figure 4.2). By reverse transcription PCRs with primers flanking the T-DNA insertions I could further show that the SALK T-DNA insertion was successfully disturbing gene transcription in all cases. The ubiquitously expressed *ACTIN 2* (*ACT2*) gene served as a control (Figure 4.2 A). In the following, the *smxl3-1*, *smxl4-1* and *smxl5-1* alleles are therefore referred to as mutants *smxl3*, *smxl4* and *smxl5*, respectively.

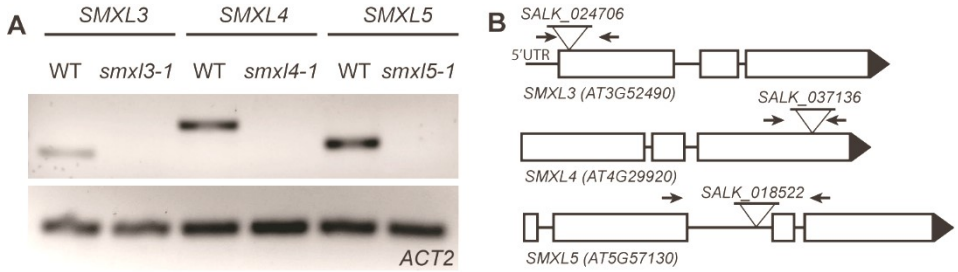

Figure 4.2: Mutant alleles *smxl3-1*, *smxl4-1* and *smxl5-1* show impaired gene transcription
A Reverse transcription PCR analysis with primers flanking the T-DNA insertions of *SMXL3*, *SMXL4* and *SMXL5* (from left to right). DNA products were only obtained for wild type (WT) and not the respective mutant alleles. RT-PCR products obtained with *ACT2* primers show that cDNA quantities were equal.
B A schematic representation of the genomic regions for *SMXL3, SMXL4* and *SMXL5* (from top to bottom) shows exon regions (white boxes), introns (black lines), T-DNA insertions (white triangles) and primers flanking the T-DNAs (black arrows).

Phenotyping of homozygous *smxl3, smxl4* and *smxl5* single mutants showed no obvious differences to wild type at the seedling stage (Figure 4.3). However, all *smxl3;smxl4*, *smxl4;smxl5* and *smxl3;smxl5* double mutant combinations were short rooted when compared to wild type (Figure 4.3 A and B). *smxl3;smxl4;smxl5* triple mutants and *smxl3;smxl5* double mutants were equally short rooted (Figure 4.2 A and C), but unlike *smxl3;smxl5*, growth of the

triple mutant was arrested at the seedling stage and *smxl3;smxl4;smxl5* plants were found to be lethal (Figure 4.3 D). Moreover, redundant roles in promoting root length were specific for *SMXL* sub-clades 2 and 3. The *smax1;smxl2* double mutant, defective for *SMXL* sub-clade 1, only showed a slight reduction in root length when compared to wild type, whereas root growth of the *smxl6;smxl7;smxl8* triple mutant, defective for *SMXL* sub-clade 4, was completely unaffected (Figure 4.3 E).

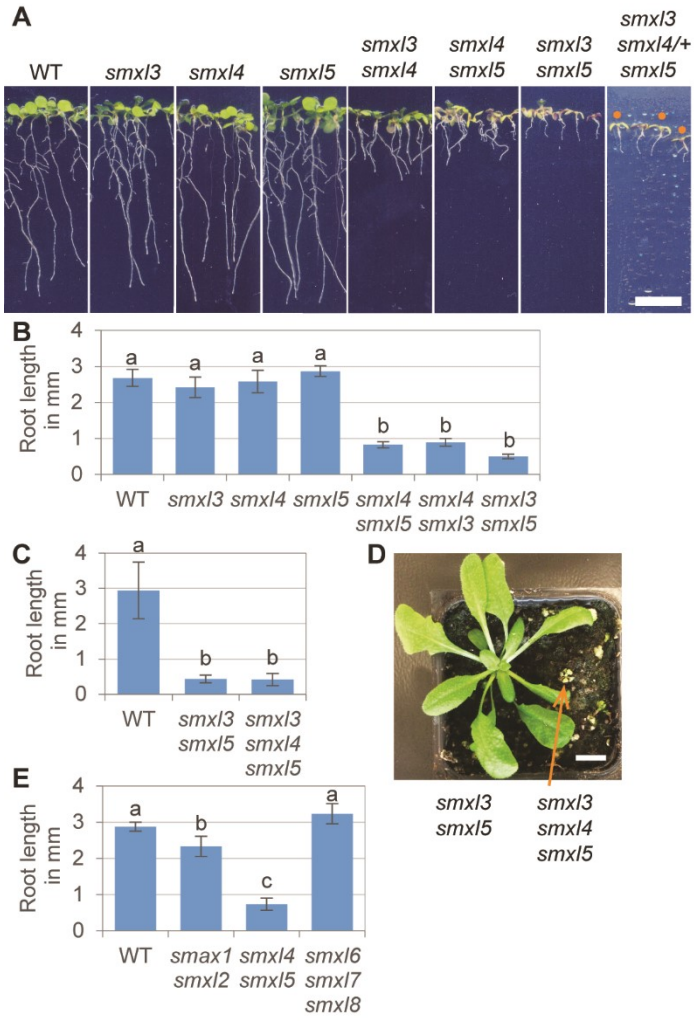

Figure 4.3: *SMXL3/4/5* act specifically on promoting root growth

A Root lengths of 10 day-old seedlings. Wild type, *smxl3, smxl4* and *smxl5* are long rooted, whereas *smxl3;smxl4, smxl4;smxl5, smxl3;smxl5* and *smxl3;smxl4/+;smxl5* are short rooted (from left to right). Homozygous *smxl3;smxl4;smxl5* mutants are indicated by orange dots. Scale bars represent 1 cm.

B Root lengths shown in A were quantified. The mean values of three independent experiments are shown (n =47-50 per experiment). Statistically different groups are indicated by letters determined by a one-way ANOVA with post-hoc Tukey HSD (95 % CI).

C -D Root lengths of 10 day-old wild type, *smxl3;smxl5* (n = 48-61) and *smxl3;smxl4;smxl5* (n = 7) were quantified and compared to each other by one-way ANOVA with post-hoc Tamhane-T2 (95 % CI). Root lengths of *smxl3;smxl5* and *smxl3;smxl4;smxl5* are comparable (C), but the latter is lethal (D). Scale bar represents 1 cm.

E The root lengths of 10 day-old *smxl4;smxl5* were significantly shorter than of *smax1;smxl2* and *smxl6;smxl7;smxl8*. Shown are the mean values of 4 independent experiments (n = 31-52 per experiment). Statistical groups determined by one-way ANOVA with post hoc Bonferroni test (95 % CI).

4.1.3 *smxl4;smxl5* loses RAM activity and phloem transport capacity

Since the SMXL3/4/5 genes acted redundantly in the root, I focused on the viable, but root growth-impaired *smxl4;smxl5* double mutant to characterize the defect in detail.

To investigate the onset of the root growth defect, I compared wild type and *smxl4;smxl5* roots over a period of 10 days after germination. At each time point analysed, I quantified the

number of cortical cells within the meristematic zone, which is a measure for RAM size (Beemster and Baskin 1998) (Figure 4.4). Surprisingly, the meristematic cortex cell number was initially equal between wild type and *smxl4;smxl5* (Figure 4.4 A-B and G), but rapidly decreased in *smxl4;smxl5* after 5 days and 10 days post germination (Figure 4.4 C-G). This indicated that the *smxl4;smxl5* mutations primarily affected root growth.

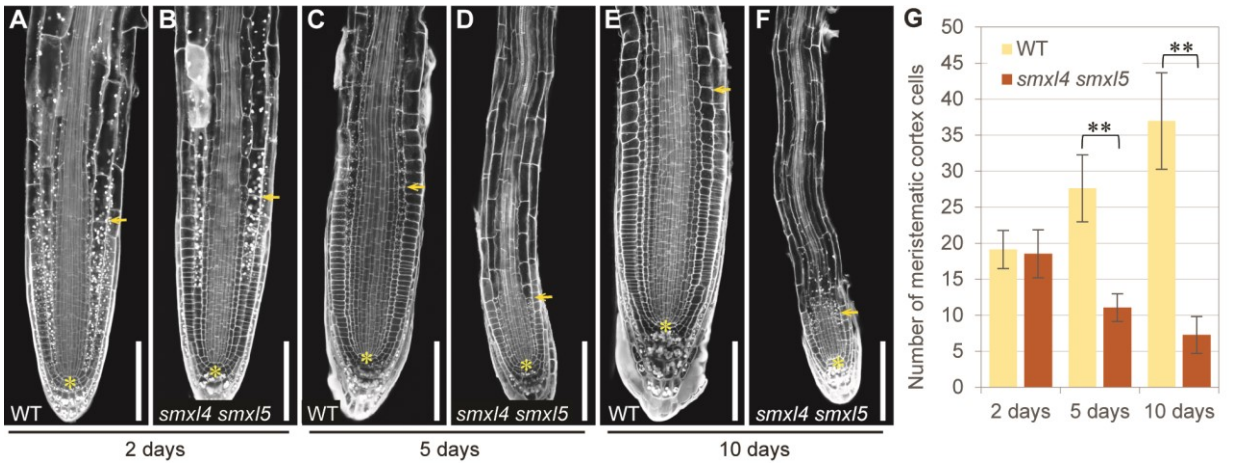

Figure 4.4: RAM size diminishes in *smxl4;smxl5* over time

A-F mPS-PI stained primary root tips 2 days (A-B), 5 days (C-D) and 10 days (E-F) after germination. Wild type roots (A, C, E) were compared to *smxl4;smxl5* roots (B, D, F) and the meristematic zone was determined by counting the cortex cells from the QC (marked by a yellow asterisk) to the first cortex cell entering the elongation zone (marked by a yellow arrow). Scale bars represent 100 µm.

G A quantification of the measurements shown in A-F revealed that the meristematic cortex cell number in *smxl4;smxl5* RAMs was equal to wild type after 2 days, but significantly decreased after 5 and 10 days post germination. Welch's t-tests were applied for each time point (n = 30-47). Significant differences are marked by asterisk.

Loss of RAM activity during vegetative growth is a well-known characteristic of phloem-defective mutants (Depuydt et al. 2013). Without proper phloem formation and/or unloading into the sink, the meristems are deprived of essential energy metabolites that maintain stem cell activity (Depuydt et al. 2013; Ross-Elliott et al. 2017). Since *SMXL3/4/5* expression was phloem related (Figure 4.1), I investigated the phloem transport capacity of *smxl4;smxl5* roots. Expressing the *GREEN FLUORESCENT PROTEIN (GFP)* under the CC-specific *SUCROSE 2 (SUC2)* promoter allows to monitor GFP movement along the phloem and its unloading into the RAM (Froelich et al. 2011). After grafting a *SUC2:GFP* reporter line onto *smxl4;smxl5* or wild type roots (Figure 4.5 A), I qualitatively and quantitatively analysed the GFP signal intensity that reached the RAM of the longest root (Figure 4.5 A-F). Comparison of the GFP intensities in wild type and *smxl4;smxl5* roots revealed that GFP transport into *smxl4;smxl5* RAMs was significantly reduced (Figure 4.5 B-F). Of note, the longest root in successfully grafted *smxl4;smxl5* plants was not the primary root, but a newly formed adventitious root that is commonly observed in *smxl4;smxl5* (Figure 4.5 G). Primary root growth of *smxl4;smxl5* seedlings was already arrested at this stage and GFP could no longer reach the root tip, nor could it be unloaded into the

RAM (Figure 4.5 G-H). This indicated that *smxl4;smxl5* seedlings gradually lose phloem transport capacities and protophloem-dependent unloading over time.

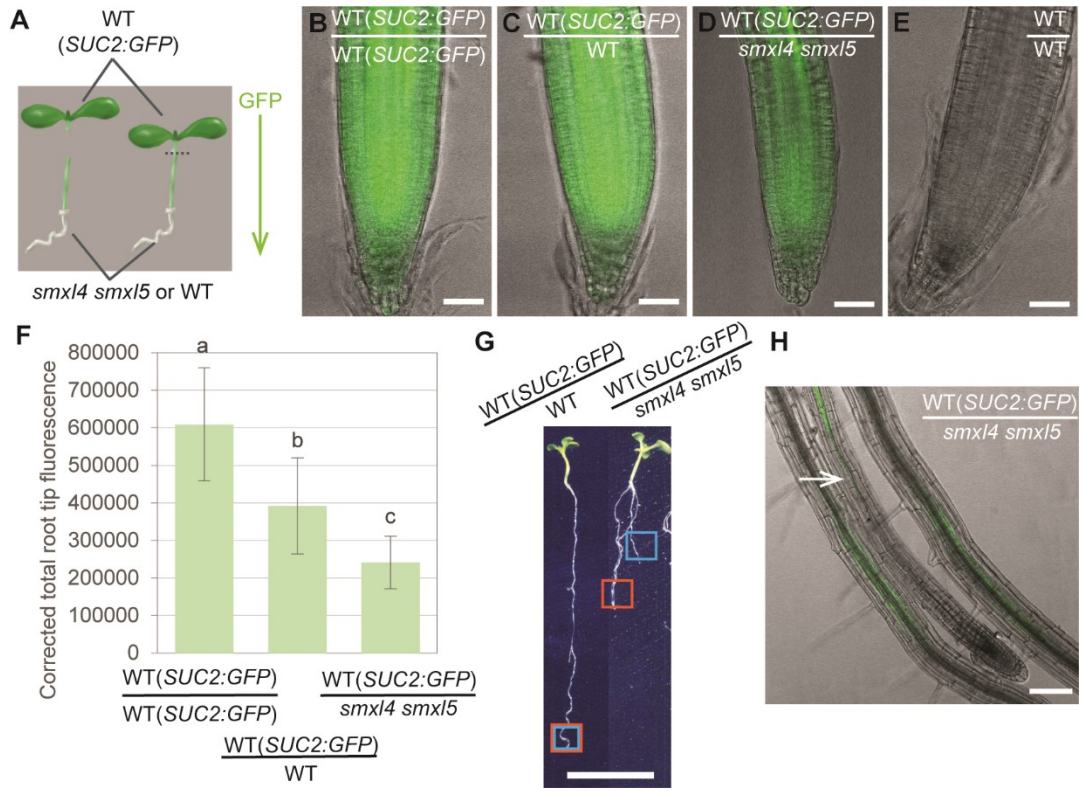

Figure 4.5: Phloem-dependent transport and unloading into the RAM is gradually lost in *smxl4;smxl5*

A A schematic representation of the grafting technique shows how 5 day-old seedlings were cut at the hypocotyl to attach a *smxl4;smxl5* root to a *SUC2:GFP* expressing upper plant body. After the vasculature connects at the graft junction, free GFP enters the *smxl4;smxl5* root and is allocated towards the root sink.

B-E The confocal pictures show the RAM of the longest root per grafted combination. The type of grafting is indicated in each image by a line that separates the genotype of the upper body part (above the line) from the root genotype (below the line). Shown are overlays of bright field (grey) and GFP signal (green). Scale bars represent 50 µm.

F The GFP intensities detected in B-E were quantified (n = 10). Error bars represent ± standard deviation. A one-way ANOVA with post-hoc Bonferroni (95 % CI) was applied to identify statistically different groups which are indicated by letters.

G Shown are seedlings 12 days after grafting. The longest root (orange square) is the primary root (blue square) in wild type (left seedling), but not in *smxl4;smxl5* (right seedling). Scale bar represents 1 cm.

H A representative primary root (n = 10) of the *smxl4;smxl5* genotype grafted to a *SUC2:GFP* plant is depicted in a confocal overlay image of bright field (grey) and GFP signal (green). The white arrow points to the last detected GFP signal within the primary root of *smxl4;smxl5*. Scale bar represents 100 µm.

4.1.4 *SMXL3/4/5* promote phloem formation

To identify the defects that lead to impaired phloem transport and unloading in *smxl4;smxl5*, I investigated the positioning of two tangential cell divisions important for the correct spatio-temporal initiation of SE precursor cells and proto- and metaphloem strands, respectively (blue and orange arrows in Figure 4.6 A and Figure 1.4). In mPS-PI stained wild type roots both tangential divisions could be located in close proximity to each other (Figure 4.6 A-B), whereas the second tangential division was significantly delayed in *smxl4;smxl5* (Figure 4.6 C-D). Moreover, protophloem strands that indicate the presence of differentiated PSEs within the RAM were absent in *smxl4;smxl5* (pink arrow in Figure 4.6 B, C and E, F). Further investigation by serial block-face scanning electron microscopy (SBEM) in collaboration with the lab of Ykä Helariutta (Cambridge, UK) revealed that PSEs in *smxl4;smxl5* indeed remain nucleated (Wallner et al. 2017). Interestingly, the stele cell number of *smxl4;smxl5* was not affected (Figure 4.6 E-G). This indicated that the delay in proto- and metaphloem initiation and the absence of PSE differentiation in *smxl4;smxl5* reflected the primary function of *SMXL4/5* and was not the consequence of a general cell division defect.

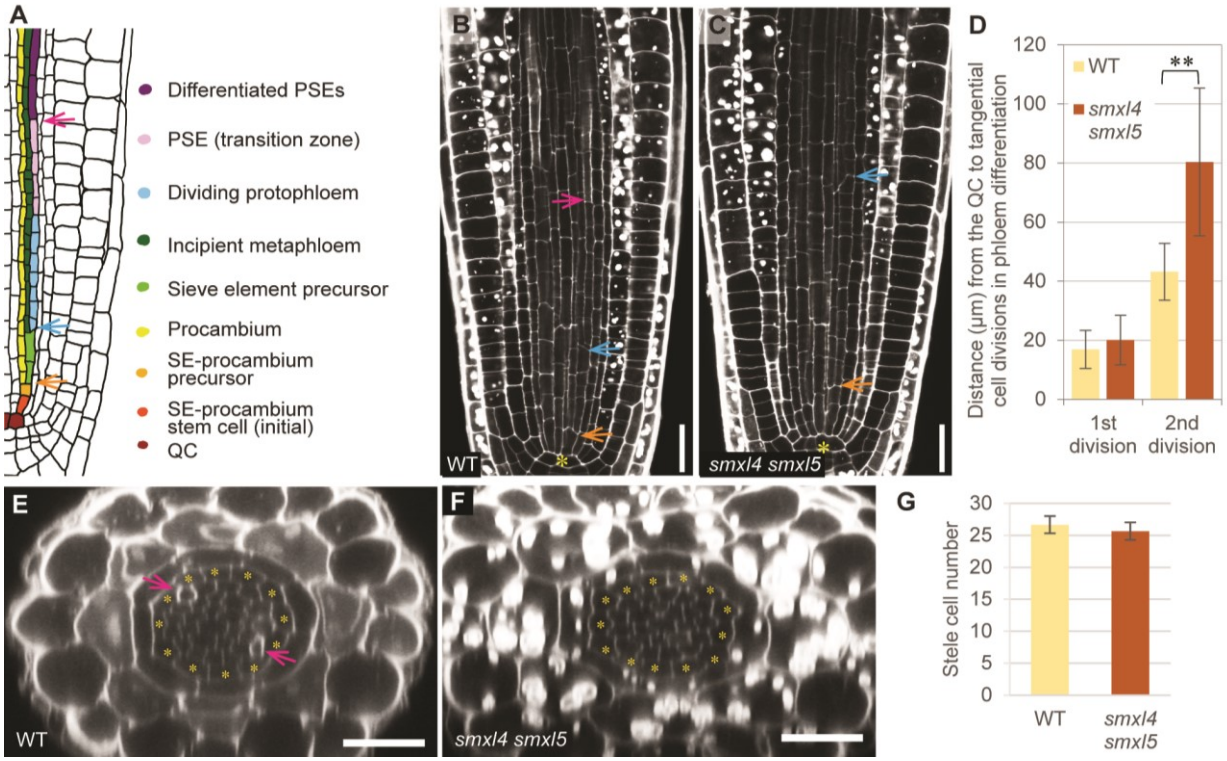

Figure 4.6: Protophloem formation and differentiation is impaired in *smxl4;smxl5*
A A schematic representation of a longitudinal root section depicting one developing phloem pole. Two tangential cell divisions spatio-temporally induce SE precursor and procambium (orange arrow) and incipient proto- and metaphloem strands (blue arrow), respectively. Differentiated SEs are marked by a pink arrow. See also Figure 1.4 and (Wallner et al. 2017).
B-C 2 day-old mPS-PI stained RAMs of wild type (B) and *smxl4;smxl5* (C). In wild type the tangential divisions (orange and blue arrow) are close to each other and the QC (yellow aster-

isks). PSEs differentiate by changing their cell wall composition, which is reflected by enhanced PI staining (pink arrow). In *smxl4;smxl5* the second tangential cell division is delayed (blue arrow) and PSEs do not differentiate. Scale bars represent 20 µm.
D The distance from the QC to the first and second tangential division shown in B-C was quantified (n = 18). Welch's t-test (95 % CI) was performed to compare the first and second division independently for wild type to *smxl4;smxl5*.
E-F Optical cross sections of 2 day-old wild type and *smxl4;smxl5* roots in 200 µm distance from the QC show the presence of shiny PSEs in wild type (pink arrows) and their absence in *smxl4;smxl5*. Pericycle cells are marked by yellow asterisk. Scale bars represent 20 µm.
G Cell numbers in the stele of optical cross sections shown in E-F were quantified and compared between wild type and *smxl4;smxl5* (n = 6) by a Student's t-test (95 % CI). No significant difference (p-value = 0.234) was detected.

Close investigation of *smxl4* and *smxl5* single mutants revealed that maturing PSEs still showed enhanced PI staining. In fact, qualitative picture analysis was not sufficient to detect differences between *smxl4, smxl5* and wild type. (Figure 4.7 A-C). Only after quantifying the distances of phloem-related tangential cell divisions, *smxl5* mutants showed a small but significant delay in the second tangential division (Figure 4.7 C and E). Of note, this defect was only mild and significantly less strong than in *smxl4;smxl5* double mutants (Figure 4.7 D-E).

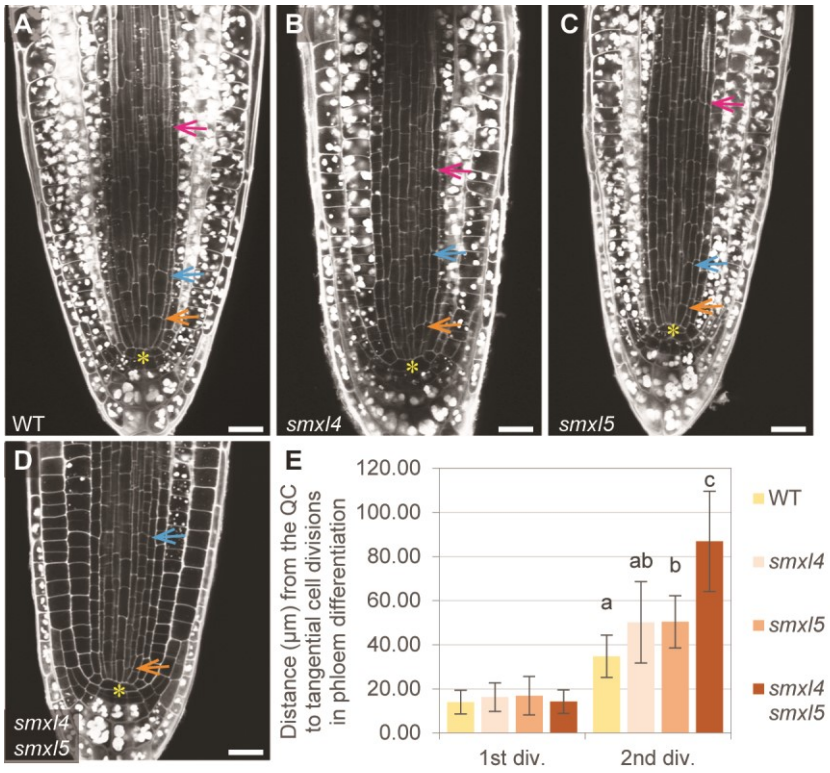

Figure 4.7: PSEs differentiate in *smxl4* and *smxl5* single mutants
A-D 2 day-old mPS-PI stained RAMs of wild type (A), *smxl4* (B), *smxl5* (C) and *smxl4;smxl5* (D). Differentiating PSEs were observed in wild type, *smxl4* and *smxl5* (pink arrows). Tangential cell divisions are marked by orange and blue arrows. The QC is indicated by a yellow asterisk. Scale bars represent 20 µm.

E The distance from the QC to the first and second tangential division shown in A-D was quantified (n = 10-12). Statistical groups marked by letters were determined by one-way ANOVA with post-hoc Tamhane-T2 (95 % CI).

To investigate whether *SMXL3* contributes to the role of *SMXL4/5* in promoting protophloem formation, I analysed optical cross sections of *smxl3, smxl4* and *smxl5* single mutants as well as *smxl3;smxl4* and *smxl3;smxl5* double mutant combinations 200 µm above the QC (Figure 4.8). At this position PSEs were detected in wild type and all single mutants (pink arrows in Figure 4.8 A-D). *smxl3;smxl4* and *smxl3;smxl5* double mutants lacked any signs of protophloem at this position, which was in line with my previous findings and indicated that *SMXL3* acted redundantly with *SMXL4/5* in protophloem formation. Strikingly, stele cell numbers were slightly reduced in *smxl3* single mutants and strongly reduced in *smxl3;smxl5* double mutants when compared to wild type (Figure 4.8 B, F and G). The *smxl3;smxl4* double mutant and the *smxl4* and *smxl5* single mutants did not differ from wild type nor *smxl3*. I thus hypothesized that *SMXL3* and *SMXL5*, which, in addition to the phloem, are expressed in the procambium (Figure 4.1), played an additional and phloem-unrelated role in procambium formation.

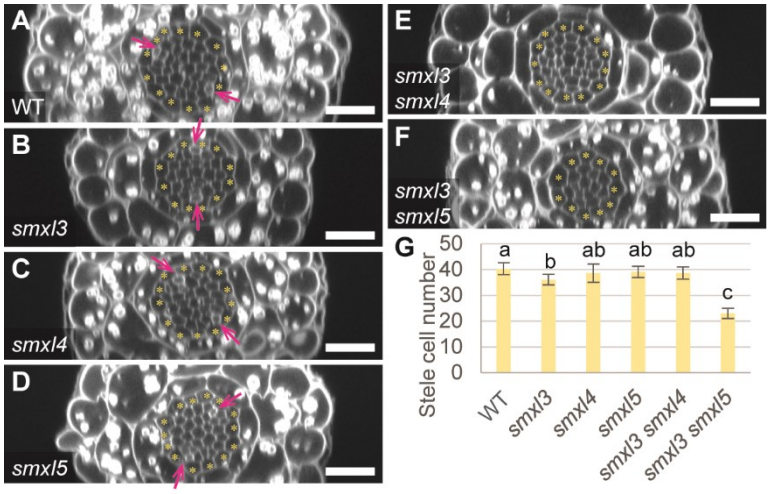

Figure 4.8: *SMXL3/5* have a role in procambium formation
A-F Optical cross sections of 2 day-old mPS-PI stained wild type (A), *smxl3* (B), *smxl4* (C), *smxl5* (D), *smxl3;smxl4* (E) and *smxl3;smxl5* (F) roots were taken 200 µm from the QC. The pericycle cells are marked by yellow asterisk and differentiated PSEs are indicated by pink arrows. Scale bars represent 20 µm.
G Stele cell numbers were quantified for each genotype (A-F, n = 8-10). Statistical groups marked by letters were determined by a one way ANOVA with post-hoc Tukey HSD (95 % CI).

This notion was further supported by the finding that *smxl3;smxl4;smxl5* triple mutants were completely deprived of callose deposition along the vasculature of cotyledons (Figure 4.9). Callose deposition is essential to regulate SE-mediated transport and therefore is used as direct indicator to analyse phloem functionality (Barratt et al. 2011; Vaten et al. 2011; Xie et al. 2011). To visualize callose, I stained 10 day-old cotyledons by aniline. Wild type cotyledons showed callose deposition along the vasculature, whereas aniline staining was absent in 9 out of 25 *smxl3;smxl4/+;smxl5* seedlings and in 18 out of 22 *smxl3;smxl4;smxl5* plants. Of note, vascular patterning of the segregating *smxl3;smxl4/+;smxl5* population could still be observed in the bright field channel (Figure 4.9 E). Based on these results, I concluded that *SMXL3/4/5* redundantly promote phloem initiation and differentiation during early vegetative growth.

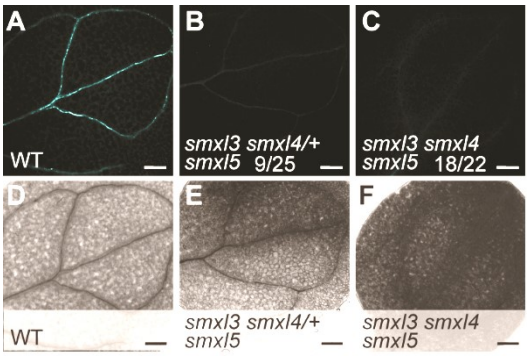

Figure 4.9: Callose deposition is largely absent in *smxl3;smxl4;smxl5*
A-F Aniline staining (A-C) and bright field images (D-F) of 10 day-old WT (A, D), heterozygous *smxl3;smxl4/+;smxl5* (B, E) and homozygous *smxl3;smxl4;smxl5* (C, F) cotyledons stained by aniline. Callose is deposited along the phloem in wild type (A), but absent in 9/25 cases in *smxl3;smxl4/+;smxl5* and 18/22 cases in *smxl3;smxl4;smxl5*. Scale bars represent 200 µm.

4.2 The role of *SMXL3/4/5* in radial growth and secondary phloem formation

To determine whether *SMXL3/4/5* specifically regulate protophloem formation or, instead, are fundamental phloem regulators in general, I investigated their role during radial growth and the de-novo formation of secondary phloem. Unlike protophloem in RAM and cotyledons (Bauby et al. 2007), secondary phloem is not pre-determined in the embryo. It derives from the cambium, which is a post-embryonically induced stem cell niche and established at the stem base of adult *Arabidopsis* plants (Altamura et al. 2001). In comparison to SAM and RAM, the organization of the cambium is still poorly understood. Whether cambium sub-domains exist and to what degree cambium daughter cells are determined towards a certain tissue type, remains largely elusive (Brackmann and Greb 2014). By investigating the novel phloem regulators *SMXL3/4/5* in this de-novo formed stem cell niche, I also aimed to clarify some of these long-standing questions about cambium regulation and secondary tissue production.

4.2.1 *SMXL4* and *SMXL5* promoters are active in the stem

Similar to the studies at early seedling stages (Figure 4.1), I first investigated expression patterns of *SMXL3/4/5* by investigating their promoter activities at the stem base (Figure 4.10). Interestingly, the detected YFP signals in *SMXL3:YFP-ER, SMXL4:YFP-ER* and *SMXL5:YFP-ER* promoter-reporter lines, respectively, showed distinct patterns (Figure 4.10). The *YFP* reporter expressed under the control of the *SMXL3* promoter was largely non-detectable and only occasionally found in primary phloem of vascular bundles (Figure 4.10 A and A'). The *SMXL4* promoter was active in differentiated primary and secondary phloem, which was in line with the phloem-specific activity pattern observed in roots (Figure 4.1 B and B'). *SMXL5:YFP-ER* activity marked the cambium and cambium-derived phloem, including differentiated primary and secondary phloem (Figure 4.10 C and C'). Again, this pattern recapitulated the phloem and procambium specific *SMXL5* promoter activity in the RAM (Figure 4.1) and nicely supported its

cambium-specific expression pattern in the stem (Agustí et al. 2011b). Since the *SMXL3* promoter activity seemed to be root-specific and mostly absent in above-ground organs (Wallner et al. 2017), I focused my stem analyses on the roles of *SMXL4* and *SMXL5*.

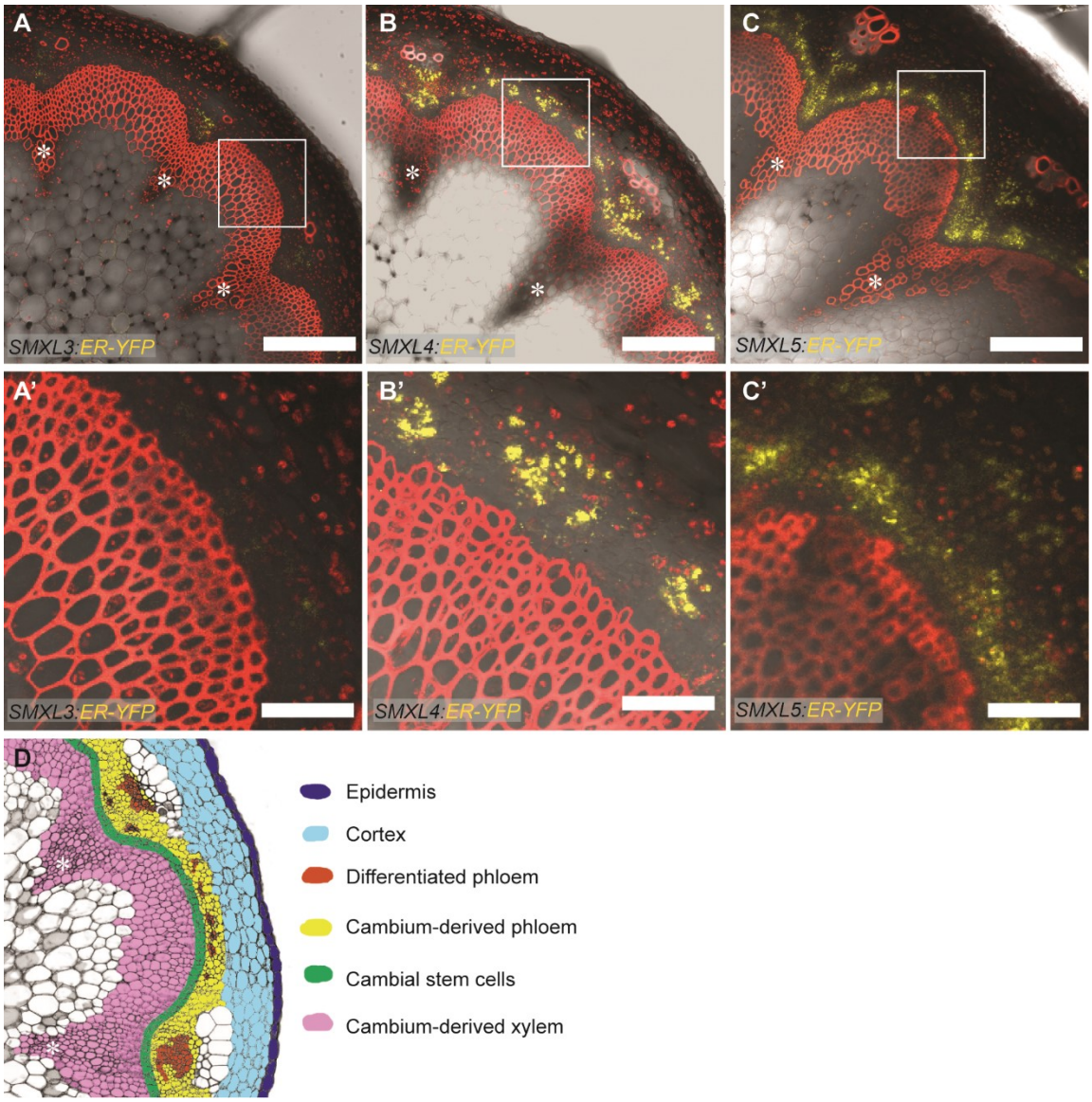

Figure 4.10: *SMXL3/4/5* promoter activities at the stem base
A-C Hand sectioned stem bases of 15-20 cm high *Arabidopsis* plants are shown. YFP signals (yellow) were detected by confocal microscopy in promoter-reporter lines *SMXL3:YFP-ER* (A), *SMXL4:YFP-ER* (B) and *SMXL5:YFP-ER* (C). Sections were counterstained by PI (red). Vascular bundles are marked by white asterisks. Scale bars represent 200 µm.
A'-C' Close-ups of the IC marked by white squared frames in A-C. *SMXL3* activity is absent in de-novo formed IC, *SMXL4* activity is localized to mature phloem and *SMXL5* activity was specific for cambium and cambium-derived phloem. Scale bars represent 50 µm.
D A schematic cross section at the stem base depicts all important tissues types that are coloured according to the legend.

4.2.2 Secondary phloem formation is largely *SMXL5*-dependent

To investigate whether *SMXL4/5* play a role in secondary phloem formation, I produced hand sections from the stem base of 15-20 cm tall *Arabidopsis* plants and stained them by aniline (Figure 4.11). Callose deposition in primary and secondary phloem was distinguishable by position: While primary phloem is solely located in phloem poles within vascular bundles, secondary phloem is found between primary phloem poles and within IC regions. *De-novo* formation of secondary phloem within IC regions can be easily distinguished from primary phloem and was therefore used as read-out to analyse cambium-derived phloem formation in this study. Almost all (98.6 %) IC regions of wild type plants showed callose deposition along secondary phloem (Figure 4.11 A, E and I). Similarly, 94.2 % of the IC regions in *smxl4* single mutants developed secondary phloem (Figure 4.11 B, F and I). Strikingly, callose deposition along IC regions was largely absent (85.2 %) in *smxl5* single mutants (Figure 4.11 C, G and I). This was surprising, since *smxl5* showed only mild phloem defects in the root (Figure 4.7) and was indistinguishable from wild type in terms of overall growth and plant morphology (Figure 4.11 J). Likewise, *smxl4;smxl5* double mutants were largely deprived of secondary phloem formation (76.1 %) (Figure 4.11D, H and I). It should be emphasized that *smxl4;smxl5* double mutants exhibit several growth defects, including changes in overall stem morphology and a delay in shoot growth (Figure 4.11 D, H and J). Those defects could have been caused by the impaired root system.

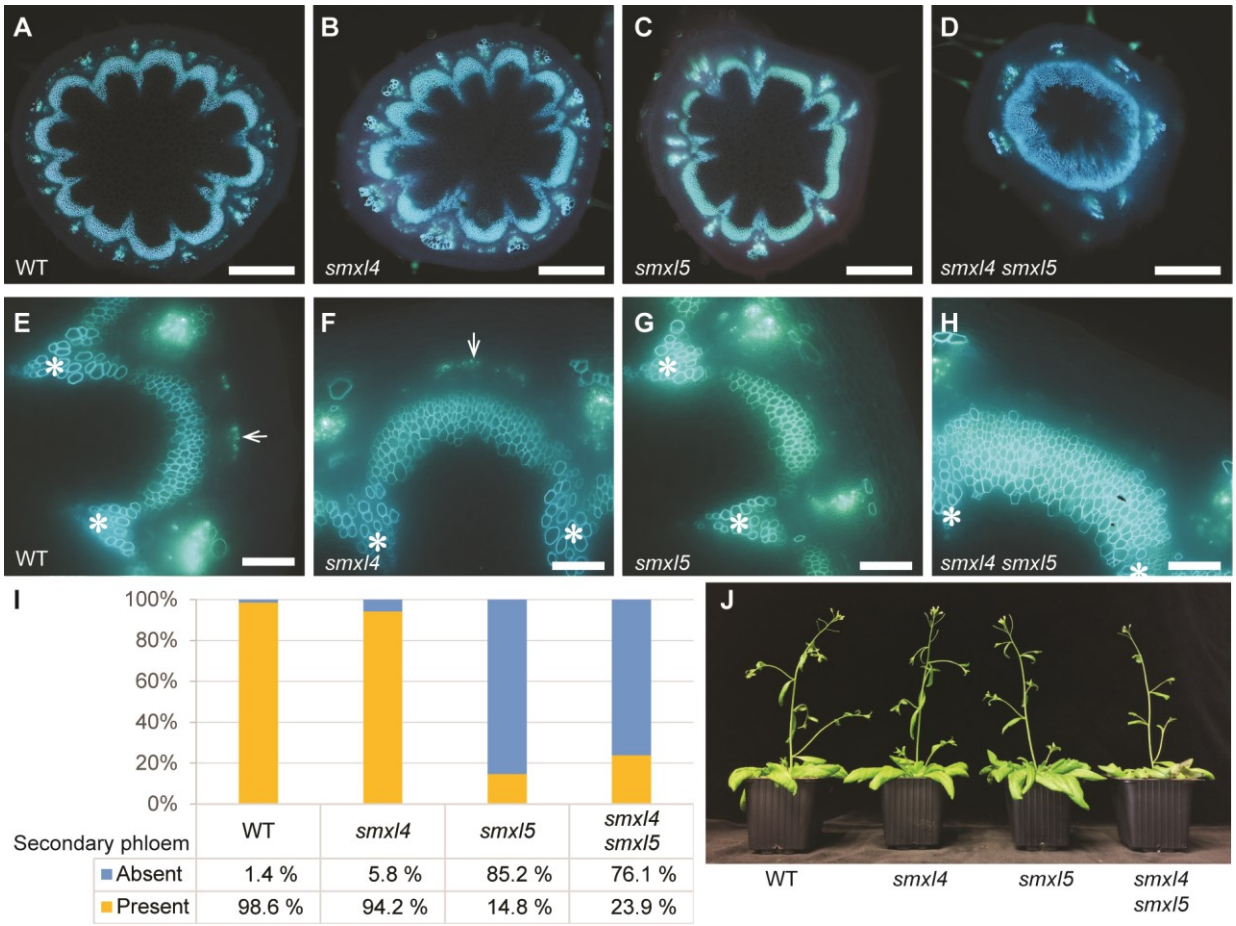

Secondary phloem	WT	*smxl4*	*smxl5*	*smxl4 smxl5*
Absent	1.4 %	5.8 %	85.2 %	76.1 %
Present	98.6 %	94.2 %	14.8 %	23.9 %

Figure 4.11: Secondary phloem formation is reduced in *smxl5* and *smxl4;smxl5*
A-D Aniline blue stained cross sections taken at the stem base of wild type (A), *smxl4* (B), *smxl5* (C) and *smxl4;smxl5* (D). Xylem autofluorescence is depicted in light blue and aniline stained callose/phloem is shown in blue/green. Scale bars represent 500 µm.
E-H Close-ups of IC regions are depicted for all samples described in A-D. Callose deposition in secondary phloem is marked by arrows in E and F and is absent in G and H. White asterisks (*) mark vascular bundles. Scale bars represent 100 µm.
I Average percentages of secondary phloem absence (blue) and presence (yellow) are depicted in a stacked histogram (n = 19-23).

4.2.3 Cambium activity is increased in *smxl4;smxl5*

To identify whether the absence of secondary phloem in *smxl5* and *smxl4;smxl5* coincides with defects in cambium formation, I analysed histological sections at the stem base of 15-20 cm tall *Arabidopsis* plants. Cambium-derived tissue (CDT) production was measured at mid-IC regions by following cambium-derived cell stacks from starch sheath to the first pith cell (indicated by a red line in Figure 4.12). The CDT production of wild type and the single mutants *smxl4* and *smxl5* was comparable (Figure 4.12 A, B, C and E). Of note, previous experiments performed under different growth conditions showed slight increases in CDT production for *smxl4* and *smxl5* (Wallner 2014). Interestingly, *smxl4;smxl5* double mutants showed on average twice as

much CDT production compared to wild type or the single mutants (Figure 4.12 D-E). This indicated that loss of secondary phloem formation in *smxl5* and *smxl4;smxl5* is not just a consequence of reduced cambium activity, but an independent defect.

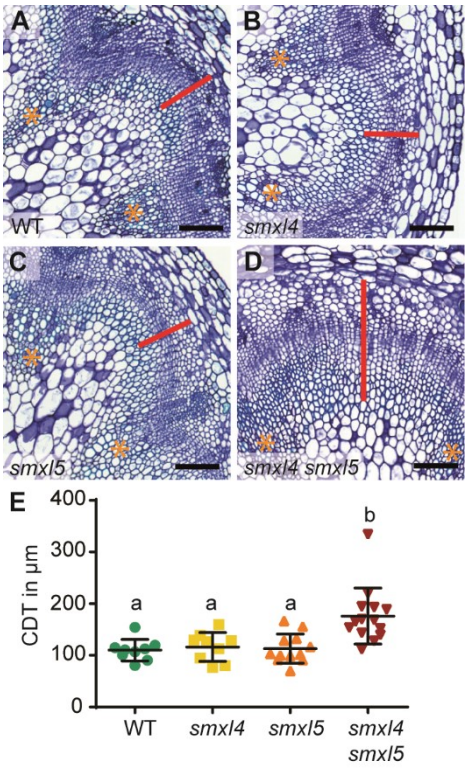

Figure 4.12: CDT production is enhanced in *smxl4;smxl5*
A-D Toluidine blue stained microtome sections taken from the stem base of 15-20 cm tall *Arabidopsis* plants. IC regions are depicted for wild type (A), *smxl4* (B), *smxl5* (C) and *smxl4;smxl5* (D). Vascular bundles are marked by yellow asterisk. Red lines indicate the measured cambium-derived tissue (CDT) production. Scale bars represent 100 µm.
E CDT production was quantified for each genotype and depicted in a scatter plot. Error bars represent ± standard deviation (n = 9-13). Statistical groups are indicated by letters and were determined by a one-way ANOVA with post-hoc Tukey-HSD (95 % CI).

4.2.4 *SMXL4/5* act locally on cambium activity

smxl4;smxl5 double mutants exhibit several growth defects and secondary stress responses (Figure 4.3 and 4.11). To decide whether the increase in CDT production is a secondary defect or reflects a local regulatory role of *SMXL4/5*, I grafted *smxl4;smxl5* shoots onto wild type roots (Figure 4.13). Wild type shoots grafted onto *smxl4;smxl5* roots served as control to determine the effects of a *smxl4;smxl5* double mutant root on plant growth (Figure 4.13 and 4.14). As expected - due to the local role of *SMXL4/5* on protophloem formation in the root (Figure 4.6) - wild type shoots grafted onto *smxl4;smxl5* roots did not restore root growth (Figure 4.13 A and B). If propagated on soil for three weeks, *smxl4;smxl5* roots negatively affected the growth of wild type rosettes. However, if a *smxl4;smxl5* rosette was sustained by a wild type root, growth was restored and the rosettes were indistinguishable from wild type self-grafts (Figure 4.13 C). Likewise, sucrose levels increased in leaves of sickish-looking plants supported by a *smxl4;smxl5* root and were reduced to wild type-levels in *smxl4;smxl5* leaves that were sustained by a wild type root (Figure 4.13 D). These data indicated that the *smxl4;smxl5* root defect is the main cause for the impaired overall growth of *smxl4;smxl5* double mutants.

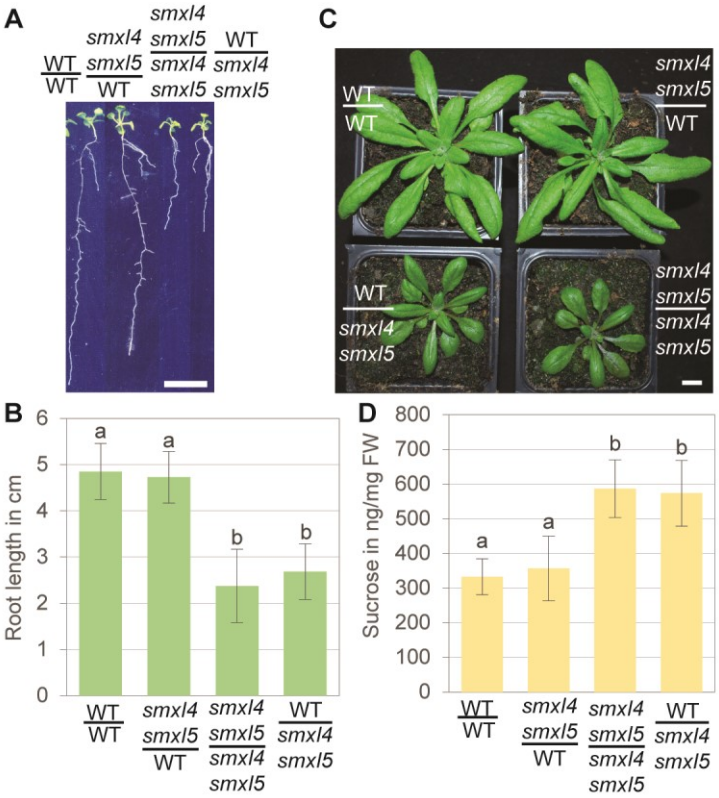

Figure 4.13: Rosette growth of *smxl4;smxl5* mutants is rescued by wild type roots

A Seedlings 2 weeks after grafting. Wild type self-grafts, *smxl4;smxl5* grafted onto wild type roots, *smxl4;smxl5* self-grafts and wild type grafted onto *smxl4;smxl5* roots are depicted from left to right. Root growth of *smxl4;smxl5* is not rescued by a wild type shoot. Scale bar represents 1 cm.

B Root lengths shown in A were quantified: Means of 3 independent experiments (n = 15-32 for the first two experiments, n = 36-50 for the third experiment). Error bars represent ± standard deviation. Statistical groups indicated by letters were determined by a one-way ANOVA with post-hoc Bonferroni (95 % CI).

C Depicted are rosettes of grafted plants that were propagated on soil for 3 weeks. Wild type roots restore rosette growth of *smxl4;smxl5*, while *smxl4;smxl5* roots induce smaller and darker leaves in wild type rosettes (n = 20). Scale bar represents 1 cm.

D Sucrose levels were quantified from rosette leaves depicted in C by the Metabolomics Core facility (EMBL Heidelberg, Germany). If supported by a *smxl4;smxl5* root, leaves accumulated more sucrose than leaves supported by a wild type root. Error bars represent ± standard deviation (n = 5). Statistical groups were determined by a one-way ANOVA with post-hoc Bonferroni (95 % CI) and are indicated by letters.

Based on these observations it was important to distinguish a local *SMXL4/5* gene function from secondary defects caused by sick *smxl4;smxl5* roots. Thus, I investigated stem morphology and CDT production in all possible graft-combinations between wild type and *smxl4;smxl5* (Figure 4.14). Histological analysis revealed that stem diameters were strongly reduced in plants supported by a *smxl4;smxl5* root but comparable to wild type in *smxl4;smxl5* stems that were supported by a wild type root (Figure 4.14 A-D and I). Interestingly, *smxl4;smxl5* roots did not influence CDT production in wild type stems (Figure 4.14 E, G and J). Since those plants showed an increase in sugar levels in leaves, similar to *smxl4;smxl5* self-grafts, it could be ruled out that over-accumulation of sugars in source organs are the reason for enhanced cambium activity in *smxl4;smxl5* (Figure 4.13 and 4.14). In fact, a significant increase in CDT production was observed in *smxl4;smxl5* stems sustained by a wild type root. Those plants were morphologically comparable to wild type self-grafts, had normal sucrose levels in leaves and a healthy root (Figure 4.13 and 4.14). Consequently, *SMXL4/5* fulfils a local function in suppressing CDT production in the stem.

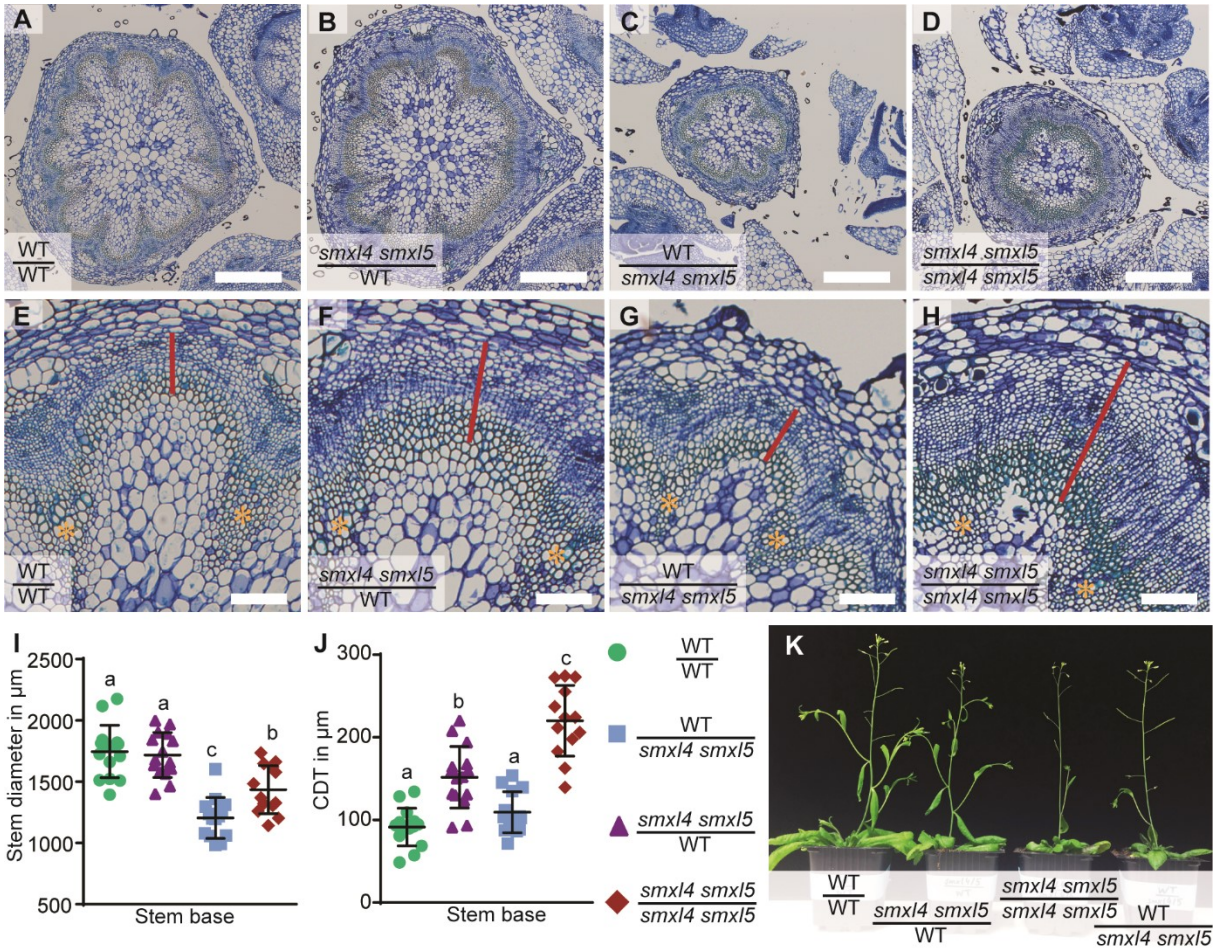

Figure 4.14: CDT production is increased in *smxl4;smxl5* independently of the root genotype

A-D Toluidine blue stained microtome sections taken at the stem base of 15-20 cm tall grafted *Arabidopsis* plants. The genotypes of shoot (written above the line) and root (written below the line) of all grafted combinations are indicated in each picture. The stem diameter of *smxl4;smxl5* plants can be rescued by a wild type root (B) and a wild type stem diameter is affected by a *smxl4;smxl5* root (C). Scale bars represent 500 µm.

E - H Close-ups of IC regions are depicted for all samples described in A-D. CDT production is indicated by a red line that follows cambium-derived cell files. Yellow asterisks (*) mark vascular bundles. Scale bars represent 100 µm.

I-J Stem diameters (I) and CDT production (J) were compared at the stem base between all grafted samples and depicted as scatter plots. Error bars represent ± standard deviation (n = 13-15). Statistical groups were determined by a one-way ANOVA with post-hoc Tukey-HSD (95 % CI) in I and J. Wild type shoots grafted on wild type roots are depicted by green cycles, wild type shoots grafted on *smxl4;smxl5* roots are depicted by blue squares, *smxl4;smxl5* shoots grafted on wild type roots are depicted by violet triangles and *smxl4;smxl5* shoots grafted on *smxl4;smxl5* roots are depicted by red rhombi.

K The pictures depict the growth habitus of 15-20 cm tall grafted *Arabidopsis* plants.

4.2.5 Secondary phloem formation is independent from CDT production

Since secondary phloem formation was largely, but not completely SMXL5-dependent, I tested the robustness of my results by analysing aniline stained stem sections taken at the base

of all grafted *smxl4;smxl5*-wild type combinations (Figure 4.15). This experiment aimed to investigate whether an increase in CDT production in *smxl4;smxl5* stems grafted onto wild type roots could compensate the deficiencies in secondary phloem formation. Compared to *smxl5* single mutants, *smxl4;smxl5* stems grafted onto wild type roots were more abundant in CDTs, while stem diameter and growth habitus were still morphologically comparable to wild type (Figure 4.11 - 4.14). Interestingly, secondary phloem formation in *smxl4;smxl5* stems could not be restored if grafted onto a wild type root (Figure 4.15 B, F and I). However, almost 100 % of all IC regions of wild type stems formed secondary phloem independently of the root genotype (Figure 4.15). This supported the idea that *SMXL5* has a dual role in promoting secondary phloem formation and suppressing CDT production together with *SMXL4*.

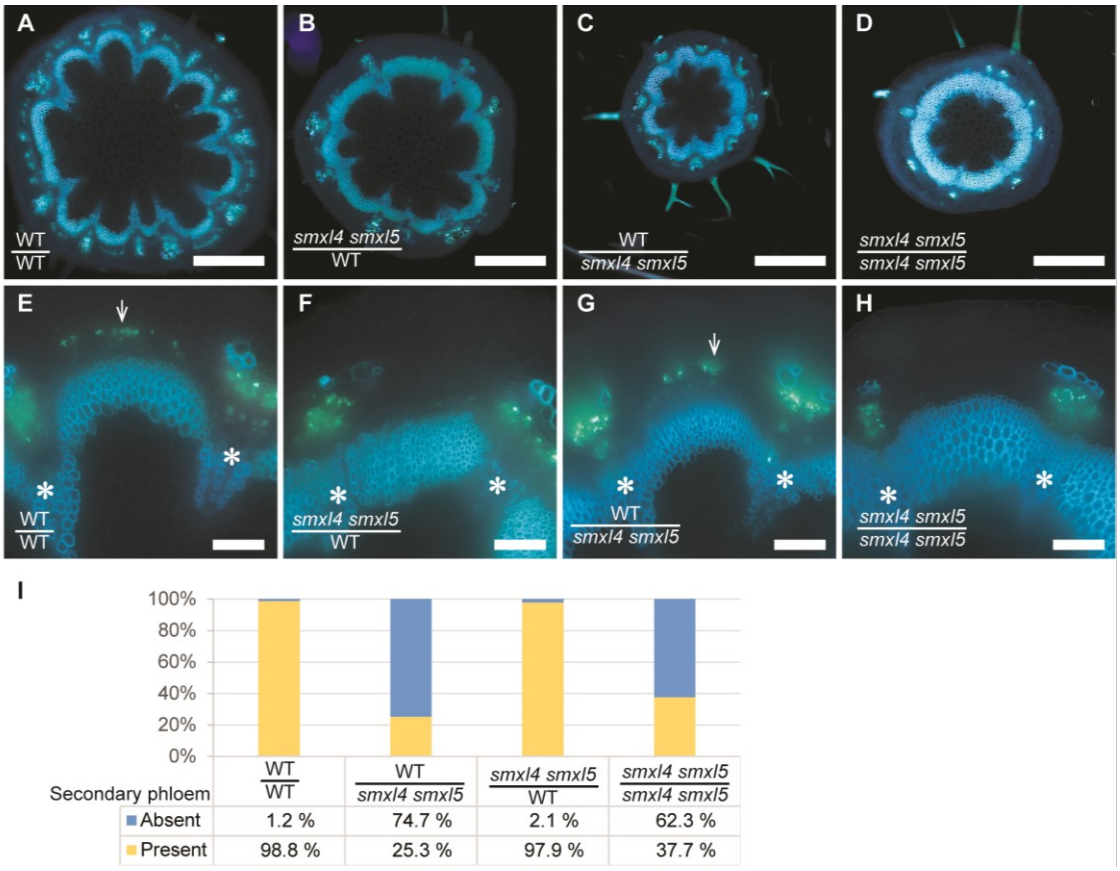

Figure 4.15: Secondary phloem formation is impaired in *smxl4;smxl5* independently of the root genotype

A - D Aniline blue stained cross sections taken at the stem base of all grafted combinations as indicated in the pictures (see also figure 4.14). Xylem autofluorescence is depicted in light blue and aniline stained callose/phloem is shown in green. Scale bars represent 500 µm.

E - H Close-ups of interfascicular regions are depicted for all samples described in A-D. Xylem autofluorescence is shown in light blue and aniline stained callose/phloem in green. Callose deposition in secondary phloem is marked by arrows in E and G and is absent in F and H. White asterisks (*) mark vascular bundles. Scale bars represent 100 µm.

I The average percentages of secondary phloem absence (blue) and presence (yellow) are depicted in a stacked histogram (n = 10-15). The results could be reproduced in an independent repetition (n = 6-12).

4.2.6 Important phloem regulators are downregulated in *smxl4;smxl5*

To back-up my phenotypic observations, I compared the transcriptomes of wild type self-grafts to *smxl4;smxl5* shoots grafted onto wild type roots. The RNA was isolated from the stem base, including the first cm above the base and therefore only contained tissues of either *smxl4;smxl5* or wild type. The grafting technique allowed again to separate unwanted secondary defects from local *SMXL4/5* functions. By applying a threshold of a fold change < 0.5 for upregulated genes and > 1.5 for downregulated genes and an adjusted p-value of 0.01, I obtained two gene sets with 273 upregulated genes and 1343 downregulated genes, respectively (Figure 4.16).

To investigate whether vascular-related genes were among those differentially expressed gene sets, I compared my transcriptional data to the “Vascular genes” dataset published in Endo et al. 2014 which contains 280 vascular-specific genes. 13 of those 280 genes were found to be upregulated, whereas 98 out of 280 vascular-specific genes were downregulated in *smxl4;smxl5* (Figure 4.16 A). Those 98 downregulated genes contained important phloem regulators, such as *APL, SEOR1, BRX, JUL1/2* or *NAC086* and many phloem-specific genes and sugar transporters, such as *SUC2* and *SUCROSE SYMPORTER* (*SUS*) (Baroja-Fernandez et al. 2012; Depuydt et al. 2013; Blob et al. 2018; Cho et al. 2018; Bonke et al. 2003). The upregulated gene fraction mostly contained stress related genes that have a reported phloem-specific expression pattern (Moseler et al. 2015; Tian et al. 2010). Interestingly and despite cambium activity was increased in *smxl4;smxl5*, cambium-related genes were not found to be significantly up- or downregulated with the applied stringency settings.

To focus on phloem-specific genes, I compared my transcriptional data with the datasets of Kondo et al. 2016. This publication provides four different phloem-specific gene sets (modules) that are reportedly expressed at specific stages during phloem development (Kondo et al. 2016). Module I contains the genes induced first during phloem formation and module IV involves genes that are expressed at the last stages of phloem differentiation (Kondo et al. 2016). All modules showed overlaps with genes that were downregulated in *smxl4;smxl5*. Only *AT5G04310*, which encodes a pectine lyase-like family protein at the latest stage of phloem formation (module IV) (Kondo et al. 2016), matched the upregulated gene set (Figure 4.16 B).

In summary, the transcriptional data of *smxl4;smxl5* stems supported the finding that *SMXL4* and *SMXL5* are fundamental and general phloem regulators. In comparison to *SMXL3* and *SMXL4*, which are redundantly acting with *SMXL5* during protophloem initiation and differentiation, *SMXL5* seems to hold a specific and unique role during secondary phloem formation.

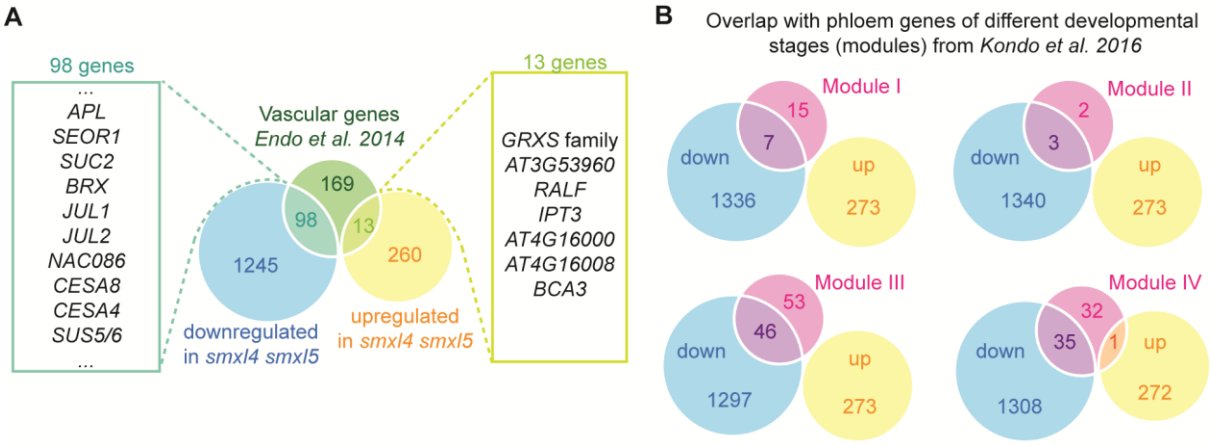

Figure 4.16: Important phloem marker genes are downregulated in *smxl4;smxl5* stems that were grafted onto wild type roots

RNA was extracted at the stem base of *smxl4;smxl5* shoots supported by a wild type root (*smxl4;smxl5*) and at the stem base of wild type self-grafts (WT). Transcriptomes of 3 independent *smxl4;smxl5* samples were compared to 3 independent wild type samples.

A Venn diagram comparing up- and downregulated genes of *smxl4;smxl5* (with an adjusted p-value < 0.01 and a fold change > 1.5 for downregulated genes and < 0.5 for upregulated genes, respectively) to the dataset of vascular genes published by Endo et al. 2014. From those 283 vascular genes, 98 overlapped with genes downregulated in *smxl4;smxl5*, including important phloem regulators, while 13 overlapped with genes upregulates in *smxl4;smxl5*, including metal ion associated and stress response genes.

B Venn diagrams depicting the same up- and downregulated genes of *smxl4;smxl5* in comparison to genes expressed during different stages of phloem formation as published by Kondo et al. 2016. Module I contains the early genes and module IV the late genes upregulated upon phloem induction (Kondo et al. 2016).

4.3 *SMXL3/4/5* act independently from SL/KAR signalling

SMXL sub-clades 1 and 4 mediate MAX2 effects in KAR- or SL-signalling, respectively (Soundappan et al. 2015; Stanga et al. 2016; Stanga et al. 2013). Several *max2*-dependent growth defects are suppressed in *smax1;smxl2;max2* and *smxl6/7/8;max2* mutants (Liang et al. 2016; Soundappan et al. 2015; Stanga et al. 2016; Wang et al. 2015). Moreover, the SL-dependent SMXL7-YFP fusion protein is rapidly degraded upon short-term treatment by the synthetic SL/KAR analogue and racemic mixture *rac*-GR24 (Liang et al. 2016). Interestingly, SMXL3/4/5 proteins lack the amino acid motif that has been proven essential for MAX2-receptor dependent ubiquitination (Figure 1.7) (Wallner et al. 2016). Whether or not *SMXL3/4/5* contribute to SL/KAR-signalling is therefore questionable and their associated molecular network and signalling pathway is still unknown.

To test a potential connection between *SMXL3/4/5* and *MAX2* and/or SL/KAR signalling, I applied genetic approaches and performed short-term protein-degradation assays with *rac*-GR24.

4.3.1 *SMXL4/5* do not mediate SL/KAR signalling

To characterize whether SMXL sub-clade 3 plays a role in a MAX2-dependent signalling pathway, I analysed root growth and protophloem formation in *max2* and *smxl4;smxl5;max2* mutants (Figure 4.17). If *SMXL4/5* were "Suppressors of *MAX2*", as suggested by their name, *max2* should exhibit developmental defects that are suppressed in *smxl4;smxl5;max2*. Since *SMXL4/5* play a major role in phloem formation and consequently root growth, I first investigated root lengths and overall seedling growth of *max2* and *smxl4;smxl5;max2* and compared them to wild type and *smxl4;smxl5* (Figure 4.17 A-B). Except for increased lateral root formation, which is a known phenotype of *max2* mutants (Kapulnik et al. 2011), wild type and *max2* primary root lengths were comparable (Figure 4.17 A-B). The phenotype of the *smxl4;smxl5;max2* triple mutant was additive and its roots were as short as roots of *smxl4;smxl5* mutants (Figure 4.17 A-B). Investigating RAM fitness yielded similar results (Figure 4.17 C-G). The RAM size of both *smxl4;smxl5* and *smxl4;smxl5;max2* was dramatically decreased in 10 day-old primary roots, whereas the RAM of *max2* mutants looked like wild type (Figure 4.17 C-G). Similarly, the spatio-temporal organization of protophloem formation was indistinguishable between wild type and *max2* (Figure H-J), and initiation of the second tangential division, which initiates proto- and metaphloem cell identities, was delayed to the same extent in *smxl4;smxl5* and *smxl4;smxl5;max2* (Figure 4.17 H-L). As expected, PSEs differentiated normally in *max2* and failed to differentiate equally in *smxl4;smxl5* and *smxl4;smxl5;max2* (Figure 4.17 M-P). Consequently, I concluded that *MAX2* is not important during protophloem formation, since root defects observed in *smxl4;smxl5;max2* triple mutants were additive and, in the case of phloem formation, exclusively based on *smxl4;smxl5*. Of note, it cannot be ruled out that *SMXL4/5* and *MAX2* genetically interact in other developmental stages or processes.

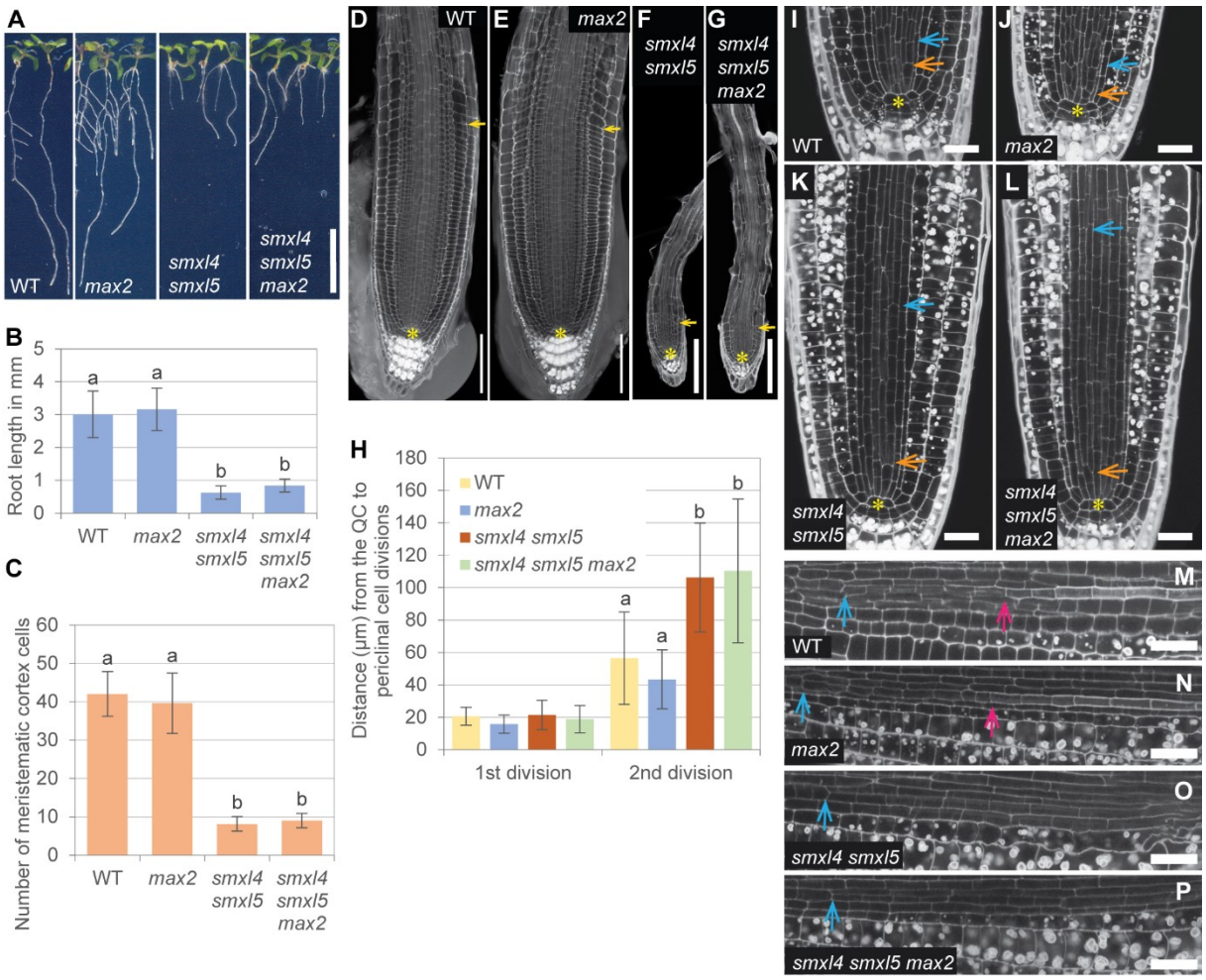

Figure 4.17: The *smxl4;smxl5;max2* phenotype is additive and combines both *smxl4;smxl5* and *max2* defects

A Root lengths of 10 day-old seedlings. Wild type, *max2, smxl4*;*smxl5* and *smxl4;smxl5;max2* are depicted (from left to right). Scale bar represents 1 cm.

B The root lengths were quantified for all genotypes shown in A. Mean values of 4 independent experiments with n = 37-52 per replicate are depicted. Error bars represent ± standard deviation. Statistical groups are marked by letters and were determined by a one-way ANOVA with post-hoc Tamhane-T2 (95 % CI).

C - G The RAM size of 10 day-old seedlings was determined by quantifying the number of meristematic cortical cells (n = 17-25). Statistical groups are indicated by letters and were determined by a one-way ANOVA with post-hoc Tamhane-T2 (95 % CI). Error bars represent ± standard deviation (C). mPS-PI stained RAMs of wild type (D), *max2* (E), *smxl4;smxl5* (F) and *smxl4;smxl5;max2* (G) are depicted. QCs are marked by yellow asterisks and yellow arrows point to the first elongating cortical cell and the end of the meristematic zone (D-G). Scale bars represent 100 µm.

H - L Distances of first and second tangential cell division to the QC were quantified in 2 day-old root tips (H) for wild type (I), *max2* (J), *smxl4;smxl5* (K) and *smxl4;smxl5;max2* (L). The QC is marked by yellow asterisks. The first tangential division is marked by orange arrows and the second tangential division is marked by blue arrows. Scale bars represent 20 µm. The Error bars represent ± standard deviation (n = 11-14). Statistical groups are indicated by letters and were determined for the second tangential divisions by a one-way ANOVA with post-hoc Tamhane-T2 (95 % CI) (H).

M - P Differentiating PSE strands after the second tangential division (blue arrows) are shown for wild type (M), *max2* (N), *smxl4;smxl5* (O) and *smxl4;smxl5;max2* (P). Differentiation of PSEs

is indicated by enhanced PI staining in M and N (pink arrows) and absent in O and P. Scale bars represent 20 µm.

4.3.2 *SMXL* family members are functionally conserved

To investigate functional similarities between *MAX2*-dependent and *MAX2*-independent *SMXL* family members, I ectopically expressed a *YFP*-fusion of the KAR-dependent *SMAX1* under the control of the *SMXL5* promoter in a *smxl4;smxl5* double mutant background. *smxl4;smxl5* double mutants carrying a *SMXL5:SMXL5-YFP* transgene served as control (Figure 4.18). Surprisingly, both transgenic lines showed restored root growth. *SMAX1* could functionally replace *SMXL5* if expressed in the *SMXL5* domain and when plant were grown on normal MS-plates without additives (mock) (Figure 4.18). Thus, I deduced that *SMXL* family members are structurally and functionally conserved across sub-clades and differences in their regulatory roles are primarily determined by distinct promoter activities (Figure 4.1). Astonishingly, if grown on MS-plates supplemented with 2 µM *rac*-GR24, the root length of *smxl4;smxl5* expressing *SMXL5:SMAX1-YFP* was reduced to the root length of *smxl4;smxl5* mutants, whereas the *SMXL5:SMXL5-YFP* transgene was still able to complement the *smxl4;smxl5* root phenotype (Figure 4.18). This promoter-swapping experiment indicated that only *SMAX1-YFP*, but not *SMXL5-YFP*, was sensitive to the SL/KAR analogue *rac*-GR24.

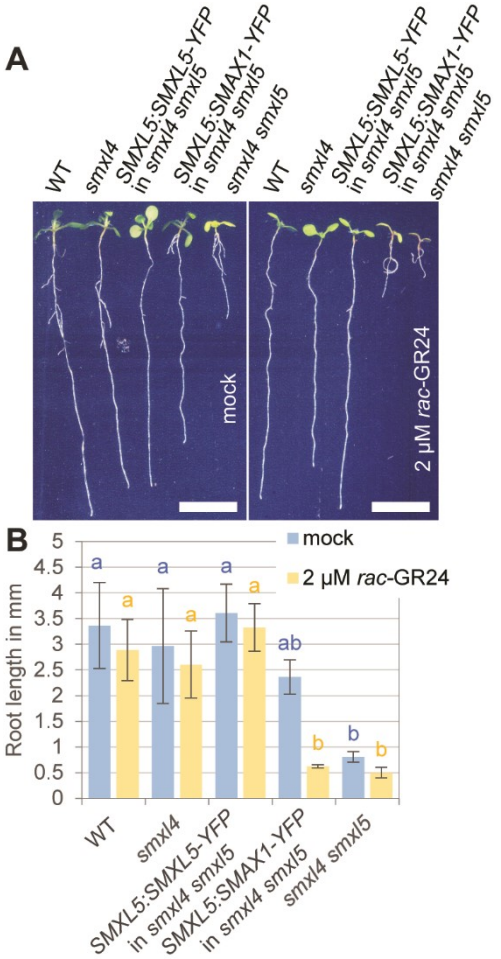

Figure 4.18: SL/KAR-independent SMXL5 can be functionally replaced by SL/KAR-dependent SMAX1

A The root length of 10 day-old seedlings are shown for wild type, *smxl4*, *smxl4;smxl5* (*SMAX5:SMXL5-YFP*), *smxl4;smxl5* (*SMXL5:SMAX1-YFP*) and *smxl4;smxl5* (from left to right). Seedlings were grown on normal MS plates (mock, left panel) and MS-plates supplemented with 2 µM *rac*-GR24 (right panel). Scale bars represent 1 cm. **B** Root lengths of all genotypes depicted in A were quantified. Error bars represent ± standard deviation. Mean values of 3 independent experiments (n = 27-55 each) are depicted. Statistical groups are indicated by letters and were determined for "mock" and "2 µM *rac*-GR24" separately by one-way ANOVA with post-hoc Bonferroni (95 % CI).

4.3.3 SMXL3/4/5 proteins are no targets of SL/KAR-dependent degradation

To determine whether the difference in *rac*-GR24 susceptibility of *SMXL5:SMXL5-YFP* and *SMXL5:SMAX1-YFP* was based on differences in SL/KAR-dependent protein stability, I compared the YFP-signal intensity of both transgenic lines during short-term *rac*-GR24 treatment (Figure 4.19). Thus, I treated *smxl4;smxl5* root tips carrying either *SMXL5:SMAX1-YFP* (Figure 4.19 A-B) or *SMXL5:SMXL5-YFP* transgenes (Figure 4.19 C-E) with liquid MS-medium (mock, Figure 4.19 A and C) or medium containing 10 µM GR24 (Figure 4.19 B and D). Initially, all root tips showed YFP signals within the *SMXL5* domain (time point 0 min, Figure 4.19) and signals were consistent for at least 12 min if treated with mock solution. Interestingly, SMAX1-YFP signals faded quickly 8 min after *rac*-GR24 application (Figure 4.19 B), whereas SMXL5-YFP signal intensities remained stable and were still observable after incubating for 60 min in *rac*-GR24 supplemented medium (Figure 4.19 D-E). Consequently, I concluded that SMAX1-YFP was a proteolytic target of SL/KAR-signalling, while SMXL5-YFP protein-fusions were resistant to *rac*-GR24-dependent degradation.

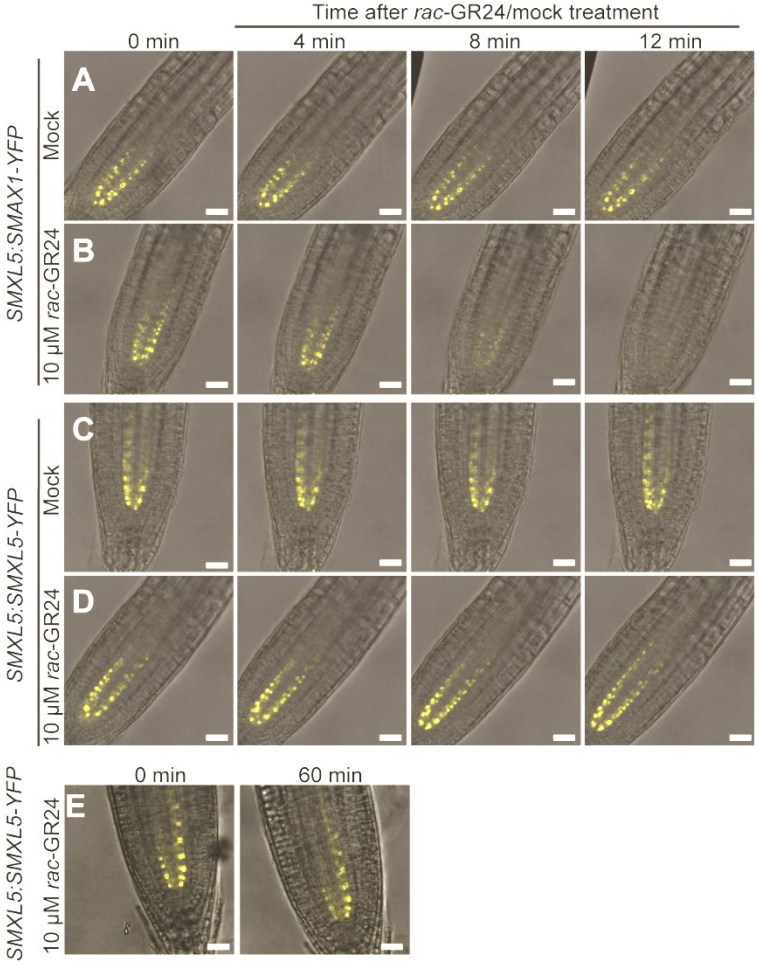

Figure 4.19: SMXL5-YFP remains stable upon GR24 treatment
A-E Confocal analysis of 5 day-old *smxl4;smxl5* root tips carrying *SMXL5:SMAX1-YFP* (A-B) or *SMXL5:SMXL5-YFP* (C-D) transgenes. The overlay of bright field image and YFP signal (yellow) is depicted. Roots were either incubated without *rac*-GR24 (mock, A and C) or with 10 µM *rac*-GR24 (B and D) over a time course of 12 min. SMAX1-YFP signals disappeared after 8 min-incubation in 10 µM *rac*-GR24 (B), while SMXL5-YFP intensities remained stable (D) even after incubating for 60 min in 10 µM *rac*-GR24 (E). Scale bars represent 25 µM.

To extend my analysis of SL/KAR-dependent protein stability also towards SMXL3 and SMXL4, I generated *SMXL3:SMXL3-YFP* and *SMXL4:SMXL4-YFP* constructs which I transformed into *smxl3;smxl5* and *smxl4;smxl5* mutant backgrounds, respectively. Since *SMXL3*, *SMXL4* and *SMXL5* shared very similar expression domains within the RAM (Figure 4.1), I did not deem it necessary to swap the endogenous promoters with the *SMXL5* promoter. Both transgenes restored root lengths in the respective double mutant backgrounds, which indicated that SMXL3-YFP and SMXL4-YFP fusion proteins were functional (Figure 4.20 G). Similar to my previous experiment (Figure 4.19), I treated root tips with either mock or 10 µM *rac*-GR24 solution over a period of 12 min. The *SMXL5:SMAX1-YFP* line served as a control (Figure 4.20 E-F). Just like SMXL5-YFP, SMXL3-YFP and SMXL4-YFP were resistant to *rac*-GR24 mediated degradation (Figure 4.20 B and C), while SMAX1-YFP signals were gone 8-12 min after *rac*-GR24 application (Figure 4.20 E). Of note, SMAX1-YFP signals were initially weaker than SMXL3-YFP and SMXL4-YFP signals. This was often observed during repetitions of these experiment (Figure 4.19 and 4.20) and might be due to endogenous SL/KAR levels that affect SMAX1-YFP stability.

In summary, I concluded that SMXL3/4/5 proteins are, unlike all other SMXL family members, resistant to SL/KAR-dependent degradation and mediate phloem formation in a MAX2- and SL/KAR-independent manner.

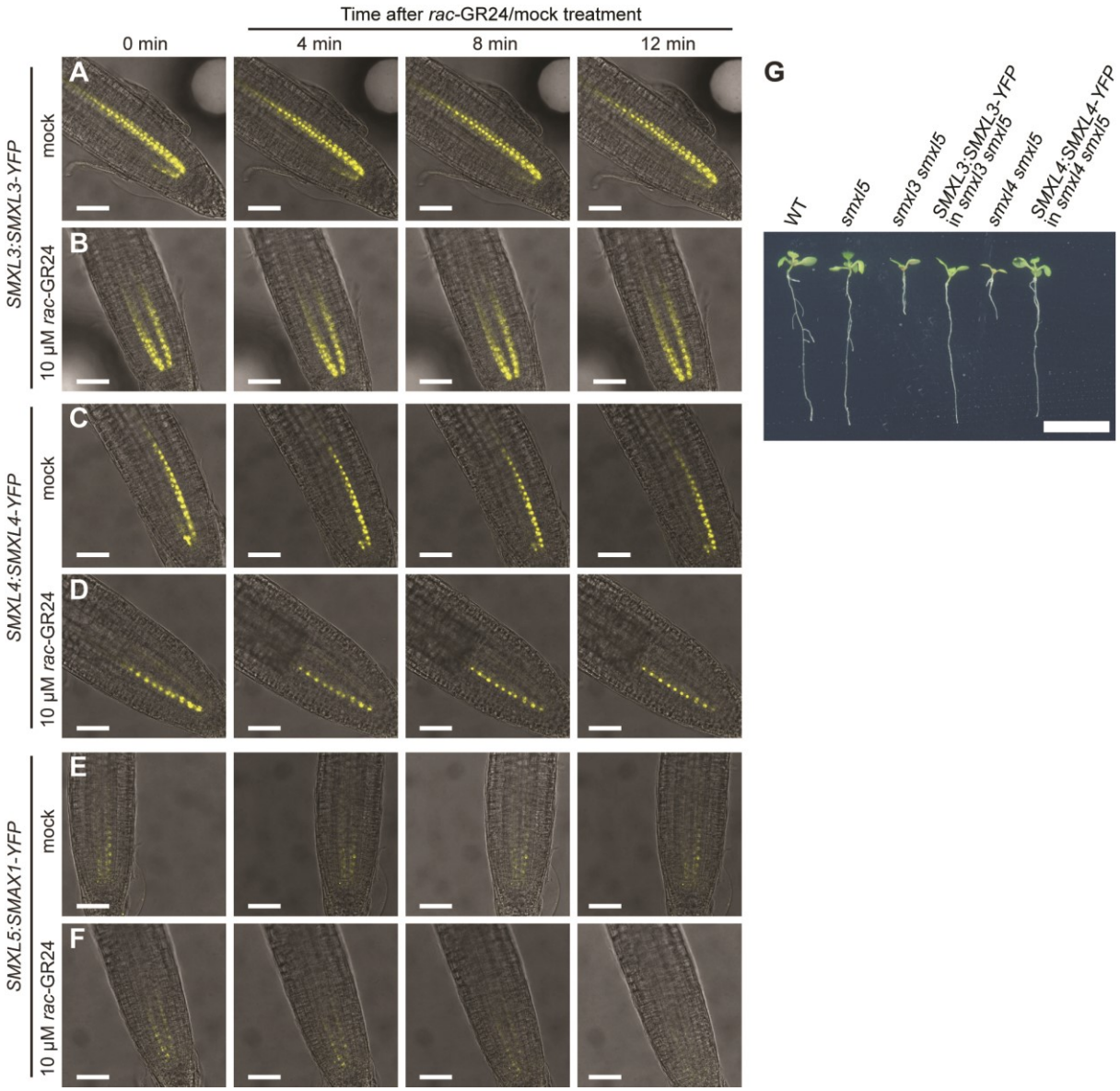

Figure 4.20: SMXL3/4 are not degraded upon GR24 treatment

A-F Shown are confocal pictures of 5 day-old *smxl4;smxl5* root tips expressing transgenes *SMXL3:SMLX3-YFP* (A-B), *SMXL4:SMXL4-YFP* (C-D) or *SMXL5:SMAX1-YFP* (E-F). The overlay of bright field image and YFP signal (yellow) is depicted. Roots were either incubated without *rac*-GR24 (mock shown in A, C and E) or with 10 µM *rac*-GR24 (B, D and F) over a time course of 12 min. While the SMAX1-YFP signal disappeared after treating the root for 8 min with 10 µM *rac*-GR24 (F), SMXL3-YFP (B) and SMXL4-YFP (D) remained stable. Scale bars represent 25 µm.

G 10 day-old wild type, *smxl5, smxl3;smxl5, smxl3;smxl5* (*SMAX3:SMXL3-YFP*), *smxl4;smxl5, smxl4;smxl5* (*SMXL4: SMAX4-YFP*) are shown (from left to right). Recovery of root lengths in *smxl4;smxl5* (*SMXL4: SMAX4-YFP*) and *smxl3;smxl5* (*SMAX3:SMXL3-YFP*) indicated that SMXL4-YFP and SMXL3-YFP fusion proteins are functional. *SMXL3:SMXL3-YFP* was also able to restore the root length of *smxl4;smxl5* (data not shown). Scale bars represent 1 cm.

4.4 OBE3 interacts with SMXL3/4/5 to promote phloem formation

To characterize the role of *SMXL3/4/5* in phloem formation from a mechanistic point of view, I explored their molecular role by investigating potential protein-protein interaction partners. A Yeast 2-Hybrid screen that was previously performed by Hybrigenics SA (Paris, France) with SMXL5 as a bait served as a starting point to select potential candidates (data unpublished). Amongst others, three PHD-finger proteins known as OBE2, OBE3 (TTA1) and OBE4 (TTA2) were identified of which OBE2 and OBE3 showed the highest confidence score. I already confirmed a direct protein-protein interaction between SMXL5 and OBE2/3 in yeast during my Master thesis (Wallner 2014). In the next step I aimed for investigating the biological relevance of this interaction *in planta*. For practical reasons and to simplify the experimental setup, I primarily focused my in-depth analyses on characterizing the SMXL5-OBE3 interaction. Interestingly, all identified *OBE3* clones identified in the Yeast 2-Hybrid screen shared base pairs 1204-1367. This region, which is designated as selected interacting domain (SID), encodes the first part of the OBE3 PHD-finger. Of note, most clones covered the whole PHD-finger, which suggested that the binding domain is localized in that area (Figure 4.21).

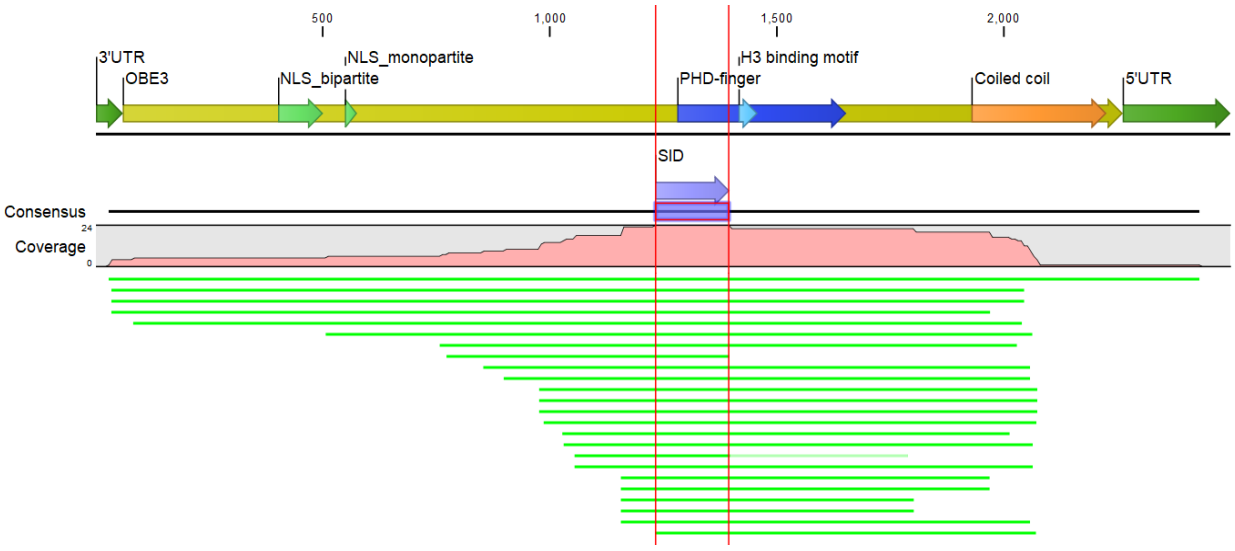

Figure 4.21: Alignment of the identified SMXL5-interacting Yeast Two-Hybrid clones in comparison to the OBE3
OBE3-encoding nucleotide sequences identified in SMXL5-interacting yeast clones (light green lines) were aligned to the full-length OBE3 coding sequence using CLC Main Workbench Version 7.6.1 (CLC Bio Qiagen, Aarhus, Denmark). Annotations mark the OBE3 exon (yellow arrow) that encodes two predicted nuclear localization signals (NLS) identified by the cNLS Mapper (Kosugi et al. 2009) (NLS_bipartite and NLS_monopartite, light green arrows), a PHD-finger domain (blue arrow) with histone 3 (H3) binding motif (light blue arrow) and a coiled coil domain (orange arrow) predicted by InterPro (EMBL-EBI, Cambridgeshire, UK). The OBE3 exon is flanked by a three prime and five prime untranslated region (3'UTR and 5'UTR, green arrow), respectively. Aligned sequences show 100 % coverage within the selected interacting domain (SID) (marked by a purple arrow and flanked by red lines). This region is thus suspected to contain the SMXL5 binding domain.

4.4.1 SMXL5 and OBE3 co-localize in the nucleus

To investigate whether the SMXL5-OBE3 interaction plays a role *in planta*, I studied protein localization of OBE3 fused to monomeric GFP (OBE3-mGFP) in relation to SMXL5 fused to monomeric Cherry (SMXL5-mCherry) (Figure 4.22). Thus, I transiently co-expressed *35S:OBE3-mGFP* with either *35S:mCherry-NLS* (Figure 4.22 A-E) or *35S:SMXL5-mCherry* (Figure 4.22 F-J) in *Nicotiana* leaves. Co-infiltration of *35S:mCherry-NLS* and *35S:mGFP-NLS* served as control, since both constructs encode fluorescent proteins coupled to a nuclear localization signal (NLS) and, therefore, localize to the nucleus (Figure 4.22 K-O). mGFP and mCherry did not compartmentalize into specific patterns in the presence of other proteins as can be seen in Figure 4.22 A-E. OBE3-mGFP was nuclear localized and accumulated in speckles (Figure 4.22 A). If co-expressed with *35S:mCherry-NLS*, the fluorescent signals showed distinct localization patterns and did not coincide (Figure 4.22 C and E). However, co-transfected cells expressing *35S:OBE3-mGFP* and *35S:SMXL5-mCherry*, showed a perfect overlap of both signals in nuclei. Of note, SMXL5-YFP is always nuclear localized and usually resides in small speckles (Wallner 2014). Interestingly, OBE3-mGFP and SMXL5-mCherry almost exclusively co-localized in fewer big speckles of unique morphology, which was in agreement with a protein-protein interaction (Figure 4.22 F-J).

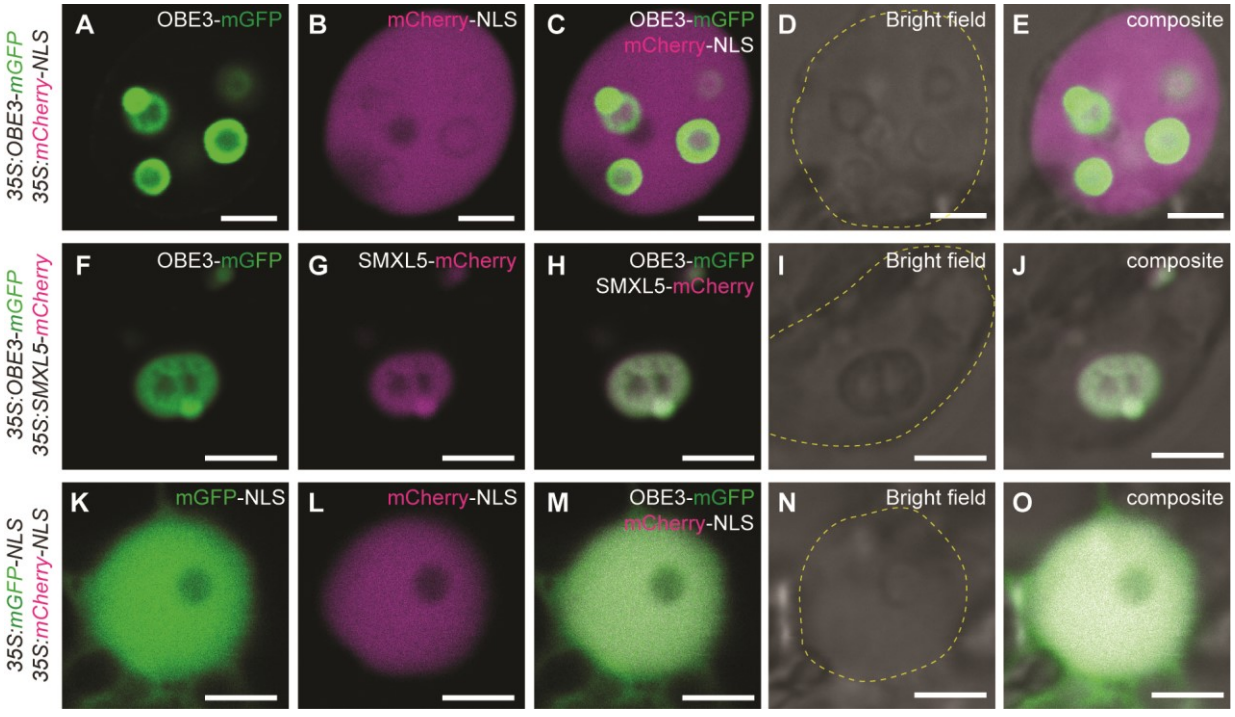

Figure 4.22: Proteins SMXL5-mCherry and OBE3-mGFP co-localize in *Nicotiana* nuclei
Fluorescent signals and bright field images of epidermal *Nicotiana* nuclei transiently co-expressing *35S:OBE3-mGFP/35S:mCherry* (A-E), *35S:OBE3-mGFP/35S:SMXL5-mCherry* (F-J) and *35S:mGFP-NLS/35S:mCherry-NLS* (K-O). A dashed yellow line indicates the outlines of nuclei in bright field images (D, I and N). The sub-nuclear localization of OBE3 fused to monomeric GFP (OBE3-mGFP) together with monomeric Cherry fused to a nuclear localization signal (mCherry-NLS) did not coincide (A-E). Fusion proteins OBE3-mGFP and SMXL5-mCherry co-

localized into special sub-nuclear patterns (F-J). Expression of the controls *mGFP-NLS* together with *mCherry-NLS* showed diffused fluorescence within the whole nucleus (K-O). Scale bars represent 5 µm.

4.4.2 SMXL5 and OBE3 proteins interact *in planta*

In a more direct approach, I tested the interaction between SMXL5 and OBE3 by co-immunoprecipitation (co-IP) and subsequent Western blotting (Figure 4.23). I thus transiently expressed *35S:6xMyc-OBE3* either alone or together with *35S:SMXL5-3xHA* in *Nicotiana* leaves (Figure 4.23 A). SMXL5 fused to a triple human influence hemagglutinin (HA) affinity tag and OBE3 fused to a sixfold c-Myc epitope tag were both soluble during protein extraction and detected by anti-HA (α HA) or anti-Myc (α Myc) antibodies, respectively (see “Input” fractions in Figure 4.23). SMXL5-3xHA was immunoprecipitated from the protein extract via HA-affinity beads and was detected in Westerns as being around 120 kDa in size matching the expected size of SMXL5 (115.25 kDa) plus 3xHA (5 kDa). A successful pull-down of SMXL5-3xHA was reflected by a decreased band intensity in the “Unbound” fractions, which contained all residual proteins that did not bind to the beads (Figure 4.23). Importantly, 6xMyc-OBE3 was co-immunoprecipitated by SMXL5-3xHA. It ran at a size of approximately 100 kDa and was thus slightly larger than the expected size of OBE3 (82.4 kDa) plus 6xMyc (10.12 kDa). Interestingly, another faint 6xcMyc-OBE3 band was detected at the expected size of around 92 kDa, but this protein did not co-immunoprecipitate with SMXL5. This observation could hint towards a yet unknown post-translational modification that is required for OBE3 interaction with SMXL5. Of note, 6xMyc-OBE3 showed no signs of unspecific binding to α-HA beads, since it could not be immunoprecipitated without the presence of SMXL5-3xHA (Figure 4.23 A).

To confirm that the detected interaction between SMXL5-3xHA and 6xMyc-OBE3 was specific, I tested the affinity of 6xMyc-OBE3 to the MAX2 protein (Figure 4.23 B). Unlike for SMXL5, the triple HA tag was fused to the N-terminus of MAX2, since this position was reported to work in interaction studies with SMXL proteins (Wang et al. 2015). In Westerns, 3xHA-MAX2 was detected at a size of approximately 80 kDa in the protein extract and was efficiently immunoprecipitated by α-HA beads (Figure 4.23 B). This size matched the expected sizes of MAX2 (76.23 kDa) plus 3xHA (5 kDa). Although 6xMyc-OBE3 again co-immunoprecipitated with SMXL5-3xHA, 6xMyc-OBE3 was absent in samples containing 3xHA-MAX2 (Figure 4.23 B). This indicated that SMXL5 specifically interacts with OBE3 *in planta*.

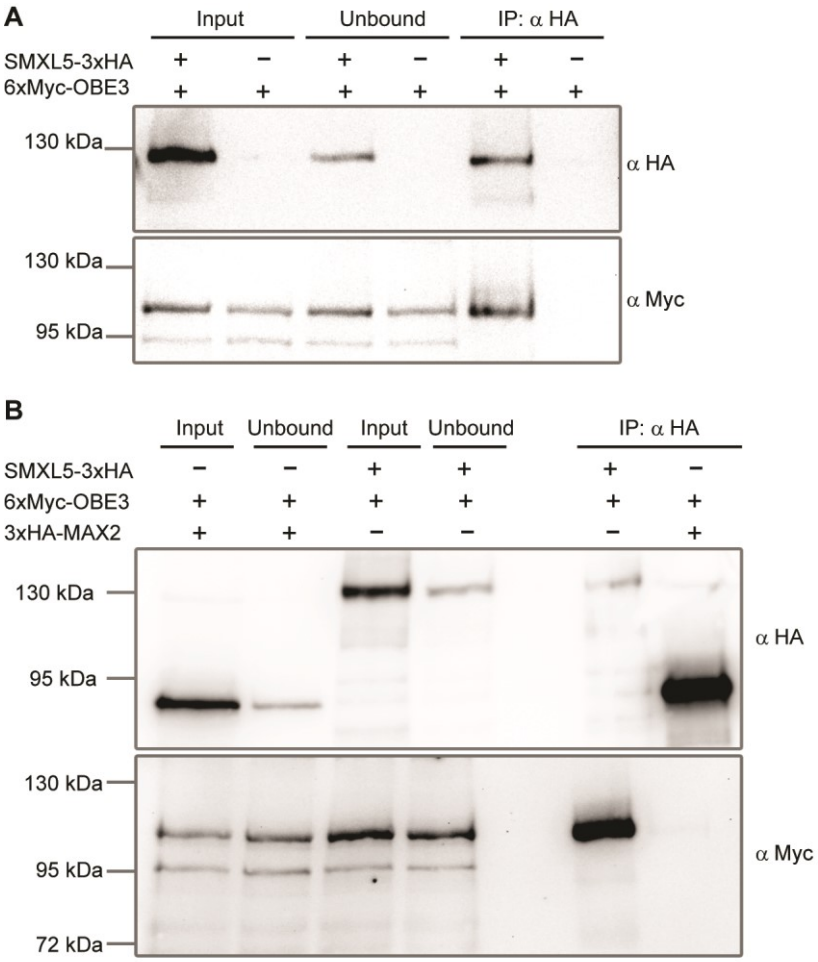

Figure 4.23: co-IP of SMXL5-OBE3 after transient expression in *Nicotiana*
Two independent Western blots depicting immunoprecipitation (IP) of SMXL5-3xHA with co-immunoprecipitation of 6xMyc-OBE3. Protein extracts were obtained from *Nicotiana* leaves after transient co-expression of *35S:SMXL5-3xHA* together with *35S:6xMyc-OBE3* (1.31 µg/µl protein in 2 ml extract) and *35S:6xMyc-OBE3* alone (1.64 µg/µl protein in 1.5 ml extract) (A) or *35S:3xHA-MAX2* together with *35S:6xMyc-OBE3* (1.86 µg/µl protein in 2 ml extract) and *35S:SMXL5-3xHA* with *35S:6xMyc-OBE3* (1.65 µg/µl protein in 2 ml extract) (B). "Input" fractions represent the protein content of the unprocessed protein extract: In A, 22.5 µl extract were loaded, resulting in 29.5 µg for SMXL5-3xHA with 6xMyc-OBE3 and 37 µg protein for 6xMyc-OBE3 alone. In B, equal amounts of 37.2 µg protein were loaded for both samples. "Unbound" fractions show proteins that remained in the extract after immunoprecipitation by α-HA-beads and "IP: α HA" depicts proteins that were immunoprecipitated after binding to α-HA-beads (SMXL5-3xHA and 3xHA-MAX2) or co-immunoprecipitated via a protein-protein interaction partner (6xMyc-OBE3). Western blots marked by "α HA" show protein bands detected by the α-HA-antibody, whereas Western blots marked by "α Myc" show protein bands detected by the α-Myc-antibody. SMXL5-3xHA runs at an expected size of approximately 120 kDa. 6xMyc-OBE3 showed a band at the expected 92 kDa and a slightly bigger one at around 100 kDA. 3xHA-MAX2 was detected as expected at around 80 kDa. α-HA-blots show IPs for SMXL5-3xHA (A) and SMXL5-3xHA and 3xHA-MAX2 (B). α-Myc-blots show that the bigger version of 6xMyc-OBE3 was co-immunoprecipitated with SMXL5-3xHA (A and B), but not with the unrelated 3xHA-MAX2 (B).

4.4.3 *SMXL3/4/5* and *OBE3* are expressed in the embryo

OBEs are known to be important regulators of embryonic meristem initiation and SAM and RAM maintenance (Lin et al. 2016; Saiga et al. 2008; Saiga et al. 2012; Thomas et al. 2009). *OBE1/2* and *OBE3/4* act redundantly in establishing the hypophysis and in orchestrating its division by modulating the expression of *ARF5/MP* downstream targets during early embryo development (Saiga et al. 2012). Among a few other functions (Lin et al. 2016), this is the best characterized role of *OBEs* so far. Consequently, I investigated the expression pattern of

OBE3:OBE3-GFP in early torpedo stage embryos and compared it to promoter activities of *SMXL3, SMXL4* and *SMXL5* at the same developmental stage (Figure 4.24). All *OBE* family members are ubiquitously expressed from early embryo stages onwards (Saiga et al. 2008; Saiga et al. 2012). I was able to confirm the ubiquitous expression of *OBE3-GFP* and additionally found that *SMXL3, SMXL4* and *SMXL5* promoters showed already provasculature-specific activity in torpedo stage embryos (Figure 4.24). This was particularly interesting since it indicated that *SMXL3/4/5* already play a role during embryogenesis and provascular pattern formation of the RAM. Interestingly, the *SMXL3* promoter was mostly active in provascular cells of the root (Figure 4.24 D-F), whereas *SMXL4* and *SMXL5* promoters were active in the whole provasculature of basal and apical organs (Figure 4.24 G-L). The location with the highest potential for protein-protein interaction was therefore the provasculature, where *SMXL3/4/5* activities and *OBE3-GFP* expression overlapped.

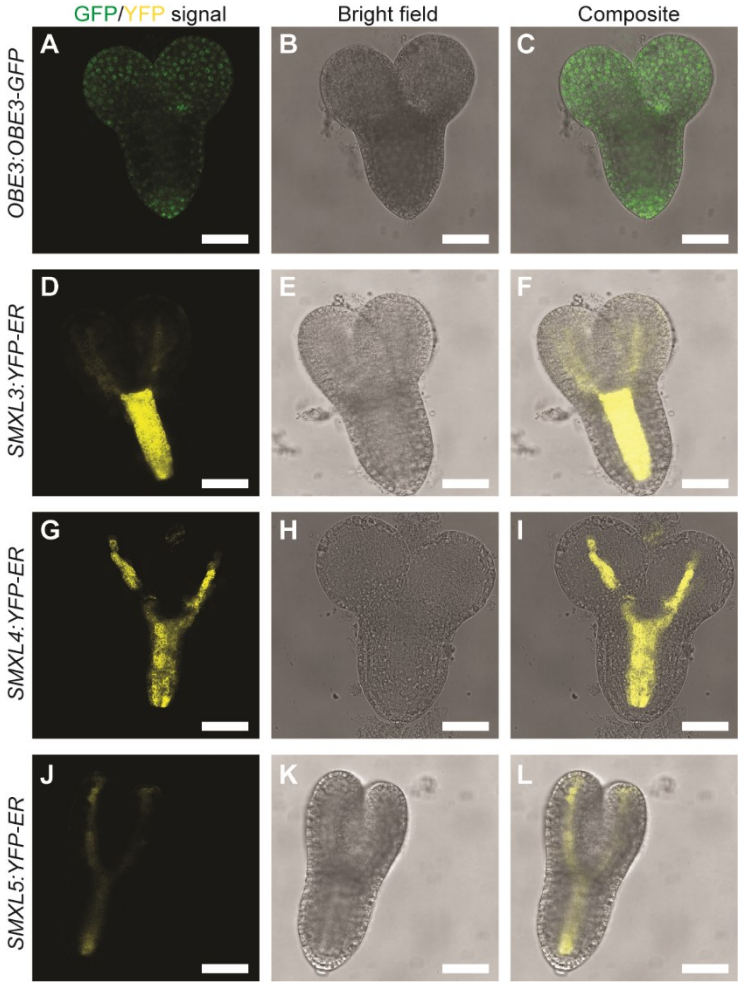

Figure 4.24: *SMXL3/4/5* promoter activities are provascular-specific while *OBE3* is ubiquitously expressed in *Arabidopsis* embryos
Confocal images of freshly extracted *Arabidopsis* embryos at the early torpedo stage. Depicted are fluorescent channels for GFP or YFP (A, D, G and J), bright field images (B, E, H and K) and composite pictures that represent an overlay of fluorescent signal and bright field image (C, F, I and L). *OBE3:OBE3-GFP* showed ubiquitous expression pattern within the embryo (green signal in A-C). SMXL3 promoter activity was specific for provascular tissues of the developing stele (D-F), whereas promoter activities of *SMXL4* (G-I) and *SMXL5* (J-L) were active in the whole provasculature (yellow signals). Scale bars represent 50 µm.

4.4.4 *OBE3* interacts with *SMXL3/4/5* to promote root length

To investigate whether *OBE3* and its redundantly acting partner *OBE4* genetically interact with *SMXL3/4/5* during early stages of embryogenesis or vegetative growth, I crossed

obe3/+;*obe4* to *smxl4;smxl5* and *smxl3* mutants. Interestingly, all double mutants were viable and RAMs were initiated in all cases (Figure 4.25 A). This indicated that establishing the hypophysis was independent from *SMXL3/4/5* function. However, roots of *smxl4;obe3* and *smxl5;obe3* double mutants were significantly shorter than those of the analysed single mutants or wild type. In contrast to my expectation based on the concerted action of *OBE3* and *OBE4* during embryogenesis, though, *smxl4;obe4* and *smxl5;obe4* showed no root growth defect (Figure 4.25 A and B), which may suggest that *OBE3* and *OBE4* execute different functions depending on their protein-binding partners. Compared to *smxl4;smxl5*, *smxl4;obe3* and *smxl5;obe3*, double mutants, *smxl3;obe3* grew equally short roots (Figure 4.25 C and D). Thus, I concluded that *OBE3* genetically interacts with *SMXL3/4/5* genes in root growth.

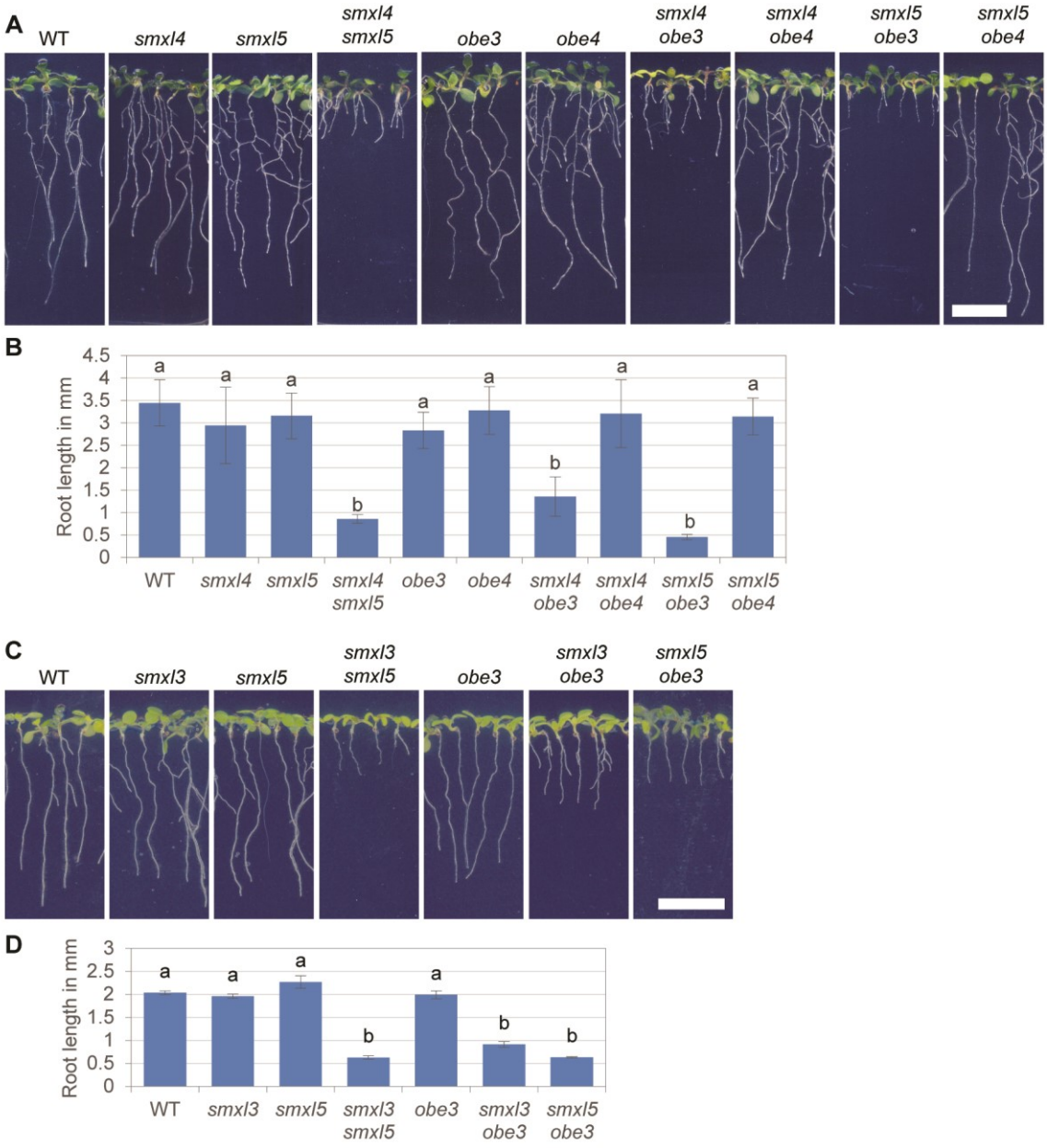

Figure 4.25: Double mutants *smxl5;obe3*, *smxl4;obe3* and *smxl3;obe3* are short rooted

A Root of 10 day-old *Arabidopsis* seedlings. Wild type, *smxl4, smxl5, smxl4;smxl5, obe3, obe4, smxl4;obe3, smxl4;obe4, smxl5;obe3, smxl5;obe4* lines are shown from left to right. Scale bar represents 1 cm.
B Lengths of roots depicted in A were quantified. Mean values of four independent experiments (n = 15-55 per experiment and genotype) were analysed by a one-way ANOVA with post-hoc Tukey HSD (95 % CI). Two statistical groups (a and b) were identified and showed that *smxl4;obe3* and *smxl5;obe3* were as short rooted as *smxl4;smxl5*.
C Roots of 10 day-old *Arabidopsis* seedlings. Wild type, *smxl3, smxl5, smxl3;smxl5, obe3, smxl3;obe3, smxl5;obe3* lines are shown from left to right. Scale bar represents 1 cm.
D Lengths of roots depicted in C were quantified. Mean values of three independent experiments (n = 62-74 per experiment and genotype) were analysed by a one-way ANOVA with post-hoc Tamhane-T2 (95 % CI). Two statistical groups (a and b) were identified and showed that *smxl3;obe3* and was as short rooted as *smxl3;smxl5*.

Besides *OBE3* and *OBE4*, which redundantly act in embryonic root initiation, the same redundant function was reported for *OBE1* and *OBE2* (Saiga et al. 2008; Saiga et al. 2012). Since *OBE2* was identified as a prey of *SMXL5* in the Yeast Two-Hybrid screen, I investigated a potential genetic interaction of *SMXL4/5* with *OBE1/2*. I thus generated *smxl4;obe1, smxl4;obe2, smxl5;obe1* and *smxl5;obe2* double mutants and compared their root lengths to wild type (Figure 4.26). Surprisingly, none of the tested double mutants showed a reduction in root length. This again indicated that the genetic interaction between *SMXL3/4/5* and *OBE3* was specific.

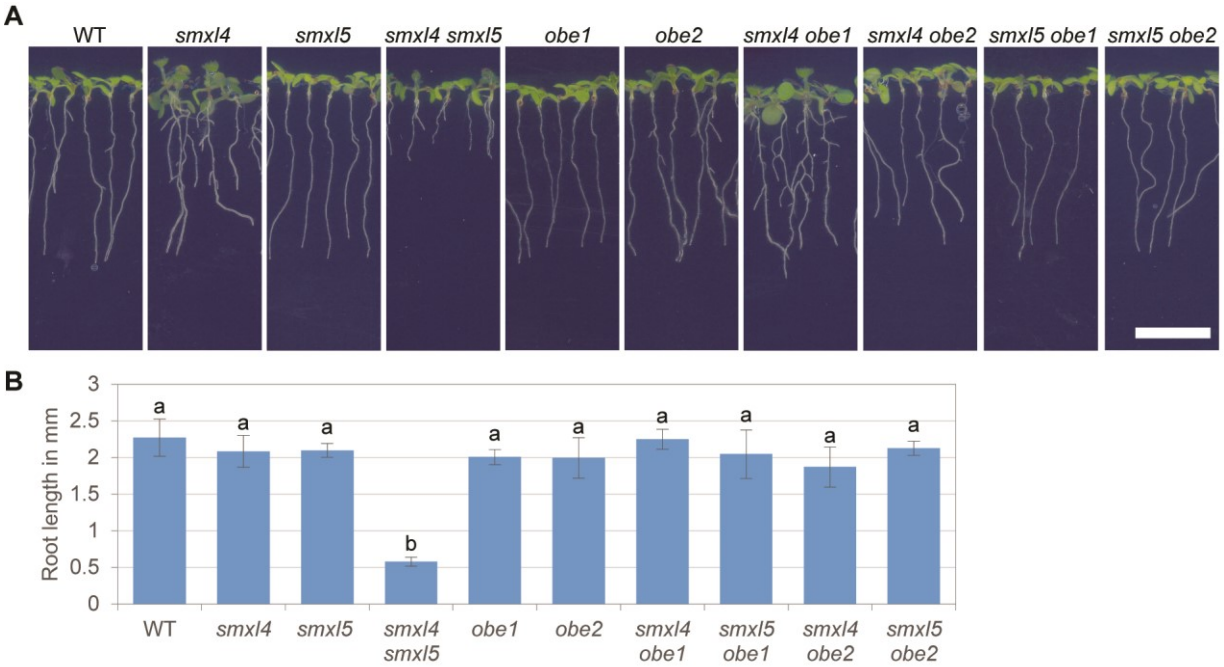

Figure 4.26: SMXL4/5 do not genetically interact with OBE1/2
A Root of 10 day-old *Arabidopsis* seedlings. Wild type, *smxl4, smxl5, smxl4;smxl5, obe1, obe2, smxl4;obe1, smxl4;obe2, smxl5;obe1, smxl5;obe2* lines are shown from left to right. Scale bar represents 1 cm.

B Lengths of roots depicted in A were quantified. Mean values of three independent experiments (n = 34-75 per experiment and genotype) were analysed by a one-way ANOVA with post-hoc Tukey HSD (95 % CI). Two statistical groups (a and b) were identified and showed that no genetic interaction between OBE1/2 and SMXL4/5 was detected in controlling root growth.

4.4.5 *OBE3* acts together with *SMXL3/4/5* in protophloem formation

To determine what causes the short-rooted *smxl3;obe3, smxl4;obe3* and *smxl5;obe3* phenotype, I analysed in which tissue type SMXL3/4/5 and OBE3 proteins potentially interact. As already shown in Figure 4.24, *OBE3* is ubiquitously expressed in the embryo, whereas *SMXL3/4/5* are very specific for (pro)-vascular phloem tissues (Figure 4.1, 4.10 and 4.24). Since *SMXL3/4/5* were identified as essential regulators of protophloem formation in young RAMs, I compared the expression patterns of *SMXL4:SMXL4-YFP* to those of *OBE1:OBE1-GFP, OBE2:OBE2-GFP, OBE3:OBE3-GFP* and *OBE4:OBE4-GFP* within root tips (Figure 4.27). I thereby aimed for identifying cell types harbouring both SMXL4 and OBE3 and potential differences to the other, not genetically interacting OBE family members. Among *SMXL3/4/5*, *SMXL4* showed the most specific expression pattern in RAMs, which was almost exclusively restricted to the developing protophloem strands (Figure 4.27 A and 4.1). To visualize PSEs, I counterstained the root tips by DirectRed, which - similarly to PI - stains cellulose and thus increases the fluorescence of differentiated PSEs (Ursache et al. 2018) (see white arrows in Figure 4.27). Interestingly, OBE1-GFP, OBE2-GFP, OBE3-GFP and OBE4-GFP indeed resided in the nuclei of all root cells, including the developing protophloem strands (Figure 4.27 B-E). Consequently, OBEs harbour the capacity to interact with SMXL3/4/5 proteins in immature protophloem strands.

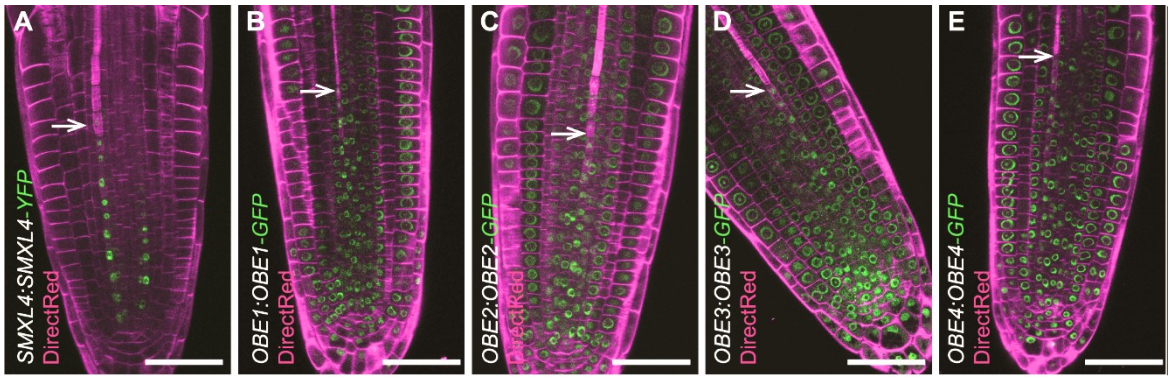

Figure 4.27: OBEs can potentially interact with SMXL3/4/5 in developing protophloem
RAMs of 7 day-old transgenic *Arabidopsis* seedlings expressing *SMXL4:SMXL4-YFP* (A), *OBE1:OBE1-GFP* (B), *OBE2:OBE2-GFP* (C), *OBE3:OBE3-GFP* (D) and *OBE4:OBE4-GFP* (E). Fluorescent signals (green) were detected by confocal microscopy and roots were counterstained by DirectRed (magenta). Differentiated PSEs showed enhanced DirectRed staining and are marked by white arrows. All OBEs are ubiquitously expressed (B-E). OBE-GFP fusion proteins were also found in developing protophloem strands, which coincides with the localization of SMXL4-YFP (A). Scale bars represent 50 µm.

To determine whether *OBE3* activity within the *SMXL5* domain was sufficient to promote root length, I generated a stable line expressing *SMXL5:OBE3-turquoise* in the *smxl5;obe3* double mutant background (Figure 4.28 A and B). Expression of *SMXL5:OBE3-turquoise* restored root growth in *smxl5;obe3* mutants (Figure 4.28 A and D). Confocal microscopy of root tips counterstained with DirectRed confirmed that OBE3-turquoise resided within the *SMXL5* domain (Figure 4.28 B and C). Additionally, I tested the genetic interaction between *SMXL5* and *OBE3* by expressing two different *miRNAs* targeting *OBE3* transcripts under the control of the *SMXL5* promoter in the *smxl5* mutant background (Figure 4.28 B and C). This *SMXL5*-domain-specific knock-down of *OBE3* significantly reduced the root length of *smxl5* (Figure 4.28 A and D). Of note, none of the two *miRNAs* supressed root growth in 100 % of the population. Whether this observed variation in root length was due to differences in copy number and *OBE3* transcript levels is subject of ongoing investigations. Nevertheless, the reduction in root length after tissue-specific expression of *OBE3-miRNAs* reinforced my previous results for which I used the only available and published *obe3* mutant allele (Figure 4.25). Taken together, my experiments indicated that the SMXL5-OBE3 interaction was specific for phloem and procambium tissues.

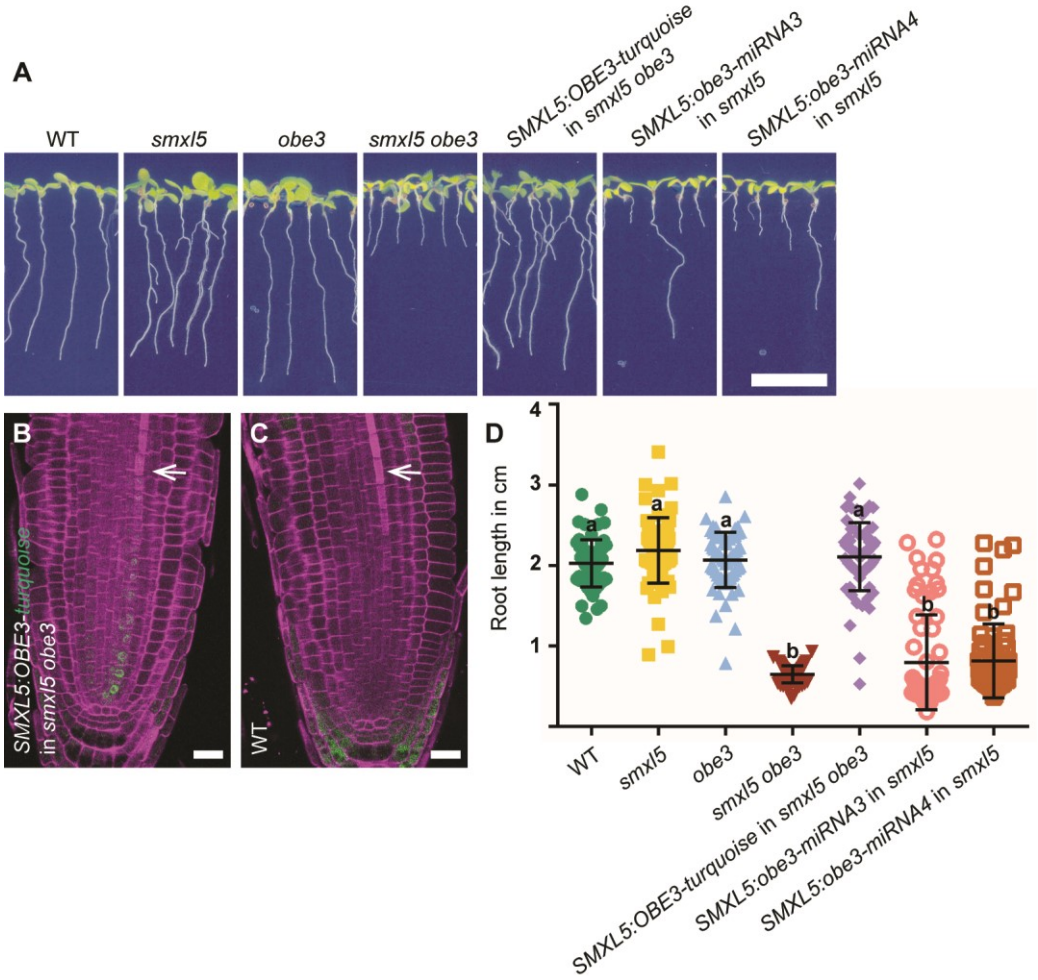

Figure 4.28: *SMXL5*-specific *OBE3* expression is sufficient to promote root growth

A Roots of 10 day-old *Arabidopsis* seedlings. Wild type, *smxl5, obe3, smxl5;obe3, SMXL5:OBE3-turquoise* in *smxl5;obe3*, *SMXL5:obe3-miRNA3* in *smx5* and *SMXL5:obe3-miRNA4* in *smx5* lines are shown from left to right. Scale bar represents 1 cm.
B-C RAMs of 7 day-old *Arabidopsis* seedlings expressing *SMXL5:OBE3-turquoise* in *smxl5;obe3* (B) were compared to a non-transformed wild type control (C). Fluorescent signals (green) were detected by confocal microscopy and roots were counterstained by DirectRed (magenta). Differentiated PSEs showed enhanced DirectRed staining and are marked by white arrows. The OBE3-turquoise fusion protein was exclusively located within the *SMXL5* domain, including the developing protophloem. Scale bars represent 20 µm.
D Lengths of roots depicted in A were quantified. One out of three independent experiments (n = 61-71 per experiment and genotype) is shown. Mean values were analysed by a one-way ANOVA with post-hoc Tamhane-T2 (95 % CI). Two statistical groups (a and b) were identified and showed that *SMXL5:OBE3-turquoise* can fully restore *smxl5;obe3* root growth, whereas *SMXL5*-specific knock down of *OBE3* by expression of *SMXL5:obe3-miRNA3* and *4* reduced root lengths.

Although the initial defect of *smxl3;obe3, smxl4;obe3* and *smxl;obe3* might have its true origin in changes during embryonic pattern formation, root growth happens post-embryonically (ten Hove et al. 2015). Since *smxl3;smxl4, smxl4;smxl5 and smxl3;smxl5* double mutants were short rooted due to impaired (proto-)phloem formation (Figure 4.3, 4.6, 4.8 and 4.17 as well as (Wallner et al. 2017)), I investigated whether a similar phloem-related defect exists in *smxl4;obe3* and *smxl5;obe3*. As before (Figure 4.6), I stained 2 day-old wild type, *obe3, obe3;smxl4* and *obe3;smxl5* root tips by mPS-PI and investigated whether enhanced PI staining revealed differentiated PSEs. Interestingly, differentiated PSEs were detected in wild type and *obe3* single mutants, but were absent in *smxl4;obe3* and *smxl5;obe3* double mutants (Figure 4.29). Moreover, I took a closer look at the two tangential divisions initiating phloem/procambium and

proto-/metaphloem cell identities, respectively (see orange and blue arrows in Figure 4.29 and 4.6). By measuring the distances of both tangential divisions to the QC, a significant delay of the second tangential phloem division was detected in *smxl4;obe3* and *smxl5;obe3* (Figure 4.29 C and D). Astonishingly, the delay of proto- and metaphloem initiation was equally pronounced as in *smxl4;smxl5* double mutants (Figure 4.29 E). Thus, I concluded that *smxl4;smxl5*, *smxl4;obe3* and *smxl5;obe3* double mutants all share the same developmental defects: Proto-phloem initiation and differentiation is impaired. Consequently, OBE3 is the first identified protein-protein interaction partner of SMXL5 that acts together with SMXL3/4/5 as an essential mediator of phloem formation.

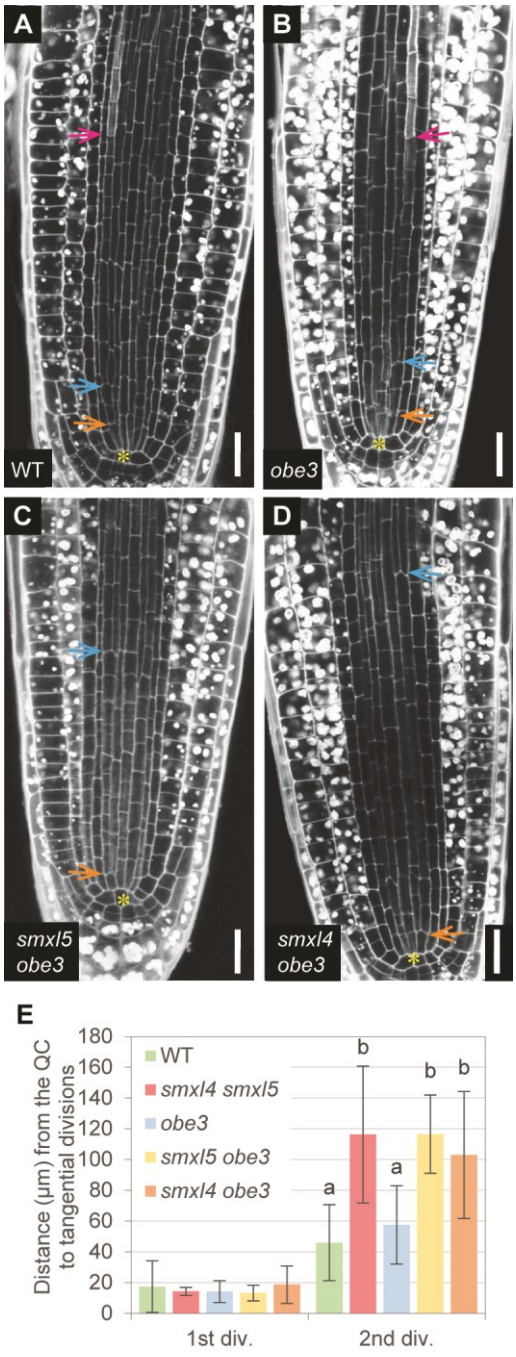

Figure 4.29: Protophloem initiation is delayed and SE differentiation is absent in *smxl5 obe3*

A-D 2 day-old mPS-PI stained RAMs of wild type (A), *obe3* (B), *smxl5;obe3* (C) and *smxl4;obe3* (D). In wild type and *obe3* the tangential divisions (orange and blue arrows) are close to each other and the QC (yellow asterisks). PSEs differentiate by changing their cell wall composition, which is reflected by enhanced PI staining (pink arrows). In *smxl4;obe3* and *smxl5;obe3* the second tangential cell division is delayed (blue arrows) and PSEs do not differentiate. Scale bars represent 20 µm.

E The distance from the QC to the first and second tangential division shown in A-D was quantified (n = 9-11). Statistical groups are indicated by letters and were determined by a one-way ANOVA with post-hoc Tukey HSD (95 % CI).

5 Discussion

5.1 *SMXL3/4/5* are early promoters of protophloem formation

Protophloem is an essential conduit that regulates transport and unloading of energy metabolites into sink organs for storage or to fuel stem cell activity (Ross-Elliott et al. 2017; Lucas et al. 2013). Spatio-temporal regulation of its development is therefore a critical hub to regulate meristem activity, which in turn affects the overall plant phenotype, growth capacity and vitality (Anne and Hardtke 2017). To understand and modulate plant morphodynamics and potentially increase crop yield, it is important to investigate the underlying molecular networks that control protophloem development.

Although several important phloem regulators have been studied in recent years and genetic interactions and dependencies are beginning to emerge (Blob et al. 2018), none of the investigated genes is required to obtain protophloem cell identity in the first place (Rodriguez-Villalon et al. 2014; Depuydt et al. 2013; Rodriguez-Villalon 2016). In this study I identified the previously underexplored *SMXL* sub-clades 2 and 3 as novel and crucial regulators of protophloem formation. Unlike other factors, *SMXL3/4/5* are already expressed in phloem initials adjacent to the QC and during early stages of embryogenesis. *OBE3* is their first identified interaction partner that acts in the same pathway: *OBE3* and *SMXL3/4/5* together promote early protophloem formation and differentiation.

5.1.1 *SMXL3/4/5-OBE3* in the context of other phloem regulators

The *SMXL3/4/5-OBE3* module in protophloem formation is a promising and important new regulator which substantially contributes to the existing network of phloem regulation. To integrate those new factors into the molecular network, it is important to discuss their potential interaction with known phloem regulators in light of their pattern of gene expression.

Since *SMXL3/4/5* are the first described phloem regulators that are already evidentially expressed in SE-procambium stem cells, it can be hypothesized that their initial role in those cells is largely independent from genes with a later onset of gene expression. *OPS* is the so far only investigated phloem regulator whose expression coincides with *SMXL3/4/5* in the first daughter cell, the SE-procambium precursor (Rodriguez-Villalon et al. 2014; Truernit et al. 2012). Other genes, such as *BRX, CVP2, CVL1, BAM3* and *CLE45* show promoter activity after the first tangential cell division of the SE-procambium precursor into the SE precursor and procambium. The mutants *brx*, *ops* and *cvp2;cvl1* are also not completely deprived of protophloem formation, but show a seemingly random failure of PSE differentiation, which results in the appearance of gap cells (Rodriguez-Villalon et al. 2015; Scacchi et al. 2009; Scacchi et al. 2010; Depuydt et al. 2013). However, in 2 day-old *smxl4;smxl5* double mutant roots none of the PSEs

differentiate, which indicates that *SMXL3/4/5* hold a quite fundamental role in protophloem formation.

In fact, the *smxl4;smxl5* double mutant phenotype can be nicely recapitulated in wild type roots treated with CLE45 (Depuydt et al. 2013). CLE45 is one of 27 different CLE peptides that are proteolytically processed into 12-14 amino acid long ligands to bind specific transmembrane receptors of the LRR-RLK family (Strabala et al. 2006; Anne et al. 2018). CLE-signalling occurs during many developmental processes and in various organs (Hazak and Hardtke 2016; Hu et al. 2018; Ogawa et al. 2008; Fletcher et al. 1999; Etchells and Turner 2010). Thus, members of the CLE family show quite diverse expression patterns and only a few members are present in vascular tissues of the root (Jun et al. 2010). Interestingly, 19 root-active CLEs can induce a short-rooted phenotype that mimics the *smxl4;smxl5* root morphology (Kinoshita et al. 2007). Recent studies especially focused on CLE45 and CLE26, which are specifically expressed in the phloem and have the strongest effect on root length (Depuydt et al. 2013; Czyzewicz et al. 2015). The LRR-RLK BAM3 has a specific affinity to CLE45 and, as expected for a receptor, *bam3* mutants are fully CLE45 insensitive (Depuydt et al. 2013; Rodriguez-Villalon et al. 2014; Hazak et al. 2017). The BAM3-CLE45 interaction negatively regulates PSE differentiation and suppresses the positive protophloem regulators *OPS* and *BRX* (Depuydt et al. 2013; Rodriguez-Villalon et al. 2014). Moreover, *BAM3* expression is enhanced by the pseudokinase CRN (Hazak et al. 2017). CRN dimerizes with the receptor-like protein CLV2 and has already been shown to act together with CLV1 in CLV3 perception (Müller et al. 2008). Likewise, an interaction of BAM3 with CRN is required for CLE45 sensing (Hazak et al. 2017). Several famous RLK-CLE-mediated signalling pathways rely on an interaction with co-receptors, such as SOMATIC EMBRYOGENESIS RECEPTOR KINASEs (SERKs) (Hu et al. 2018; Zhang et al. 2016; Hohmann et al. 2018). Of note, SERKS do not play a role in BAM3-CLE45 signalling and CRN lacks a kinase domain, which suggests that it cannot act as a classical co-receptor (Müller et al. 2008; Hazak et al. 2017). In fact, the CRN-CLV2 dimer seems to mediate sensitivity to several - if not all - root-active CLE peptides via a yet unidentified mechanism (Hazak et al. 2017). CLE26, whose sensing also requires an interaction of CRN-CLV2, acts redundantly to the BAM3-CLE45 pathway, but its receptor is still unknown (Anne et al. 2018). The *LRR-RLK CLE-RESISTANT RECEPTOR KINASE (CLERK)* was identified in a forward genetic screen of CLE26-insensitive mutants (Anne et al. 2018). Unlike BAM3 which has 20-30 LRR extracellular domains, CLERK exhibits only 3-4 extracellular LRR domains and is a SERK homologue (Shiu and Bleecker 2001; Anne et al. 2018). Surprisingly, *CLERK* is very specifically expressed in the developing protophloem and its promoter is already active in the phloem initial (Anne et al. 2018). Thus, *CLERK* is the only so far reported gene whose expression pattern completely overlaps with those of *SMXL3/4/5*. Although *clerk* mutants show resistance to CLE26 and CLE45 treatments, CLERK does neither bind CLE26 nor CLE45. Consequently, CLERK is yet another potential co-receptor

that is involved in CLE-sensing (Anne et al. 2018). Since *clerk;brx* mutants were still CLE26 sensitive, CLERK-mediated CLE-perception seems to act independently of the BAM3-CLE45 and BRX network. What makes *CLERK* so interesting with regard to *SMXL3/4/5* is the observation that promoter activity of the phloem-specific *CVP2*-marker appeared earlier in *clerk* mutants than in wild type. Thus, *CLERK* seems to restrict the transition from meristematic protophloem to differentiation, similar to *BAM3* (Anne et al. 2018; Depuydt et al. 2013). Considering the role of *SMXL3/4/5* as promoters of protophloem initiation and differentiation, protophloem-specific CLE-signalling seems to counteract their function. Unlike *brx, ops* or *cvl1;cvp2*, the *smxl4;smxl5* double mutant does not only show gap cells, but perfectly mimics CLE-treated wild type seedling. Consequently, *SMXL3/4/5* could be involved in suppressing endogenous CLE levels in the root or attenuating the expression or activity of RLK-CLE downstream effectors, such as *MEMBRANE-ASSOCIATED KINASE REGULATOR 5* (*MAKR5*), which is a positive amplifier of CLE45-mediated signalling (Kang and Hardtke 2016). Likewise, *SMXL3/4/5* gene or protein activity could be also affected by CLE-signalling in roots. Further studies are needed to integrate *SMXL3/4/5* into this complex and tightly regulated network of phloem regulators.

5.1.2 Does it all start in the embryo?

Besides promoting PSE differentiation, *SMXL3/4/5* play an additional role in spatio-temporal regulation of proto- and metaphloem initiation. The initiation of those cell identities takes place in form of a tangential cell division within the SE precursor cell lineage. In 2 day-old *smxl4;smxl5* double mutants this tangential division is already significantly delayed compared to wild type. Similarly, a delay or even absence of the tangential division was reported for *apl, ops, brx* and *cvp2;cvl2* mutants (Bonke et al. 2003; Rodriguez-Villalon et al. 2014; Rodriguez-Villalon et al. 2015). Likewise, CLE45 treatment of 4 day-old wild type roots induces loss of PSE differentiation within 20 hours and loss of the tangential division within 30 hours (Rodriguez-Villalon et al. 2015). Moreover, the tangential division is negligible when it comes to PSE and MSE differentiation: After recovering roots from CLE45 treatment, PSEs start to differentiate before the tangential division is re-established and mutants, such as *brx* or *ops*, still specify MSEs at the correct position. Although the exact mechanism was not specifically investigated, it was suggested that procambium cells adopt proto- or metaphloem cell identity even if those cells were not initiated by a tangential division in the first place (Rodriguez-Villalon et al. 2014). Based on these observations it has been hypothesized that the missing tangential division is an indirect side effect following an interrupted PSE differentiation (Rodriguez-Villalon et al. 2015). Although this is a valid assumption, the dynamics and position of the tangential division was not followed over time and the respective experiments were conducted at least 4 days post germination. At this time-point *smxl4;smxl5* RAMs are already too impaired to dissect primary from secondary defects. Thus, I conducted the experiments in 2 day-old seedlings, whose RAM morphology is still comparable to wild type. At this stage, *smxl4;smxl5* seedlings already showed a

very definite and reproducible delay of the tangential division. There are two possible explanations: First of all, the delay could be induced with the onset of vegetative growth, meaning that the distance between QC and tangential division increases over time at a certain rate. Secondly, the delay of this tangential division could have been pre-determined during embryogenesis. The pattern formation of the primary root is already completed in late-stage embryos (Scheres et al. 1995). Consequently, incipient proto- and metaphloem are established and the tangential division that initiates proto- and metaphloem identity can be already observed (Bauby et al. 2007). This indicates that embryonic establishment of proto- and metaphloem cell identities does not depend on the presence of differentiated PSEs or MSEs. Since *SMXL3/4/5* promoters show specific activity within provascular tissues of torpedo-stage embryos, they could contribute to RAM pattern formation already during embryogenesis. One aspect that makes this hypothesis interesting, is the observation that grafted *smxl4;smxl5* seedlings show GFP translocation within the phloem quite efficiently in adventitious roots. Moreover, adventitious roots tend to outgrow primary roots in *smxl4;smxl5* and possibly contribute to overall plant fitness. Of note, adventitious and lateral roots are not pre-determined in the embryo, but are post-embryonically induced by de-differentiation of pericycle cells (Laskowski et al. 1995). Consequently, the origin and initial regulation of primary and secondary roots differs fundamentally. The notion that *smxl4;smxl5* primary roots are especially impaired suggests early developmental defects, which could already be determined in the embryo.

5.2 *SMXL3/4/5* regulation by hormones

SMXL family members of sub-clade 1 and sub-clade 4 are the central mediators of KAR and SL signalling, respectively (Soundappan et al. 2015; Stanga et al. 2016; Stanga et al. 2013; Wang et al. 2015). To identify whether *SMXL3/4/5*, which build sub-clade 2 and 3, mediate hormonal signalling pathways or are even proteolytic targets of SL/KAR signalling, I conducted several experiments.

5.2.1 SMXL3/4/5 proteins are SL/KAR independent

Interestingly, SMXL3/4/5 proteins differ in a specific amino acid sequence (RGKTGI) that was reported essential for MAX2-dependent ubiquitination (Wang et al. 2015; Wallner et al. 2016; Jiang et al. 2013; Zhou et al. 2013). Of note, a deletion of those amino acids only affects ubiquitination and not binding of the MAX2/D3-D14 complex to the SMXL rice orthologue D53 (Jiang et al. 2013; Zhou et al. 2013). In *Arabidopsis*, SMXL6/7/8 are specifically targeted for ubiquitination by MAX2-D14 in a SL-dependent manner (Wang et al. 2015; Jiang et al. 2013; Soundappan et al. 2015). A mutagenized version of SMXL6, SMXL6D, that shows a deletion of four amino acids within the RGKTGI-motif is no longer ubiquitinated nor degraded upon *rac-*

GR24 treatment (Wang et al. 2015). Moreover, overexpression of *SMXL6D* induces a branchy phenotype similar to the high-tillering mutant *d53*, which indicates that SL-signalling was successfully compromised by the constitutively active and non-degradable SMXL6D version (Jiang et al. 2013; Wang et al. 2015). Interestingly, the RGKTGI amino acid sequence is conserved throughout SMXL orthologues of various species and can even be found in non-vascular plants, such as the liverwort *Marchantia spp* (Moturu et al. 2018). Only among angiosperms, SMXL3/4/5 have incorporated distinct changes in the RGKTGI degron (Moturu et al. 2018; Wallner et al. 2016). In line with this observation, my findings indicate that SMXL3/4/5 proteins are resistant to SL/KAR-mediated degradation. Moreover, *SMXL3/4/5* are not mediators of *MAX2* activity, since the phenotype of *smxl4;smxl5;max2* is simply additive and *max2* does not show any defects during protophloem formation. Although a genetic interaction cannot be ruled out in other developmental processes and growth stages, previous studies already investigated a potential contribution of *SMXL4/5* to branching regulation and came to the same conclusion: *SMXL4/5* play no role in branching regulation and act independently from *MAX2* (Soundappan et al. 2015). Since *SMXL3/4/5* are not directly involved in mediating SL- or KAR-signalling, the question whether there is a signalling pathway that targets SMXL3/4/5 proteins remains. One repeatedly discussed potential regulator of SMXL3/4/5 is the receptor DWARF14-LIKE2 (DLK2). D14, KAI2 and DLK2 all belong to the same family of α/β-hydrolases (Bythell-Douglas et al. 2017). DLK2 possesses the catalytic triade (Ser-102, Asp-223, His-253) and can weakly hydrolyse the synthetic SL enantiomer GR24$^{ent\text{-}5DS}$ (Vegh et al. 2017). While KAI2 and D14 bind KAR and SL, respectively, the natural ligand for DLK2 is so far unknown (Vegh et al. 2017; Kagiyama et al. 2013; Zhao et al. 2015). Similar to SMXL3/4/5, DLK2 behaves a bit differently from its homologues when it comes to *rac*-GR24 induced degradation. Unlike D14 and KAI2, degradation of DLK2 is not induced upon *rac*-GR24 treatment (Chevalier et al. 2014; Waters et al. 2014; Vegh et al. 2017). Moreover, *dlk2* mutants show normal growth and exhibit no *max2*-specific phenotypes, such as branching or abnormal photomorphogenic responses (Vegh et al. 2017; Shen et al. 2007; Waters et al. 2012). Interestingly, not protein activity, but *DLK2* expression is dependent on *MAX2* and *KAI2* and upregulated during SL/KAR signalling (Waters and Smith 2013; Stanga et al. 2013; Scaffidi et al. 2014). Consequently, *DLK2* is tightly connected to SL/KAR signalling pathways, but most likely not directly involved (Vegh et al. 2017). This behaviour is very similar to *SMXL3/4/5*, which can be functionally replaced by the KAR-signalling target *SMAX1* if expressed under the *SMXL5* promoter, but are themselves SL/KAR resistant. Whether DLK2 is indeed the long-sought receptor that signals via SMXL3/4/5 has yet to be investigated.

5.2.2 PSE differentiation and *SMXL5* expression are regulated by auxin

The plant hormone auxin plays a role in many fundamental growth processes and was recently described as important regulator of protophloem formation in a *BRX*-mediated molecular rheostat. The study showed that BRX interacts with the D6 PROTEIN KINASE (D6PK)-like protein kinase PROTEIN KINASE ASSOCIATED WITH BRX (PAX) at the rootward end of the PM to modulate the auxin flux within PSEs (Marhava et al. 2018). Auxin is polarly transported by PIN-FORMED (PIN) proteins that co-localize with BRX and PAX at the basal PM (Marhava et al. 2018; Adamowski and Friml 2015). Cellular auxin flux and definite auxin levels determine organ patterning (Blilou et al. 2005). During root formation, an auxin maximum positions the QC, comparatively low auxin levels are found in dividing daughter cells and higher levels can be observed in differentiating cells, such as PSEs (Marhava et al. 2018; Santuari et al. 2011; Grieneisen et al. 2007; Sabatini et al. 1999). Auxin efflux is modulated by D6PK- and PINOID (PID)-dependent phosphorylation of PINs (Barbosa et al. 2014; Zourelidou et al. 2014; Weller et al. 2017). In protophloem formation, it was proposed that BRX blocks auxin efflux by binding PAX at the PM. Consequently, auxin levels within the cell rise until a certain threshold is reached at which BRX dispatches and PAX becomes active. If PAX is not bound to BRX, it phosphorylates PIN and auxin is transported out of the cell. If the auxin efflux is inhibited, PSEs fail to differentiate. This important dynamic rheostat is genetically supported, since the *pax* mutant phenotype shows gap cells similar to *brx* (Marhava et al. 2018). Of note, BRX also modulates ARF activity and is in itself activated by the transcription factor ARF5/MP (Santuari et al. 2011). Thus, there is a tight interplay between auxin and important protophloem regulators.

Since *SMXL3/4/5* are fundamental and novel protophloem regulators, it would be interesting to explore a possible connection to auxin flux or signalling. Interestingly, *SMXL5* is a reported target of ARF3, which is also known as ETTIN (ETT) (Simonini et al. 2017). During canonical auxin signalling, auxins, such as IAA, bind the F-box protein and receptor TRANSPORT INHIBITOR RESPONSE 1 (TIR1). This induces ubiquitination of Aux/IAA repressor proteins, which otherwise repress ARF activity by binding to their PB1 (Phox/BemIp) domain (Guilfoyle 2015; Dharmasiri et al. 2005). ARF3 lacks the PB1 domain and is therefore not directly involved in canonical auxin signalling (Simonini et al. 2016). Instead of modulating ARF3 activity via Aux/IAA suppressors, auxin changes the ARF3 binding capacity to certain promoters, such as *SMXL5*. Consequently, *SMXL5* transcription is induced by ARF3 binding to its promoter, but downregulated in the presence of the natural auxin IAA, since IAA leads to detachment of ARF3 from the *SMXL5* promoter region. Of note, the ARF3 targets were identified by chromatin immunoprecipitation sequencing (ChIPseq) analysis conducted in inflorescence tissues. Although *SMXL3* and *SMXL4* also appear in the ChIPseq, their potential modulation by ARF3 is not conclusive (Simonini et al. 2017). For *SMXL3* this could be for instance explained by the weak

expression pattern in above-ground organs. Nevertheless, *SMXL3/4/5* are promising candidates for playing an important role in auxin-dependent protophloem formation.

5.3 *SMXL4/5* are regulated on the mRNA level

Post-transcriptional regulation is an important and common mechanism to modulate transcript abundance and consequently protein synthesis rates. So far, two interesting and completely independent mechanisms have been described to target *SMXL4/5* mRNAs for silencing or translational inhibition (Cho et al. 2018; Wu et al. 2017).

5.3.1 *SMXL4/5* are targets of post-translational gene silencing

Gene silencing utilizes many different regulatory mechanisms which involve small, double-stranded RNA sequences commonly known as small interfering RNAs (siRNAs) (Borges and Martienssen 2015). One pathway that targets unwanted transcripts involves trans-acting small interfering RNAs (ta-siRNAs) that originate from *TAS* genes. *TAS* gene transcripts are processed by ARGONAUTE (AGO) proteins AGO1 or AGO7 within a RNA-induced silencing complex (RISC) according to a micro RNA (miRNA) template. The processed transcript is converted into double stranded RNA (dsRNA) by RNA-DEPENDENT RNA POLYMERASE 6 (RDR6) and SUPPRESSOR OF GENE SILENCING 3 (SGS3) and cleaved by the DICER-LIKE 4 (DCL4) ribonuclease into 21 nucleotide (nt) long ta-siRNAs and DCL2 in 22 nt long ta-siRNAs (Dunoyer et al. 2005; Xie et al. 2005; Yoshikawa et al. 2005; Parent et al. 2015). Those ta-siRNAs are loaded into AGO1 as template to target specific transcripts for degradation (Yoshikawa 2013). An important target of ta-siRNA-mediated silencing is for instance *ARF3* (Williams et al. 2005; Fahlgren et al. 2006). In *dcl4* mutants or when DCL4 function is compromised by viral infections, DCL2 substitutes for DCL4, which leads to accumulation of 22 nt long ta-siRNAs (Xie et al. 2005; Wu et al. 2017; Bouche et al. 2006). Cleavage products of 22 nt long ta-siRNAs are not degraded, but further processed into secondary siRNAs by the siRNA pathway that is usually triggered after viral infection or after introducing a transgene (Chen et al. 2010; Jouannet 2011; Baulcombe 2004). Surprisingly, secondary siRNAs are produced in *dcl4* mutants that target the protein-coding transcripts of *SMXL4* and *SMXL5*. Consequently, *dcl4* mutants exhibit the same developmental defects and phenotypes that can be found in *smxl4;smxl5* double mutants, including short roots and increased sugar and starch levels in source tissues (Wu et al. 2017). Unlike viral genes or transgenes, *SMXL4* and *SMXL5* show only low transcript abundance within a very restricted tissue type. It is thus unclear why they are targeted by post-transcriptional gene silencing in the absence of DCL4. However, it is intriguing that besides *SMXL4* and *SMXL5* also *BAM3* is among the five genes that show the highest production of siRNAs in *dcl4* mutants (Wu et al. 2017). Taken those observations together, I hypothesize that *SMXL4* and *SMXL5* are not just coincidental off-targets. Summarizing the so far discussed aspects, an evident pattern

emerges: *ARF3* is a target of DCL4-dependent ta-siRNAs to regulate spatio-temporal organ patterning and positively regulates *SMXL5* transcription if auxin levels are low (Fahlgren et al. 2006; Simonini et al. 2017). Auxin levels spatio-temporally control protophloem formation (Marhava et al. 2018). *SMXL4/5* are fundamental phloem regulators whose mutant phenotype can be mimicked by CLE45 treatments (Depuydt et al. 2013; Wallner et al. 2017). Transcripts encoding for the CLE45 receptor *BAM3* and both positive phloem regulators *SMXL4* and *SMXL5* are targeted for gene silencing if DCL4 function is compromised (Wu et al. 2017). Consequently, I propose that a complex molecular network involving post-transcriptional gene silencing, *SMXL4/5*, CLE-mediated signalling and auxin-mediated responses is required for proper spatio-temporal protophloem formation.

5.3.2 JULGI controls *SMXL4/5* translation by RNA G-quadruplex formation

A quite fascinating mechanism that regulates *SMXL4* and *SMXL5* translation was identified by a collaborating research group. The mechanism centres around a zinc-finger RNA-binding protein called JULGI (JUL) that binds the 5' UTR of *SMXL4* and *SMXL5* to induce and stabilize a G-quadruplex structure that inhibits *SMXL4/5* mRNA translation (Cho et al. 2018). G-quadruplexes are 3D structures of DNA or RNA that represent an alternative interaction and folding mechanism to the commonly known Watson-Crick model. The formation of G-quadruplexes requires guanine (G)-rich sequences that are folded into stacked G-quartets and hold together by hydrogen-bonds. Each G-quartet consists out of four G bases that are assembled in a planar fashion (reviewed in Bugaut and Balasubramanian 2012). Those structures are found in both prokaryotes and eukaryotes and serve important regulatory functions (Song et al. 2016). DNA G-quadruplexes, for instance, are formed at the 3' overhang of telomeres to protect chromosomes from telomerase activity (Wang and Patel 1993; Bugaut and Balasubramanian 2012). RNA G-quadruplexes are found in translational control of many transcripts encoding for human oncogenes, epigenetic regulators or transcription factors (Song et al. 2016; Wolfe et al. 2014).

In plants, G-quadruplex motifs can be detected in many cambium and phloem-specific mRNAs, such as *SMXL4/5, BAM3, HIGH CAMBIUM ACTIVITY 2 (HCA2), NEN1* or *SEOR2* (Cho et al. 2018). Of note, G-quadruplex formation via JUL was so far only investigated and proven for *SMXL4/5* transcripts. The *JUL* and *SMXL3/4/5* expression patterns nicely coincide in phloem and (pro-)cambium. If sucrose levels are high, *JUL1/2* are induced to stabilize G-quadruplex formation at the 5'UTR of *SMXL4/5* transcripts. This dampens their translation and consequently suppresses phloem formation. The mechanism builds a unique regulatory hub within vascular plants to balance phloem formation: Overexpression of *JUL1* and its homologue *JUL2* leads to *smxl4;smxl5*-specific phloem defects, whereas suppression of *JUL1/2* results in enhanced phloem formation and an increase in sink strength due to accumulation of SMXL4/5 proteins. Seeds produced in *JUL1/2* knock-down lines were significantly larger, which again

highlights the importance of *SMXL4/5* as promoters of plant fitness and even suggests potential applications to increase crop yield (Cho et al. 2018). Interestingly, *SMXL3* transcripts do not seem to form a G-quadruplex. Since *SMXL3* promoter activity is predominantly found in the root, it could be speculated that *SMXL3* is required to ensure protophloem formation in the RAM. Even if sucrose levels are high and JUL1/2 targets *SMXL4/5* transcripts to restrict additional sugar transport into sinks, the connection of differentiating PSEs to the RAM has to be maintained.

5.4 *SMXL3/4/5* fulfil distinct functional roles

Although *SMXL3/4/5* act redundantly during protophloem formation in the RAM, those three genes show distinct differences in expression pattern, onset of expression, regulation and subtle differences in function.

For instance, *SMXL3* and *SMXL5* expression is induced at different time points during phloem formation. In the *in-vitro* system called Vascular Cell Induction Culture System Using *Arabidopsis* Leaves (VISUAL) leaf mesophyll cells are reprogrammed into procambium cells and subsequently into phloem and xylem by exposing leaves to the Glycogen synthase kinase 3 proteins (GSK3) inhibitor bikini (Kondo et al. 2015; Kondo et al. 2014). Even if procambium, phloem and xylem formation is ectopically induced, the underlying molecular regulators remain the same and can be investigated under controlled conditions (Kondo et al. 2015; Kondo et al. 2016). Interestingly, Kondo et al. 2016 categorized genes involved in phloem formation according to their onset of gene expression into four different modules. While *SMXL5* resides together with *BAM3, HCA2, SEOR2* and other important and early phloem regulators in the first module, *SMXL3* was grouped into module III. *SMXL4* could not be detected by the array (Kondo et al. 2016). Of note, VISUAL is an artificial system and I did not detect different onsets of *SMXL3/4/5* activity in promoter-reporter lines. Nonetheless, this data suggests that *SMXL3/4/5* might be differentially regulated and could fulfil slightly diverse roles during phloem formation.

5.4.1 *SMXL3* and *SMXL5* act on procambium formation

In comparison to the phloem-specific *SMXL4* gene, promoter activities of *SMXL3* and *SMXL5* are slightly broader and can not only be found in developing proto- and metaphloem but also in the procambium. Moreover, *SMXL3* promoter activity is even detected in the PPP. It is therefore likely that *SMXL3/5* fulfil additional roles in the procambium that are independent from *SMXL4*. Indeed, *SMXL3* acts together with *SMXL5* in promoting procambial divisions in the stele. Already in 2 day-old roots, *smxl3;smxl5* double mutants show a significant reduction in stele cell number, whereas procambial divisions are unaffected in *smxl4;smxl5* and *smxl3;smxl4* mutants. This is a very interesting and defined difference between the functional role of *SMXL4* and *SMXL3/5*. Recent data from one of our collaborating groups proposes a complex, regulatory

machinery that spatio-temporally determines vascular divisions during radial root growth (Miyashima et al. personal communication). In this study, the role of *PHLOEM EARLY DOF 1 (PEAR1)* and *PEAR2* transcription factors, also known as *DOF2.4* and *DOF 5.1*, respectively, was investigated. *PEAR* transcription factors are specifically expressed in developing PSEs, but show protein movement into adjacent procambium cells. The expression of *PEAR1/2* and its homologues *OBP2/DOF1.1, DOF6/DOF3.2, TMO6/DOF3.4* and *HCA2/DOF5.6* is induced by cytokinin signalling to promote periclinal cell divisions in the procambium. Consequently, the data suggests that initial radial growth in form of procambial divisions occurs around PSEs. *Class III HOMEODOMAIN LEUCINE ZIPPER (HD-ZIP III)* genes act in a negative feedback loop to counteract *PEAR* activity. Interestingly, *SMXL3* is a reported direct downstream-target of PEAR transcription factors. Ectopic overexpression of either *PEAR2* or *SMXL3* results in a massive increase of vascular cells in the stele (Miyashima et al. personal communication). Although *SMXL5* seems to act together with *SMXL3* in inducing periclinal procambium divisions, *SMXL5* was not reported to be a direct downstream target of PEARs. Consequently, several possible scenarios exist: *SMXL3* and *SMXL5* could fulfil the same function within their expression domain, although being differentially regulated by PEARs or ARF3, respectively (Miyashima et al. personal communication) (Simonini et al. 2017).

5.4.2 *SMXL5* promotes secondary phloem formation

Differences in the regulatory roles of *SMXL3/4/5* become especially apparent when looking at cambium dynamics and phloem formation in the stem. While *SMXL3* expression is largely absent in above ground organs, *SMXL4* and *SMXL5* show distinct promoter activities in differentiated phloem and proposed phloem-precursors, respectively. Even more surprisingly, *SMXL5* activity alone is sufficient to induce secondary phloem formation within IC regions. Interestingly, only *smxl4;smxl5* double mutant stems show an additional increase in CDT production, which is absent in the respective single mutants. This indicates that the increased CDT production in *smxl4;smxl5* reflects a pleiotropic gene function and not a secondary side effect induced by the absence of phloem differentiation. Moreover, grafting *smxl4;smxl5* plants onto wild type roots also indicates that the observed cambium phenotype in *smxl4;smxl5* stems is caused by a local absence of *SMXL4/5* and not by an impaired root system or by elevated sugar levels. I thus hypothesize that *SMXL5* acts on phloem formation and additionally suppresses cambium activity in concert with *SMXL4*. These observations not only indicate that *SMXL4* and *SMXL5* hold special functional roles, they could also help to elucidate long-standing questions about cambium regulation and potential cambium sub-domains.

Unlike in the RAM, above-ground organs establish phloem and xylem *de-novo* from (pro-)cambium cells (Scarpella and Helariutta 2010). Although this suggests a tight interconnectedness between cambium activity and vascular tissue production, the relation between

those two processes has proven to be quite complex. Overexpression of the transcription factor *HCA2/DOF5.6*, for instance, induces IC activity and the abundance of secondary phloem, but downregulates xylem-related genes (Guo et al. 2009). This exemplifies that cambium activity not necessarily correlates with the amounts of produced xylem and phloem tissues. In fact, known cambium markers are either expressed towards the distal phloem or the proximal xylem side. This bipartite organization can be observed for the LRR-RLKs *MOL1* and *PXY*, which counteract each other to balance cambium homeostasis (Etchells et al. 2016; Gursanscky et al. 2016). Besides *MOL1*, *SMXL5* is the first gene that marks both phloem and distal cambium cells during radial growth. Its investigation is therefore of great interest to determine cambial sub-domains and to understand their dynamics. While cell identities and spatio-temporally controlled division events can be determined for each cell within the RAM (Cederholm et al. 2012; Rodriguez-Villalon et al. 2014), it is up-to date not clear which cells actually divide within the cambium nor if a dormant organizing centre exists (Sánchez 2013). *SMXL5* fulfils a much conserved role as a major phloem regulator across different organs and growth stages. Comparing its function in phloem proliferation and differentiation between the well-studied RAM and the IC could therefore help to shed some light on cambium regulation. The RAMs of *smxl4;smxl5* show a delay of the second tangential cell division within the phloem cell lineage. Consequently, one possibility would be that more SE precursor cells are produced without splitting tangentially to acquire proto- and metaphloem cell fate (Wallner et al. 2017; De Rybel et al. 2016). Of note, the actual cell identity of those additional, non-tangentially dividing cells still needs to be determined. Comparing this phenotype to the cambium, we can observe a similar behaviour: More cambium-derived vascular cells are produced in *smxl4;smxl5*. Towards the phloem side those “phloem-precursors” fail to differentiate. Their cell identity and differentiation stage is still unknown. However, deducing the situation from the RAM, we can hypothesize that those “precursors” are the cells dividing excessively in *smxl4;smxl5* and not necessarily the actual cambium stem cells. This hypothesis assumes the existence of different cambium sub-domains with distinct behaviour.

5.4.3 *SMXL4* is the most specific phloem gene and linked to salt stress

The astonishing vascular-specificity of *SMXL4* was already described in 2014, before its actual role in plant development became clear (Zhang et al. 2014a). Interestingly, the promoter region of *SMXL4*, which is also known as *Arabidopsis HEAT SHOCK PROTEIN RELATED (AtHSPR)*, contains several proposed cis-regulatory elements that are mostly involved in stress- and environmental responses, such as cold, heat, salt, pathogen or wounding (Zhang et al. 2014a). It has been shown that *SMXL4* expression can be enhanced by treating plants with the hormone abscisic acid (ABA) or salt (Yang et al. 2015; Finkelstein 2013). Mutants of *smxl4* react hypersensitive to salt and are impaired in ABA-induced closure of stomata (Yang et al. 2015;

Lim et al. 2015). Since stomata opening and closure is an essential hub for regulating transpiration and gas exchange, *smxl4* single mutants are especially prone to drought stress (Yang et al. 2015). Based on transcriptome analysis and an increase in stress and reactive oxygen species (ROS) responsive genes in *smxl4*, it was thus hypothesized that *SMXL4* plays a role in promoting antioxidative response mechanisms against salt-induced ROS (Yang et al. 2016). Of note, similar stress-responsive and redox-homeostasis-mediating genes, such as *GLUTAREDOXINs (GRXSs)* (Meyer et al. 2008) are also up-regulated in the transcriptome of our grafted *smxl4;smxl5* stem bases. There are two possible explanations: First of all, those stress responses are a consequence of impaired phloem formation and the resulting imbalance in metabolite homeostasis and transport. Since *SMXL3/4/5* acts dose-dependently in phloem formation, *smxl4* single mutants are - although not phenotypically apparent in our laboratory conditions - slightly compromised in growth and therefore hypersensitive to a variety of stresses (Yang et al. 2016). The second possibility is that *SMXL4* is indeed directly and actively involved in antioxidative stress responses. SMXL family members are closely related to HSP101, which is an essential regulator of thermotolerance (Queitsch et al. 2000). Thus, it can be speculated that *SMXLs* are involved in modulating growth responses according to environmental conditions. This is an interesting aspect for future studies, since it could directly link environmental cues to phloem formation.

5.5 Hypothesizing about a SMXL-OBE3 chromatin remodelling complex

The PHD-finger protein OBE3 is the first identified interaction partner of SMXL3/4/5. OBEs act in SAM maintenance as well as embryonic root initiation and vascular patterning during embryogenesis (Lin et al. 2016; Saiga et al. 2008; Saiga et al. 2012; Thomas et al. 2009). OBEs are proposed members of a chromatin remodelling complex that modulates chromatin states and thereby regulates transcription. During embryogenesis, OBEs are reported key factors for transcription of the *MP/ARF5* downstream targets *TMO5* and *TMO7* (Saiga et al. 2008; Saiga et al. 2012). Since OBE3 is nuclear localized and ubiquitously expressed, its contribution to several diverse growth processes is not surprising. It is therefore tempting to speculate about a role of SMXL3/4/5-OBE3 complexes in transcriptional regulation of important phloem regulators. Deciphering the role of the SMXL5-OBE3 protein complex could thus provide new knowledge about transcriptional regulation and chromatin remodelling.

Chromatin describes a tightly organized association between genomic DNA that is wrapped twice (147 bp) around octamers of histone proteins formed by H2A-H2B and H3-H4 dimers (Hauer and Gasser 2017; Luger et al. 1997). Together, histones and DNA form nucleosomes, which are the core building blocks of chromatin and stabilized by H1 (Figure 5.1) (Hauer and Gasser 2017; Hergeth and Schneider 2015). Histone modifications fundamentally determine the strength of interaction between negatively-charged DNA and positively-charged amino

acid-residues on histones (Hauer and Gasser 2017). This fine-tuned modulation of chromatin states and thus accessibility of promoter regions is an essential regulatory hub that controls gene transcription in eukaryotes. Whereas euchromatin is associated with active gene transcription, heterochromatin is densely packed and found in transcriptionally inactive regions, such as telo- and centromeres (Tamaru 2010). Post-translational histone modifications can be manifold and include heterochromatin-promoting methylation of lysine or arginine as well as euchromatin-promoting acetylation of lysine residues at H3 (Lachner and Jenuwein 2002; Shahbazian and Grunstein 2007). Chromatin remodelling complexes are essential machineries that modulate and translocate nucleosomes to regulate transcription (Erdel et al. 2011; Voss and Hager 2014). Their function is ATP-dependent and requires a nucleosome-interacting domain, such as a bromo-associated homology domain (BAH), a plant homeodomain (PHD) or chromodomain (CHD) as well as ATPase activity (Erdel et al. 2011).

Interestingly, OBE3 carries a PHD zinc-finger (Figure 5.1) (Saiga et al. 2008). PHD fingers can read the modification state of H3K4, H3K14 and H3R2 and - depending on the protein - bind preferentially to methylated, unmodified or even acetylated H3 residues (Sanchez and Zhou 2011).

Quite fittingly, most SMXLs display one or more predicted pore-loop NTPase domains that - if mapped by InterPro (EMBL-EBI, Cambridgeshire, UK) - are closely related to ATPases of the SNF2 superfamily and were also identified as AAA ATPase domains in D53 (Ma et al. 2017). The majority of chromatin remodellers with ATPase activity belong to the SNF2 family (Erdel et al. 2011). Moreover, AAA ATPases, such as SMXLs and D53, are known to allow hexamer formation, which suggests that SMXLs form homo- or heterohexamers with each other (Ma et al. 2017; Gardner et al. 2018). Preliminary data from our lab show that SMXL5 has the capacity to interact with itself after transient expression in *Nicotiana* (Vadir López-Salmerón, personal communication). Whether SMXLs truly interact in hexamers and whether their interaction is restricted to homo-hexamers, involves only members of a specific sub-clade or can transcend clades by incorporating all eight SMXL family members into a hetero-hexamer has yet to be determined. Interestingly, *SMXL5* can be functionally replaced by *SMAX1* if the latter is expressed under the *SMXL5* promoter. This indicates that *SMXL* family members are not restricted to a certain function by their sub-clade, but by their expression domain. Considering this, I speculate that all SMXL family members have the potential to be incorporated into a hexamer if residing in the same nucleus. The MAX2-dependent ubiquitination-motif of D53 and SMXL sub-clade 1 and 4 has recently been predicted to form a pore-loop, although the usually conserved tyrosine is replaced by a lysine. This additional positive charge could help to thread DNA through the pore-loop of a D53-hexamer for transcriptional regulation (Ma et al. 2017; Zhou et al. 2013). The fact that SMXL3/4 lack this amino acid sequence and that SMXL5 has no predicted pore-loop NTPase domain at all (Figure 5.1), could also significantly alter their role in DNA-interaction and transcriptional regulation. Consequently, the altered RGKTGI-sequence of SMXL3/4/5

makes them - once again - special in comparison to all other SMXL family members and their closer investigation even more compelling.

5.6 Conclusion and outlook

This study revealed novel and fundamental roles of the so far underexplored SMXL family members *SMXL3/4/5* in phloem formation and (pro-)cambium regulation. *SMXL3/4/5* act redundantly in spatio-temporal regulation of protophloem initiation and differentiation within the RAM. They are the first identified phloem regulators that are already active in phloem initials and the first reported genes whose double mutants are completely deprived of protophloem formation. Their function is therefore irreplaceable in maintaining the stem cell niche, root growth and plant vitality in general. Apart from their redundant function in protophloem formation, *SMXL3/4/5* show subtle, but important differences in expression pattern and function. *SMXL3* and *SMXL5* play additional roles in procambium formation of roots. *SMXL5* alone is sufficient to promote secondary phloem formation during radial growth, but acts together with *SMXL4* in suppressing CDT production. Unlike all other *SMXL* family members, *SMXL3/4/5* act independently from MAX2-mediated SL- and KAR-signalling and their encoded proteins are non-degradable by the SL/KAR-analogue *rac*-GR24. Interestingly, work from other groups show that *SMXL3/4/5* are transcriptionally regulated by *DOF* transcription factors, salt stress or auxin-dependent *ETT/ARF3*, respectively. Moreover, *SMXL4/5* protein levels are controlled post-transcriptionally by RNA silencing mechanisms and JUL-mediated G-quadruplex formation. The PHD-finger OBE3 is the first identified protein-protein interaction partner that mediates SMXL3/4/5-dependent protophloem formation during early vegetative growth. Intriguingly, 6xcMyc-OBE3 showed two bands in my Western blots: One with the expected size that did not co-immunoprecipitate with SMXL5-3xHA and another slightly larger version that did co-immunoprecipitate. Consequently, further studies should investigate whether OBE3 is post-translationally modified and whether this modification is required for a protein-protein-interaction with SMXL5. Moreover, the lack of genetic interaction with the other OBE family members should be further investigated. Similar to the study in OBE3-mediated SAM maintenance (Lin et al. 2016), only one mutant allele was used in this study for each *OBE* gene. Although they are published as functional knock-outs that show convincing effects on embryogenesis (Saiga et al. 2008; Saiga et al. 2012), it is not clear whether truncated versions of OBE1/2 and OBE4 proteins are still produced and sufficient to fulfil their function during phloem formation.

Based on the OBE and SMXL protein domains it can be hypothesized that OBE3-SMXL3/4/5 form chromatin remodelling complexes to control transcription of downstream targets, such as important phloem regulators (Figure 5.1). The identification of downstream targets is therefore an essential next step to gain a better mechanistic understanding of the SMXL3/4/5-OBE3 interaction. Moreover, it will allow to integrate *SMXL3/4/5* into the molecular network of

phloem regulation by either revealing a link to known phloem regulators or by describing a completely new pathway. Of note, SMXL and OBE proteins do not carry an obvious DNA-binding domain. If involved in chromatin remodelling, SMXL3/4/5-OBE3 complexes must contain additional binding partners with DNA-binding capability mediating target specificity. Identifying those transcription factors could generate fantastic new insights into phloem development that are of great interest for gaining a deeper understanding of phloem formation in particular and cell differentiation in general.

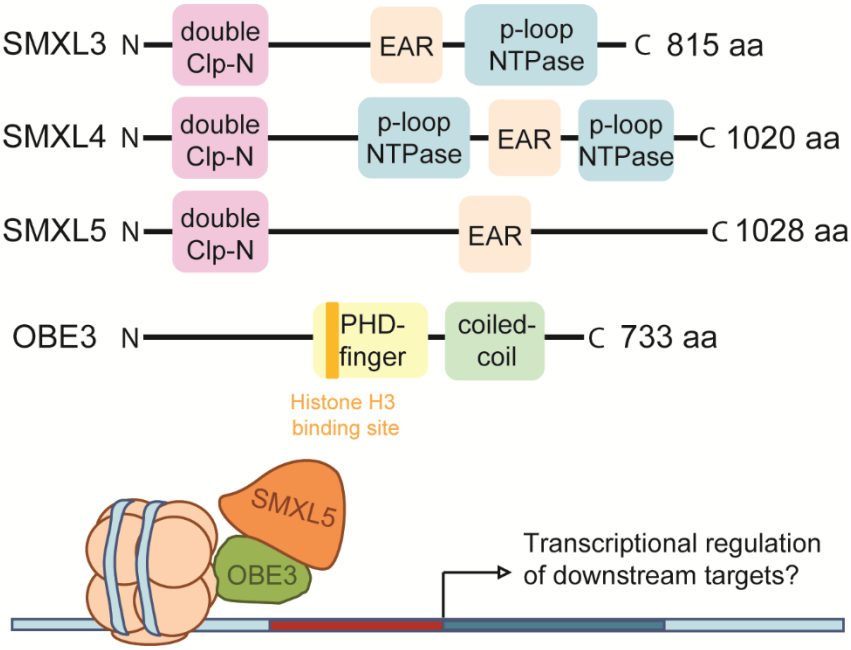

Figure 5.1 SMXL3/4/5 and OBE3 protein domains and working hypothesis
Shown are schematic representations of SMXL3, SMXL4, SMXL5 and OBE3 amino acid sequences with important protein domains predicted by InterPro (EMBL-EBI, Cambridgeshire, UK). In my working hypothesis, SMXL3/4/5 interact with OBE3 in a chromatin remodelling complex to modulate transcription of downstream targets.

6 List of publications

First-authorships:

Strigolactone- and Karrikin-Independent SMXL Proteins Are Central Regulators of Phloem Formation. **(2017)** Wallner ES, López-Salmerón V, Belevich I, Poschet G, Jung I, Grünwald K, Sevilem I, Jokitalo E, Hell R, Helariutta Y, Agustí J, Lebovka I, Greb T Curr Biol

Strigolactone versus gibberellin signaling: reemerging concepts? **(2016)** Wallner ES, López-Salmerón V, Greb T Planta

In preparation:
- *SMXL4/5 promote secondary phloem formation in the stem* (working title)
- *SMXL3/4/5 interact with OBE3 in phloem development* (working title)

Co-authorships:

Spatial specificity of auxin responses coordinates wood formation. (2018) Brackmann K, Qi J, Gebert M, Jouannet V, Schlamp T, Grünwald K, Wallner ES, Novikova DD, Levitsky VG, Agustí J, Sanchez P, Lohmann JU, Greb T Nat Commun, 9, 1, 875

Translational control of phloem development by RNA G-quadruplex–JULGI determines plant sink strength (2018) Cho H., Cho HS., Nam H., Jo H., Yoon J., Park C., Dang TVT., Kim E., Jeong J., Park S., Wallner ES., Youn H., Park J., Jeon J., Ryu H., Greb T., Choi K., Lee Y., Jang SK., Ban C., Hwang I. Nature Plants volume 4, pages 376–390

7 Index of figures and tables

8 References

Abe S, Sado A, Tanaka K, Kisugi T, Asami K, Ota S, Kim HI, Yoneyama K, Xie X, Ohnishi T, Seto Y, Yamaguchi S, Akiyama K, Yoneyama K, Nomura T (2014) Carlactone is converted to carlactonoic acid by MAX1 in Arabidopsis and its methyl ester can directly interact with AtD14 in vitro. Proceedings of the National Academy of Sciences of the United States of America 111 (50):18084-18089

Adamowski M, Friml J (2015) PIN-dependent auxin transport: action, regulation, and evolution. Plant Cell 27 (1):20-32

Agustí J, Herold S, Schwarz M, Sanchez P, Ljung K, Dun EA, Brewer PB, Beveridge CA, Sieberer T, Sehr EM, Greb T (2011a) Strigolactone signaling is required for auxin-dependent stimulation of secondary growth in plants. Proc Natl Acad Sci USA 108 (50):20242-20247

Agustí J, Lichtenberger R, Schwarz M, Nehlin L, Greb T (2011b) Characterization of Transcriptome Remodeling during Cambium Formation Identifies MOL1 and RUL1 as Opposing Regulators of Secondary Growth. PLoS Genet 7 (2):e1001312

Aichinger E, Kornet N, Friedrich T, Laux T (2012) Plant stem cell niches. Annual review of plant biology 63:615-636

Akiyama K, Matsuzaki K, Hayashi H (2005) Plant sesquiterpenes induce hyphal branching in arbuscular mycorrhizal fungi. Nature 435 (7043):824-827

Alberts BJ, A.; Lewis, J.; et al. (2002) Molecular Biology of the Cell. 4th edn. Garland Science, New York

Alder A, Jamil M, Marzorati M, Bruno M, Vermathen M, Bigler P, Ghisla S, Bouwmeester H, Beyer P, Al-Babili S (2012) The path from beta-carotene to carlactone, a strigolactone-like plant hormone. Science 335 (6074):1348-1351

Altamura MM, Possenti M, Matteucci A, Baima S, Ruberti I, Morelli G (2001) Development of the vascular system in the inflorescence stem of Arabidopsis. New Phytologist 151 (2):381-389

Anne P, Amiguet-Vercher A, Brandt B, Kalmbach L, Geldner N, Hothorn M, Hardtke CS (2018) CLERK is a novel receptor kinase required for sensing of root-active CLE peptides in Arabidopsis. Development (Cambridge, England) 145 (10)

Anne P, Hardtke CS (2017) Phloem function and development-biophysics meets genetics. Curr Opin Plant Biol 43:22-28

Atkinson NJ, Urwin PE (2012) The interaction of plant biotic and abiotic stresses: from genes to the field. Journal of experimental botany 63 (10):3523-3543

Awad AA, Sato D, Kusumoto D, Kamioka H, Takeuchi Y, Yoneyama K (2006) Characterization of Strigolactones, Germination Stimulants for the Root Parasitic Plants Striga and Orobanche, Produced by Maize, Millet and Sorghum. Plant Growth Regulation 48 (3):221

Barbosa IC, Zourelidou M, Willige BC, Weller B, Schwechheimer C (2014) D6 PROTEIN KINASE activates auxin transport-dependent growth and PIN-FORMED phosphorylation at the plasma membrane. Developmental cell 29 (6):674-685

Baroja-Fernandez E, Munoz FJ, Li J, Bahaji A, Almagro G, Montero M, Etxeberria E, Hidalgo M, Sesma MT, Pozueta-Romero J (2012) Sucrose synthase activity in the sus1/sus2/sus3/sus4 Arabidopsis mutant is sufficient to support normal cellulose and starch production. Proceedings of the National Academy of Sciences of the United States of America 109 (1):321-326

Barratt DH, Kolling K, Graf A, Pike M, Calder G, Findlay K, Zeeman SC, Smith AM (2011) Callose synthase GSL7 is necessary for normal phloem transport and inflorescence growth in Arabidopsis. Plant physiology 155 (1):328-341

Basson MA (2012) Signaling in cell differentiation and morphogenesis. Cold Spring Harb Perspect Biol 4 (6)

Bauby H, Divol F, Truernit E, Grandjean O, Palauqui JC (2007) Protophloem differentiation in early Arabidopsis thaliana development. Plant & cell physiology 48 (1):97-109

Baulcombe D (2004) RNA silencing in plants. Nature 431 (7006):356-363

Becraft PW (2002) Receptor kinase signaling in plant development. Annu Rev Cell Dev Biol 18:163-192

Beemster GT, Baskin TI (1998) Analysis of cell division and elongation underlying the developmental acceleration of root growth in Arabidopsis thaliana. Plant physiology 116 (4):1515-1526

Bennett T, Leyser O (2014) Strigolactone signalling: standing on the shoulders of DWARFs. Curr Opin Plant Biol 22:7-13

Bennett T, Scheres B (2010) Root development-two meristems for the price of one? Curr Top Dev Biol 91:67-102

Bennett T, Sieberer T, Willett B, Booker J, Luschnig C, Leyser O (2006) The Arabidopsis MAX pathway controls shoot branching by regulating auxin transport. Current biology : CB 16 (6):553-563

Bentsink L, Koornneef M (2008) Seed dormancy and germination. Arabidopsis Book 6:e0119

Bergmann DC, Sack FD (2007) Stomatal development. Annual review of plant biology 58:163-181

Beveridge CA, Kyozuka J (2010) New genes in the strigolactone-related shoot branching pathway. Curr Opin Plant Biol 13 (1):34-39

Blilou I, Xu J, Wildwater M, Willemsen V, Paponov I, Friml J, Heidstra R, Aida M, Palme K, Scheres B (2005) The PIN auxin efflux facilitator network controls growth and patterning in Arabidopsis roots. Nature 433 (7021):39-44

Blob B, Heo JO, Helariutta Y (2018) Phloem differentiation: an integrative model for cell specification. J Plant Res 131 (1):31-36

Bonke M, Thitamadee S, Mähönen AP, Hauser MT, Helariutta Y (2003) APL regulates vascular tissue identity in Arabidopsis. Nature 426 (6963):181-186

Booker J, Sieberer T, Wright W, Williamson L, Willett B, Stirnberg P, Turnbull C, Srinivasan M, Goddard P, Leyser O (2005) MAX1 encodes a cytochrome P450 family member that acts downstream of MAX3/4 to produce a carotenoid-derived branch-inhibiting hormone. Developmental cell 8 (3):443-449

Borges F, Martienssen RA (2015) The expanding world of small RNAs in plants. Nat Rev Mol Cell Biol 16 (12):727-741

Bouche N, Lauressergues D, Gasciolli V, Vaucheret H (2006) An antagonistic function for Arabidopsis DCL2 in development and a new function for DCL4 in generating viral siRNAs. The EMBO journal 25 (14):3347-3356

Bouwmeester HJ, Roux C, Lopez-Raez JA, Becard G (2007) Rhizosphere communication of plants, parasitic plants and AM fungi. Trends in plant science 12 (5):224-230

Brackmann K, Greb T (2014) Long- and short-distance signaling in the regulation of lateral plant growth. Physiologia plantarum 151 (2):134-141

Brackmann K, Qi J, Gebert M, Jouannet V, Schlamp T, Grünwald K, Wallner ES, Novikova DD, Levitsky VG, Agusti J, Sanchez P, Lohmann JU, Greb T (2018) Spatial specificity of auxin responses coordinates wood formation. Nat Commun 9 (1):875

Brand U, Fletcher JC, Hobe M, Meyerowitz EM, Simon R (2000) Dependence of stem cell fate in Arabidopsis on a feedback loop regulated by CLV3 activity. Science 289 (5479):617-619

Breda AS, Hazak O, Hardtke CS (2017) Phosphosite charge rather than shootward localization determines OCTOPUS activity in root protophloem. Proceedings of the National Academy of Sciences of the United States of America 114 (28):E5721-E5730

Brewer PB, Dun EA, Ferguson BJ, Rameau C, Beveridge CA (2009) Strigolactone acts downstream of auxin to regulate bud outgrowth in pea and Arabidopsis. Plant physiology 150 (1):482-493

Brewer PB, Dun EA, Gui R, Mason MG, Beveridge CA (2015) Strigolactone Inhibition of Branching Independent of Polar Auxin Transport. Plant physiology 168 (4):1820-1829

Brewer PB, Koltai H, Beveridge CA (2013) Diverse roles of strigolactones in plant development. Molecular plant 6 (1):18-28

Brewer PB, Yoneyama K, Filardo F, Meyers E, Scaffidi A, Frickey T, Akiyama K, Seto Y, Dun EA, Cremer JE, Kerr SC, Waters MT, Flematti GR, Mason MG, Weiller G, Yamaguchi S, Nomura T, Smith SM, Yoneyama K, Beveridge CA (2016) LATERAL BRANCHING OXIDOREDUCTASE acts in the final stages of strigolactone biosynthesis in Arabidopsis. Proceedings of the National Academy of Sciences of the United States of America 113 (22):6301-6306

Brown HR (2013) The Theory of the Rise of Sap in Trees: Some Historical and Conceptual Remarks. Physics in Perspective 15 (3):320-358

Bugaut A, Balasubramanian S (2012) 5'-UTR RNA G-quadruplexes: translation regulation and targeting. Nucleic acids research 40 (11):4727-4741

Burgess A, Vigneron S, Brioudes E, Labbe JC, Lorca T, Castro A (2010) Loss of human Greatwall results in G2 arrest and multiple mitotic defects due to deregulation of the cyclin B-Cdc2/PP2A balance. Proceedings of the National Academy of Sciences of the United States of America 107 (28):12564-12569

Bythell-Douglas R, Rothfels CJ, Stevenson DWD, Graham SW, Wong GK, Nelson DC, Bennett T (2017) Evolution of strigolactone receptors by gradual neo-functionalization of KAI2 paralogues. BMC Biol 15 (1):52

Campbell NA, Reece JB, Urry LA, Cain ML, Wasserman SA, Minorsky PV, Jackson RB (2016) Biologie, vol 10. Pearson Deutschland,

Cederholm HM, Iyer-Pascuzzi AS, Benfey PN (2012) Patterning the primary root in Arabidopsis. Wiley interdisciplinary reviews Developmental biology 1 (5):675-691

Chen HM, Chen LT, Patel K, Li YH, Baulcombe DC, Wu SH (2010) 22-Nucleotide RNAs trigger secondary siRNA biogenesis in plants. Proceedings of the National Academy of Sciences of the United States of America 107 (34):15269-15274

Chevalier F, Nieminen K, Sanchez-Ferrero JC, Rodriguez ML, Chagoyen M, Hardtke CS, Cubas P (2014) Strigolactone promotes degradation of DWARF14, an alpha/beta hydrolase essential for strigolactone signaling in Arabidopsis. Plant Cell 26 (3):1134-1150

Cho H, Cho HS, Nam H, Jo H, Yoon J, Park C, Dang TVT, Kim E, Jeong J, Park S, Wallner ES, Youn H, Park J, Jeon J, Ryu H, Greb T, Choi K, Lee Y, Jang SK, Ban C, Hwang I (2018) Translational control of phloem development by RNA G-quadruplex-JULGI determines plant sink strength. Nature plants:doi: 10.1038/s41477-41018-40157-41472

Conn CE, Bythell-Douglas R, Neumann D, Yoshida S, Whittington B, Westwood JH, Shirasu K, Bond CS, Dyer KA, Nelson DC (2015) Convergent evolution of strigolactone perception enabled host detection in parasitic plants. Science 349 (6247):540-543

Conn CE, Nelson DC (2015) Evidence that KARRIKIN-INSENSITIVE2 (KAI2) Receptors may Perceive an Unknown Signal that is not Karrikin or Strigolactone. Front Plant Sci 6:1219

Cook CE, Whichard LP, Turner B, Wall ME, Egley GH (1966) Germination of witchweed (Striga lutea Lour.): Isolation and properties of a potent stimulant. Science 154 (3753):1189-1190

Crawford S, Shinohara N, Sieberer T, Williamson L, George G, Hepworth J, Muller D, Domagalska MA, Leyser O (2010) Strigolactones enhance competition between shoot branches by dampening auxin transport. Development (Cambridge, England) 137 (17):2905-2913

Czyzewicz N, Shi CL, Vu LD, Van De Cotte B, Hodgman C, Butenko MA, De Smet I (2015) Modulation of Arabidopsis and monocot root architecture by CLAVATA3/EMBRYO SURROUNDING REGION 26 peptide. Journal of experimental botany 66 (17):5229-5243

Dastidar MG, Jouannet V, Maizel A (2012) Root branching: mechanisms, robustness, and plasticity. Wiley Interdisciplinary Reviews: Developmental Biology 1 (3):329-343

Daum G, Medzihradszky A, Suzaki T, Lohmann JU (2014) A mechanistic framework for noncell autonomous stem cell induction in Arabidopsis. Proceedings of the National Academy of Sciences of the United States of America 111 (40):14619-14624

Davies P (2010) Plant hormones: Biosynthesis, signal transduction, action!

De Rybel B, Adibi M, Breda AS, Wendrich J, Smit ME, Novák O, Yamaguchi N, Yoshida S, Van Isterdael G, Palovaara J, Nijsse B, Boekschoten MV, Hooiveld G, Beeckman T, Wagner D, Ljung K, Fleck C, Weijers D (2014) Integration of growth and patterning during vascular tissue formation in Arabidopsis. Science 345 (6197):1255215

De Rybel B, Mahonen AP, Helariutta Y, Weijers D (2016) Plant vascular development: from early specification to differentiation. Nat Rev Mol Cell Biol 17 (1):30-40

de Saint Germain A, Bonhomme S, Boyer FD, Rameau C (2013) Novel insights into strigolactone distribution and signalling. Curr Opin Plant Biol 16 (5):583-589

De Smet I, Vanneste S, Inze D, Beeckman T (2006) Lateral root initiation or the birth of a new meristem. Plant molecular biology 60 (6):871-887

De Smet I, Vassileva V, De Rybel B, Levesque MP, Grunewald W, Van Damme D, Van Noorden G, Naudts M, Van Isterdael G, De Clercq R, Wang JY, Meuli N, Vanneste S, Friml J, Hilson P, Jurgens G, Ingram GC, Inze D, Benfey PN, Beeckman T (2008) Receptor-like kinase ACR4 restricts formative cell divisions in the Arabidopsis root. Science 322 (5901):594-597

Delaux PM, Xie X, Timme RE, Puech-Pages V, Dunand C, Lecompte E, Delwiche CF, Yoneyama K, Becard G, Sejalon-Delmas N (2012) Origin of strigolactones in the green lineage. New Phytol 195 (4):857-871

Depuydt S, Rodriguez-Villalon A, Santuari L, Wyser-Rmili C, Ragni L, Hardtke CS (2013) Suppression of Arabidopsis protophloem differentiation and root meristem growth by CLE45 requires the receptor-like kinase BAM3. Proceedings of the National Academy of Sciences of the United States of America 110 (17):7074-7079

Dettmer J, Ursache R, Campilho A, Miyashima S, Belevich I, O'Regan S, Mullendore DL, Yadav SR, Lanz C, Beverina L, Papagni A, Schneeberger K, Weigel D, Stierhof YD, Moritz T, Knoblauch M, Jokitalo E, Helariutta Y (2014) CHOLINE TRANSPORTER-LIKE1 is required for sieve plate development to mediate long-distance cell-to-cell communication. Nat Commun 5:4276

Dharmasiri N, Dharmasiri S, Estelle M (2005) The F-box protein TIR1 is an auxin receptor. Nature 435 (7041):441-445

Dolan L, Janmaat K, Willemsen V, Linstead P, Poethig S, Roberts K, Scheres B (1993) Cellular organisation of the Arabidopsis thaliana root. Development (Cambridge, England) 119 (1):71-84

Dolzblasz A, Nardmann J, Clerici E, Causier B, van der Graaff E, Chen J, Davies B, Werr W, Laux T (2016) Stem Cell Regulation by Arabidopsis WOX Genes. Molecular plant 9 (7):1028-1039

Dun EA, de Saint Germain A, Rameau C, Beveridge CA (2012) Antagonistic action of strigolactone and cytokinin in bud outgrowth control. Plant physiology 158 (1):487-498

Dunoyer P, Himber C, Voinnet O (2005) DICER-LIKE 4 is required for RNA interference and produces the 21-nucleotide small interfering RNA component of the plant cell-to-cell silencing signal. Nat Genet 37 (12):1356-1360

Dupuy L, Mackenzie J, Haseloff J (2010) Coordination of plant cell division and expansion in a simple morphogenetic system. Proceedings of the National Academy of Sciences of the United States of America 107 (6):2711-2716

Elo A, Immanen J, Nieminen K, Helariutta Y (2009) Stem cell function during plant vascular development. Semin Cell Dev Biol 20 (9):1097-1106

Endo M, Shimizu H, Nohales MA, Araki T, Kay SA (2014) Tissue-specific clocks in Arabidopsis show asymmetric coupling. Nature 515 (7527):419-422

Erdel F, Krug J, Langst G, Rippe K (2011) Targeting chromatin remodelers: signals and search mechanisms. Biochim Biophys Acta 1809 (9):497-508

Esau K (1950) Development and structure of the phloem tissue. II. The Botanical Review 16 (2):67

Etchells JP, Provost CM, Mishra L, Turner SR (2013) WOX4 and WOX14 act downstream of the PXY receptor kinase to regulate plant vascular proliferation independently of any role in vascular organisation. Development (Cambridge, England) 140 (10):2224-2234

Etchells JP, Smit ME, Gaudinier A, Williams CJ, Brady SM (2016) A brief history of the TDIF-PXY signalling module: balancing meristem identity and differentiation during vascular development. New Phytol 209 (2):474-484

Etchells JP, Turner SR (2010) The PXY-CLE41 receptor ligand pair defines a multifunctional pathway that controls the rate and orientation of vascular cell division. Development (Cambridge, England) 137 (5):767-774

Evert RF, Eichhorn SE (2006) Esau's Plant Anatomy. 3 edn. John Wiley & Sons, Hoboken, New Jersey

Fahlgren N, Montgomery TA, Howell MD, Allen E, Dvorak SK, Alexander AL, Carrington JC (2006) Regulation of AUXIN RESPONSE FACTOR3 by TAS3 ta-siRNA affects developmental timing and patterning in Arabidopsis. Current biology : CB 16 (9):939-944

Finkelstein R (2013) Abscisic Acid synthesis and response. Arabidopsis Book 11:e0166

Fisher K, Turner S (2007) PXY, a Receptor-like Kinase Essential for Maintaining Polarity during Plant Vascular-Tissue Development. Current biology : CB 17 (12):1061-1066

Flematti GR, Ghisalberti EL, Dixon KW, Trengove RD (2004) A compound from smoke that promotes seed germination. Science 305 (5686):977

Flematti GR, Scaffidi A, Goddard-Borger ED, Heath CH, Nelson DC, Commander LE, Stick RV, Dixon KW, Smith SM, Ghisalberti EL (2010) Structure-activity relationship of karrikin germination stimulants. J Agric Food Chem 58 (15):8612-8617

Fletcher JC, Brand U, Running MP, Simon R, Meyerowitz EM (1999) Signaling of cell fate decisions by CLAVATA3 in Arabidopsis shoot meristems. Science 283 (5409):1911-1914

Fowler JE, Quatrano RS (1997) Plant cell morphogenesis: plasma membrane interactions with the cytoskeleton and cell wall. Annu Rev Cell Dev Biol 13:697-743

Froelich DR, Mullendore DL, Jensen KH, Ross-Elliott TJ, Anstead JA, Thompson GA, Pelissier HC, Knoblauch M (2011) Phloem ultrastructure and pressure flow: Sieve-Element-Occlusion-Related agglomerations do not affect translocation. Plant Cell 23 (12):4428-4445

Fukuda H (2000) Programmed cell death of tracheary elements as a paradigm in plants. Plant molecular biology 44 (3):245-253

Furuta KM, Hellmann E, Helariutta Y (2014a) Molecular control of cell specification and cell differentiation during procambial development. Annual review of plant biology 65:607-638

Furuta KM, Yadav SR, Lehesranta S, Belevich I, Miyashima S, Heo JO, Vaten A, Lindgren O, De Rybel B, Van Isterdael G, Somervuo P, Lichtenberger R, Rocha R, Thitamadee S, Tahtiharju S, Auvinen P, Beeckman T, Jokitalo E, Helariutta Y (2014b) Arabidopsis NAC45/86 direct sieve element morphogenesis culminating in enucleation. Science 345 (6199):933-937

Gaillochet C, Daum G, Lohmann JU (2015) O cell, where art thou? The mechanisms of shoot meristem patterning. Curr Opin Plant Biol 23:91-97

Gaillochet C, Lohmann JU (2015) The never-ending story: from pluripotency to plant developmental plasticity. Development (Cambridge, England) 142 (13):2237-2249

Gardner BM, Castanzo DT, Chowdhury S, Stjepanovic G, Stefely MS, Hurley JH, Lander GC, Martin A (2018) The peroxisomal AAA-ATPase Pex1/Pex6 unfolds substrates by processive threading. Nat Commun 9 (1):135

Geldner N (2013) The endodermis. Annual review of plant biology 64:531-558

Gomez-Roldan V, Fermas S, Brewer PB, Puech-Pages V, Dun EA, Pillot JP, Letisse F, Matusova R, Danoun S, Portais JC, Bouwmeester H, Becard G, Beveridge CA, Rameau C, Rochange SF (2008) Strigolactone inhibition of shoot branching. Nature 455 (7210):189-194

Greb T, Lohmann JU (2016) Plant Stem Cells. Current biology : CB 26 (17):R816-821

Grieneisen VA, Xu J, Maree AF, Hogeweg P, Scheres B (2007) Auxin transport is sufficient to generate a maximum and gradient guiding root growth. Nature 449 (7165):1008-1013

Guilfoyle TJ (2015) The PB1 domain in auxin response factor and Aux/IAA proteins: a versatile protein interaction module in the auxin response. Plant Cell 27 (1):33-43

Guo Y, Qin G, Gu H, Qu L-J (2009) Dof5.6/HCA2, a Dof Transcription Factor Gene, Regulates Interfascicular Cambium Formation and Vascular Tissue Development in Arabidopsis. Plant Cell 21 (11):3518-3534

Guo Y, Zheng Z, La Clair JJ, Chory J, Noel JP (2013) Smoke-derived karrikin perception by the alpha/beta-hydrolase KAI2 from Arabidopsis. Proceedings of the National Academy of Sciences of the United States of America 110 (20):8284-8289

Gursanscky N, Jouannet V, Grünwald K, Sanchez P, Laaber-Schwarz M, Greb T (2016) *MOL1* is required for cambium homeostasis in Arabidopsis. The Plant journal : for cell and molecular biology 86 (3):210-220

Ha CV, Leyva-Gonzalez MA, Osakabe Y, Tran UT, Nishiyama R, Watanabe Y, Tanaka M, Seki M, Yamaguchi S, Dong NV, Yamaguchi-Shinozaki K, Shinozaki K, Herrera-Estrella L, Tran LS (2014) Positive regulatory role of strigolactone in plant responses to drought and salt stress. Proceedings of the National Academy of Sciences of the United States of America 111 (2):851-856

Hagen G (2015) Auxin signal transduction. Essays Biochem 58:1-12

Hamann T, Mayer U, Jurgens G (1999) The auxin-insensitive bodenlos mutation affects primary root formation and apical-basal patterning in the Arabidopsis embryo. Development (Cambridge, England) 126 (7):1387-1395

Hamiaux C, Drummond RS, Janssen BJ, Ledger SE, Cooney JM, Newcomb RD, Snowden KC (2012) DAD2 is an alpha/beta hydrolase likely to be involved in the perception of the plant branching hormone, strigolactone. Current biology : CB 22 (21):2032-2036

Hauer MH, Gasser SM (2017) Chromatin and nucleosome dynamics in DNA damage and repair. Genes Dev 31 (22):2204-2221

Haupt S, Duncan GH, Holzberg S, Oparka KJ (2001) Evidence for symplastic phloem unloading in sink leaves of barley. Plant physiology 125 (1):209-218

Hayward A, Stirnberg P, Beveridge C, Leyser O (2009) Interactions between Auxin and Strigolactone in Shoot Branching Control. Plant physiology 151 (1):400-412

Hazak O, Brandt B, Cattaneo P, Santiago J, Rodriguez-Villalon A, Hothorn M, Hardtke CS (2017) Perception of root-active CLE peptides requires CORYNE function in the phloem vasculature. EMBO reports

Hazak O, Hardtke CS (2016) CLAVATA 1-type receptors in plant development. Journal of experimental botany 67 (16):4827-4833

Hergeth SP, Schneider R (2015) The H1 linker histones: multifunctional proteins beyond the nucleosomal core particle. EMBO reports 16 (11):1439-1453

Hernandez-Leon O, Rodriguez-Villalonga OL, Perez-Nogueira FR, Guillen-Canovas EJ, Alvarez-Toledo N, Lemus-Saraceni A (2014) [Endoscopic approach to ventricular atrium for biopsy of pineal region tumour: case report]. Neurocirugia (Astur) 25 (1):43-47

Hershko A, Ciechanover A (1998) The ubiquitin system. Annu Rev Biochem 67:425-479

Hirakawa Y, Kondo Y, Fukuda H (2010) TDIF peptide signaling regulates vascular stem cell proliferation via the WOX4 homeobox gene in Arabidopsis. Plant Cell 22 (8):2618-2629

Hohmann U, Santiago J, Nicolet J, Olsson V, Spiga FM, Hothorn LA, Butenko MA, Hothorn M (2018) Mechanistic basis for the activation of plant membrane receptor kinases by SERK-family coreceptors. Proceedings of the National Academy of Sciences of the United States of America 115 (13):3488-3493

Hu C, Zhu Y, Cui Y, Cheng K, Liang W, Wei Z, Zhu M, Yin H, Zeng L, Xiao Y, Lv M, Yi J, Hou S, He K, Li J, Gou X (2018) A group of receptor kinases are essential for CLAVATA signalling to maintain stem cell homeostasis. Nature plants 4 (4):205-211

Huala E, Dickerman AW, Garcia-Hernandez M, Weems D, Reiser L, LaFond F, Hanley D, Kiphart D, Zhuang M, Huang W, Mueller LA, Bhattacharyya D, Bhaya D, Sobral BW, Beavis W, Meinke DW, Town CD, Somerville C, Rhee SY (2001) The Arabidopsis Information Resource (TAIR): a comprehensive database and web-based information retrieval, analysis, and visualization system for a model plant. Nucleic acids research 29 (1):102-105

Imaichi R, Hiratsuka R (2007) Evolution of shoot apical meristem structures in vascular plants with respect to plasmodesmatal network. Am J Bot 94 (12):1911-1921

Imlau A, Truernit E, Sauer N (1999) Cell-to-cell and long-distance trafficking of the green fluorescent protein in the phloem and symplastic unloading of the protein into sink tissues. Plant Cell 11 (3):309-322

Ito Y, Nakanomyo I, Motose H, Iwamoto K, Sawa S, Dohmae N, Fukuda H (2006) Dodeca-CLE peptides as suppressors of plant stem cell differentiation. Science 313 (5788):842-845

Jiang L, Liu X, Xiong G, Liu H, Chen F, Wang L, Meng X, Liu G, Yu H, Yuan Y, Yi W, Zhao L, Ma H, He Y, Wu Z, Melcher K, Qian Q, Xu HE, Wang Y, Li J (2013) DWARF 53 acts as a repressor of strigolactone signalling in rice. Nature 504 (7480):401-405

Jouannet V (2011) Cell biology and role of TAS3-derived trans-acting small interfering RNA during Arabidopsis thaliana development. University of Paris,

Jun J, Fiume E, Roeder AH, Meng L, Sharma VK, Osmont KS, Baker C, Ha CM, Meyerowitz EM, Feldman LJ, Fletcher JC (2010) Comprehensive analysis of CLE polypeptide signaling gene expression and overexpression activity in Arabidopsis. Plant physiology 154 (4):1721-1736

Jura-Morawiec J, Tulik M, Iqbal M (2015) Lateral Meristems Responsible for Secondary Growth of the Monocotyledons: A Survey of the State of the Art. Bot Rev 81 (2):150-161

Kagiyama M, Hirano Y, Mori T, Kim SY, Kyozuka J, Seto Y, Yamaguchi S, Hakoshima T (2013) Structures of D14 and D14L in the strigolactone and karrikin signaling pathways. Genes Cells 18 (2):147-160

Kang J, Dengler N (2002) Cell cycling frequency and expression of the homeobox gene ATHB-8 during leaf vein development in Arabidopsis. Planta 216 (2):212-219

Kang YH, Hardtke CS (2016) Arabidopsis MAKR5 is a positive effector of BAM3-dependent CLE45 signaling. EMBO reports 17 (8):1145-1154

Kapulnik Y, Delaux PM, Resnick N, Mayzlish-Gati E, Wininger S, Bhattacharya C, Sejalon-Delmas N, Combier JP, Becard G, Belausov E, Beeckman T, Dor E, Hershenhorn J, Koltai H (2011) Strigolactones affect lateral root formation and root-hair elongation in Arabidopsis. Planta 233 (1):209-216

Katari MS, Nowicki SD, Aceituno FF, Nero D, Kelfer J, Thompson LP, Cabello JM, Davidson RS, Goldberg AP, Shasha DE, Coruzzi GM, Gutierrez RA (2010) VirtualPlant: a software platform to support systems biology research. Plant physiology 152 (2):500-515

Kawashima T, Goldberg RB (2010) The suspensor: not just suspending the embryo. Trends in plant science 15 (1):23-30

Kenrick P, Crane PR (1997) The origin and early evolution of plants on land. Nature 389:33

Kim D, Pertea G, Trapnell C, Pimentel H, Kelley R, Salzberg SL (2013) TopHat2: accurate alignment of transcriptomes in the presence of insertions, deletions and gene fusions. Genome biology 14 (4):R36

Kinoshita A, Nakamura Y, Sasaki E, Kyozuka J, Fukuda H, Sawa S (2007) Gain-of-function phenotypes of chemically synthetic CLAVATA3/ESR-related (CLE) peptides in Arabidopsis thaliana and Oryza sativa. Plant & cell physiology 48 (12):1821-1825

Knoblauch M, Knoblauch J, Mullendore DL, Savage JA, Babst BA, Beecher SD, Dodgen AC, Jensen KH, Holbrook NM (2016) Testing the Munch hypothesis of long distance phloem transport in plants. Elife 5

Knoblauch M, Vendrell M, de Leau E, Paterlini A, Knox K, Ross-Elliot T, Reinders A, Brockman SA, Ward J, Oparka K (2015) Multispectral phloem-mobile probes: properties and applications. Plant physiology 167 (4):1211-1220

Kondo Y, Fujita T, Sugiyama M, Fukuda H (2015) A novel system for xylem cell differentiation in Arabidopsis thaliana. Molecular plant 8 (4):612-621

Kondo Y, Ito T, Nakagami H, Hirakawa Y, Saito M, Tamaki T, Shirasu K, Fukuda H (2014) Plant GSK3 proteins regulate xylem cell differentiation downstream of TDIF-TDR signalling. Nat Commun 5:3504

Kondo Y, Nurani AM, Saito C, Ichihashi Y, Saito M, Yamazaki K, Mitsuda N, Ohme-Takagi M, Fukuda H (2016) Vascular Cell Induction Culture System Using Arabidopsis Leaves (VISUAL) Reveals the Sequential Differentiation of Sieve Element-like Cells. Plant Cell 28 (6):1250-1262

Kosugi S, Hasebe M, Tomita M, Yanagawa H (2009) Systematic identification of cell cycle-dependent yeast nucleocytoplasmic shuttling proteins by prediction of composite motifs. Proceedings of the National Academy of Sciences of the United States of America 106 (25):10171-10176

Krogan NT, Long JA (2009) Why so repressed? Turning off transcription during plant growth and development. Curr Opin Plant Biol 12 (5):628-636

Kubo M, Udagawa M, Nishikubo N, Horiguchi G, Yamaguchi M, Ito J, Mimura T, Fukuda H, Demura T (2005) Transcription switches for protoxylem and metaxylem vessel formation. Genes Dev 19 (16):1855-1860

Kucukoglu M, Nilsson O (2015) CLE peptide signaling in plants - the power of moving around. Physiologia plantarum 155 (1):74-87

Kumar M, Pandya-Kumar N, Kapulnik Y, Koltai H (2015) Strigolactone signaling in root development and phosphate starvation. Plant signaling & behavior 10 (7):e1045174

Kurihara D, Mizuta Y, Sato Y, Higashiyama T (2015) ClearSee: a rapid optical clearing reagent for whole-plant fluorescence imaging. Development (Cambridge, England) 142 (23):4168-4179

Lachner M, Jenuwein T (2002) The many faces of histone lysine methylation. Curr Opin Cell Biol 14 (3):286-298

Lalonde S, R Franceschi V, Frommer W (2001) Companion Cells.

Lalonde S, Weise A, Walsh RP, Ward JM, Frommer WB (2003) Fusion to GFP blocks intercellular trafficking of the sucrose transporter SUT1 leading to accumulation in companion cells. BMC Plant Biol 3:8

Lampropoulos A, Sutikovic Z, Wenzl C, Maegele I, Lohmann JU, Forner J (2013) GreenGate---a novel, versatile, and efficient cloning system for plant transgenesis. PloS one 8 (12):e83043

Laskowski MJ, Williams ME, Nusbaum HC, Sussex IM (1995) Formation of lateral root meristems is a two-stage process. Development (Cambridge, England) 121 (10):3303-3310

Lau OS, Bergmann DC (2012) Stomatal development: a plant's perspective on cell polarity, cell fate transitions and intercellular communication. Development (Cambridge, England) 139 (20):3683-3692

Lee I, Kim K, Lee S, Lee S, Hwang E, Shin K, Kim D, Choi J, Choi H, Cha JS, Kim H, Lee RA, Jeong S, Kim J, Kim Y, Nam HG, Park SK, Cho HS, Soh MS (2018) A missense allele of KARRIKIN-INSENSITIVE2 impairs ligand-binding and downstream signaling in Arabidopsis thaliana. Journal of experimental botany 69 (15):3609-3623

Lee Y, Lee WS, Kim SH (2013) Hormonal regulation of stem cell maintenance in roots. Journal of experimental botany 64 (5):1153-1165

Lemoine R, La Camera S, Atanassova R, Dedaldechamp F, Allario T, Pourtau N, Bonnemain JL, Laloi M, Coutos-Thevenot P, Maurousset L, Faucher M, Girousse C, Lemonnier P, Parrilla J, Durand M (2013) Source-to-sink transport of sugar and regulation by environmental factors. Front Plant Sci 4:272

Leyser O (2009) The control of shoot branching: an example of plant information processing. Plant Cell Environ 32 (6):694-703

Li H, Ilin S, Wang W, Duncan EM, Wysocka J, Allis CD, Patel DJ (2006) Molecular basis for site-specific read-out of histone H3K4me3 by the BPTF PHD finger of NURF. Nature 442 (7098):91-95

Liang Y, Ward S, Li P, Bennett T, Leyser O (2016) SMAX1-LIKE7 Signals from the Nucleus to Regulate Shoot Development in Arabidopsis via Partially EAR Motif-Independent Mechanisms. Plant Cell 28 (7):1581-1601

Lim CW, Baek W, Jung J, Kim JH, Lee SC (2015) Function of ABA in Stomatal Defense against Biotic and Drought Stresses. Int J Mol Sci 16 (7):15251-15270

Lin TF, Saiga S, Abe M, Laux T (2016) OBE3 and WUS Interaction in Shoot Meristem Stem Cell Regulation. PloS one 11 (5):e0155657

Love MI, Huber W, Anders S (2014) Moderated estimation of fold change and dispersion for RNA-seq data with DESeq2. Genome biology 15 (12):550

Lucas WJ, Groover A, Lichtenberger R, Furuta K, Yadav SR, Helariutta Y, He XQ, Fukuda H, Kang J, Brady SM, Patrick JW, Sperry J, Yoshida A, Lopez-Millan AF, Grusak MA, Kachroo P (2013) The plant vascular system: evolution, development and functions. Journal of integrative plant biology 55 (4):294-388

Luger K, Mader AW, Richmond RK, Sargent DF, Richmond TJ (1997) Crystal structure of the nucleosome core particle at 2.8 A resolution. Nature 389 (6648):251-260

Ma H, Duan J, Ke J, He Y, Gu X, Xu TH, Yu H, Wang Y, Brunzelle JS, Jiang Y, Rothbart SB, Xu HE, Li J, Melcher K (2017) A D53 repression motif induces oligomerization of TOPLESS corepressors and promotes assembly of a corepressor-nucleosome complex. Science advances 3 (6):e1601217

Mallory A, Vaucheret H (2010) Form, function, and regulation of ARGONAUTE proteins. Plant Cell 22 (12):3879-3889

Marhava P, Bassukas AEL, Zourelidou M, Kolb M, Moret B, Fastner A, Schulze WX, Cattaneo P, Hammes UZ, Schwechheimer C, Hardtke CS (2018) A molecular rheostat adjusts auxin flux to promote root protophloem differentiation. Nature

Masubelele NH, Dewitte W, Menges M, Maughan S, Collins C, Huntley R, Nieuwland J, Scofield S, Murray JA (2005) D-type cyclins activate division in the root apex to promote seed germination in Arabidopsis. Proceedings of the National Academy of Sciences of the United States of America 102 (43):15694-15699

Matsunaga KK, Tomescu AM (2016) Root evolution at the base of the lycophyte clade: insights from an Early Devonian lycophyte. Annals of botany 117 (4):585-598

Mattsson J, Ckurshumova W, Berleth T (2003) Auxin signaling in Arabidopsis leaf vascular development. Plant physiology 131 (3):1327-1339

McCarty DR, Chory J (2000) Conservation and innovation in plant signaling pathways. Cell 103 (2):201-209

Melnyk CW, Meyerowitz EM (2015) Plant grafting. Current biology : CB 25 (5):R183-188

Meng Y, Shuai H, Luo X, Chen F, Zhou W, Yang W, Shu K (2016) Karrikins: Regulators Involved in Phytohormone Signaling Networks during Seed Germination and Seedling Development. Front Plant Sci 7:2021

Meyer Y, Siala W, Bashandy T, Riondet C, Vignols F, Reichheld JP (2008) Glutaredoxins and thioredoxins in plants. Biochim Biophys Acta 1783 (4):589-600

Miyashima S, Koi S, Hashimoto T, Nakajima K (2011) Non-cell-autonomous microRNA165 acts in a dose-dependent manner to regulate multiple differentiation status in the Arabidopsis root. Development (Cambridge, England) 138 (11):2303-2313

Miyashima S, Sebastian J, Lee JY, Helariutta Y (2013) Stem cell function during plant vascular development. The EMBO journal 32 (2):178-193

Morffy N, Faure L, Nelson DC (2016) Smoke and Hormone Mirrors: Action and Evolution of Karrikin and Strigolactone Signaling. Trends Genet 32 (3):176-188

Moseler A, Aller I, Wagner S, Nietzel T, Przybyla-Toscano J, Muhlenhoff U, Lill R, Berndt C, Rouhier N, Schwarzlander M, Meyer AJ (2015) The mitochondrial monothiol glutaredoxin S15 is essential for iron-sulfur protein maturation in Arabidopsis thaliana. Proceedings of the National Academy of Sciences of the United States of America 112 (44):13735-13740

Moturu TR, Thula S, Singh RK, Nodzynski T, Varekova RS, Friml J, Simon S (2018) Molecular evolution and diversification of the SMXL gene family. Journal of experimental botany 69 (9):2367-2378

Müller R, Bleckmann A, Simon R (2008) The Receptor Kinase CORYNE of Arabidopsis Transmits the Stem Cell-Limiting Signal CLAVATA3 Independently of CLAVATA1. Plant Cell:tpc.107.057547

Muraro D, Mellor N, Pound MP, Help H, Lucas M, Chopard J, Byrne HM, Godin C, Hodgman TC, King JR, Pridmore TP, Helariutta Y, Bennett MJ, Bishopp A (2014) Integration of hormonal signaling networks and mobile microRNAs is required for vascular patterning in Arabidopsis roots. Proceedings of the National Academy of Sciences of the United States of America 111 (2):857-862

Nakamura H, Xue YL, Miyakawa T, Hou F, Qin HM, Fukui K, Shi X, Ito E, Ito S, Park SH, Miyauchi Y, Asano A, Totsuka N, Ueda T, Tanokura M, Asami T (2013) Molecular mechanism of strigolactone perception by DWARF14. Nat Commun 4:2613

Nelson DC, Flematti GR, Riseborough JA, Ghisalberti EL, Dixon KW, Smith SM (2010) Karrikins enhance light responses during germination and seedling development in Arabidopsis thaliana. Proceedings of the National Academy of Sciences of the United States of America 107 (15):7095-7100

Nelson DC, Scaffidi A, Dun EA, Waters MT, Flematti GR, Dixon KW, Beveridge CA, Ghisalberti EL, Smith SM (2011) F-box protein MAX2 has dual roles in karrikin and strigolactone signaling in Arabidopsis thaliana. Proceedings of the National Academy of Sciences of the United States of America 108 (21):8897-8902

Nieminen K, Blomster T, Helariutta Y, Mähönen AP (2015) Vascular Cambium Development. The Arabidopsis Book:e0177

Ogawa M, Shinohara H, Sakagami Y, Matsubayashi Y (2008) Arabidopsis CLV3 peptide directly binds CLV1 ectodomain. Science 319 (5861):294

Oliveros JC (2007) VENNY. An interactive tool for comparing lists with Venn diagrams. http://bioinfogp.cnb.csic.es/tools/venny/index.html.

Oparka KJ, Turgeon R (1999) Sieve elements and companion cells-traffic control centers of the phloem. Plant Cell 11 (4):739-750

Otero S, Helariutta Y (2017) Companion cells: a diamond in the rough. Journal of experimental botany 68 (1):71-78

Parent JS, Bouteiller N, Elmayan T, Vaucheret H (2015) Respective contributions of Arabidopsis DCL2 and DCL4 to RNA silencing. The Plant journal : for cell and molecular biology 81 (2):223-232

Parent JS, Martinez de Alba AE, Vaucheret H (2012) The origin and effect of small RNA signaling in plants. Front Plant Sci 3:179

Patrick JW (1997) PHLOEM UNLOADING: Sieve Element Unloading and Post-Sieve Element Transport. Annu Rev Plant Physiol Plant Mol Biol 48:191-222

Perilli S, Di Mambro R, Sabatini S (2012) Growth and development of the root apical meristem. Curr Opin Plant Biol 15 (1):17-23

Peris CI, Rademacher EH, Weijers D (2010) Green beginnings - pattern formation in the early plant embryo. Curr Top Dev Biol 91:1-27

Pi L, Aichinger E, van der Graaff E, Llavata-Peris CI, Weijers D, Hennig L, Groot E, Laux T (2015) Organizer-Derived WOX5 Signal Maintains Root Columella Stem Cells through Chromatin-Mediated Repression of CDF4 Expression. Developmental cell 33 (5):576-588

Poschet G, Hannich B, Raab S, Jungkunz I, Klemens PA, Krueger S, Wic S, Neuhaus HE, Buttner M (2011) A novel Arabidopsis vacuolar glucose exporter is involved in cellular sugar homeostasis and affects the composition of seed storage compounds. Plant physiology 157 (4):1664-1676

Purves WS, D.;Orians, G.; Heller, H. C.; Hillis, D.; Berenbaum, M. R. (2007) Purves, Biologie.

Queitsch C, Hong SW, Vierling E, Lindquist S (2000) Heat shock protein 101 plays a crucial role in thermotolerance in Arabidopsis. Plant Cell 12 (4):479-492

Ragni L, Greb T (2017) Secondary growth as a determinant of plant shape and form. Semin Cell Dev Biol

Raissig MT, Gagliardini V, Jaenisch J, Grossniklaus U, Baroux C (2013) Efficient and rapid isolation of early-stage embryos from Arabidopsis thaliana seeds. J Vis Exp (76)

Rasmussen A, Depuydt S, Goormachtig S, Geelen D (2013) Strigolactones fine-tune the root system. Planta 238 (4):615-626

Reddy GV, Heisler MG, Ehrhardt DW, Meyerowitz EM (2004) Real-time lineage analysis reveals oriented cell divisions associated with morphogenesis at the shoot apex of Arabidopsis thaliana. Development (Cambridge, England) 131 (17):4225-4237

Reddy GV, Meyerowitz EM (2005) Stem-cell homeostasis and growth dynamics can be uncoupled in the Arabidopsis shoot apex. Science 310 (5748):663-667

Rodriguez-Villalon A (2016) Wiring a plant: genetic networks for phloem formation in Arabidopsis thaliana roots. New Phytol 210 (1):45-50

Rodriguez-Villalon A, Gujas B, Kang YH, Breda AS, Cattaneo P, Depuydt S, Hardtke CS (2014) Molecular genetic framework for protophloem formation. Proceedings of the National Academy of Sciences of the United States of America 111 (31):11551-11556

Rodriguez-Villalon A, Gujas B, van Wijk R, Munnik T, Hardtke CS (2015) Primary root protophloem differentiation requires balanced phosphatidylinositol-4,5-biphosphate levels and systemically affects root branching. Development (Cambridge, England) 142 (8):1437-1446

Ross-Elliott TJ, Jensen KH, Haaning KS, Wager BM, Knoblauch J, Howell AH, Mullendore DL, Monteith AG, Paultre D, Yan D, Otero S, Bourdon M, Sager R, Lee JY, Helariutta Y, Knoblauch M, Oparka KJ (2017) Phloem unloading in Arabidopsis roots is convective and regulated by the phloem-pole pericycle. Elife 6

Ruiz Sola MA, Coiro M, Crivelli S, Zeeman SC, Schmidt Kjolner Hansen S, Truernit E (2017) OCTOPUS-LIKE 2, a novel player in Arabidopsis root and vascular development, reveals a key role for OCTOPUS family genes in root metaphloem sieve tube differentiation. New Phytol 216 (4):1191-1204

Russell J, Bulman S (2005) The liverwort Marchantia foliacea forms a specialized symbiosis with arbuscular mycorrhizal fungi in the genus Glomus. New Phytol 165 (2):567-579

Ruzicka K, Ursache R, Hejatko J, Helariutta Y (2015) Xylem development - from the cradle to the grave. New Phytol 207 (3):519-535

Sabatini S, Beis D, Wolkenfelt H, Murfett J, Guilfoyle T, Malamy J, Benfey P, Leyser O, Bechtold N, Weisbeek P, Scheres B (1999) An auxin-dependent distal organizer of pattern and polarity in the Arabidopsis root. Cell 99 (5):463-472

Sachs T (1981) The control of the patterned differentiation of vascular tissues. Adv Bot Res 9:151-162

Saiga S, Furumizu C, Yokoyama R, Kurata T, Sato S, Kato T, Tabata S, Suzuki M, Komeda Y (2008) The Arabidopsis OBERON1 and OBERON2 genes encode plant homeodomain finger proteins and are required for apical meristem maintenance. Development (Cambridge, England) 135 (10):1751-1759

Saiga S, Moller B, Watanabe-Taneda A, Abe M, Weijers D, Komeda Y (2012) Control of embryonic meristem initiation in Arabidopsis by PHD-finger protein complexes. Development (Cambridge, England) 139 (8):1391-1398

Sánchez P (2013) Cell fate regulation in the *Arabidopsis thaliana* stem: analysis of interfascicular cambium formation and development of a method for tissue-specific transcriptome analysis. University of Vienna, Vienna

Sanchez P, Nehlin L, Greb T (2012) From thin to thick – major transitions during stem development. Trends in plant science 17 (2):113-121

Sanchez R, Zhou MM (2011) The PHD finger: a versatile epigenome reader. Trends Biochem Sci 36 (7):364-372

Santuari L, Scacchi E, Rodriguez-Villalon A, Salinas P, Dohmann EM, Brunoud G, Vernoux T, Smith RS, Hardtke CS (2011) Positional information by differential endocytosis splits auxin response to drive Arabidopsis root meristem growth. Current biology : CB 21 (22):1918-1923

Sarkar AK, Luijten M, Miyashima S, Lenhard M, Hashimoto T, Nakajima K, Scheres B, Heidstra R, Laux T (2007) Conserved factors regulate signalling in Arabidopsis thaliana shoot and root stem cell organizers. Nature 446 (7137):811-814

Sauer M, Robert S, Kleine-Vehn J (2013) Auxin: simply complicated. Journal of experimental botany 64 (9):2565-2577

Scacchi E, Osmont KS, Beuchat J, Salinas P, Navarrete-Gomez M, Trigueros M, Ferrandiz C, Hardtke CS (2009) Dynamic, auxin-responsive plasma membrane-to-nucleus movement of Arabidopsis BRX. Development (Cambridge, England) 136 (12):2059-2067

Scacchi E, Salinas P, Gujas B, Santuari L, Krogan N, Ragni L, Berleth T, Hardtke CS (2010) Spatio-temporal sequence of cross-regulatory events in root meristem growth. Proceedings of the National Academy of Sciences of the United States of America 107 (52):22734-22739

Scaffidi A, Waters MT, Sun YK, Skelton BW, Dixon KW, Ghisalberti EL, Flematti GR, Smith SM (2014) Strigolactone hormones and their stereoisomers signal through two related receptor proteins to induce different physiological responses in Arabidopsis. Plant physiology 165 (3):1221-1232

Scarpella E, Francis P, Berleth T (2004) Stage-specific markers define early steps of procambium development in Arabidopsis leaves and correlate termination of vein formation with mesophyll differentiation. Development (Cambridge, England) 131 (14):3445-3455

Scarpella E, Helariutta Y (2010) Vascular pattern formation in plants. Curr Top Dev Biol 91:221-265

Schenk ST, Schikora A (2015) Staining of Callose Depositions in Root and Leaf Tissues. Bio-protocol 5 (6):e1429

Scheres B (2007) Stem-cell niches: nursery rhymes across kingdoms. Nat Rev Mol Cell Biol 8 (5):345-354

Scheres B, Di Laurenzio L, Willemsen V, Hauser MT, Janmaat K, Weisbeek P, Benfey PN (1995) Mutations affecting the radial organisation of the Arabidopsis root display specific defects throughout the embryonic axis. Development (Cambridge, England) 121 (1):53-62

Scheres B, Wolkenfelt H, Willemsen V, Terlouw M, Lawson E, Dean C, Weisbeek P (1994) Embryonic origin of the Arabidopsis primary root and root meristem initials. Development (Cambridge, England) 120 (9):2475-2487

Schlereth A, Moller B, Liu W, Kientz M, Flipse J, Rademacher EH, Schmid M, Jurgens G, Weijers D (2010) MONOPTEROS controls embryonic root initiation by regulating a mobile transcription factor. Nature 464 (7290):913-916

Scholthof HB (2006) The Tombusvirus-encoded P19: from irrelevance to elegance. Nat Rev Microbiol 4 (5):405-411

Schoof H, Lenhard M, Haecker A, Mayer KF, Jurgens G, Laux T (2000) The stem cell population of Arabidopsis shoot meristems in maintained by a regulatory loop between the CLAVATA and WUSCHEL genes. Cell 100 (6):635-644

Seago JL, Jr., Fernando DD (2013) Anatomical aspects of angiosperm root evolution. Annals of botany 112 (2):223-238

Sehr EM, Agustí J, Lehner R, Farmer EE, Schwarz M, Greb T (2010) Analysis of secondary growth in the Arabidopsis shoot reveals a positive role of jasmonate signalling in cambium formation. The Plant journal : for cell and molecular biology 63 (5):811-822

Shahbazian MD, Grunstein M (2007) Functions of site-specific histone acetylation and deacetylation. Annu Rev Biochem 76:75-100

Sheard LB, Tan X, Mao H, Withers J, Ben-Nissan G, Hinds TR, Kobayashi Y, Hsu FF, Sharon M, Browse J, He SY, Rizo J, Howe GA, Zheng N (2010) Jasmonate perception by inositol-phosphate-potentiated COI1-JAZ co-receptor. Nature 468 (7322):400-405

Shen H, Luong P, Huq E (2007) The F-box protein MAX2 functions as a positive regulator of photomorphogenesis in Arabidopsis. Plant physiology 145 (4):1471-1483

Shiu SH, Bleecker AB (2001) Receptor-like kinases from Arabidopsis form a monophyletic gene family related to animal receptor kinases. Proceedings of the National Academy of Sciences of the United States of America 98 (19):10763-10768

Sieburth LE (1999) Auxin is required for leaf vein pattern in Arabidopsis. Plant physiology 121 (4):1179-1190

Simonini S, Bencivenga S, Trick M, Ostergaard L (2017) Auxin-Induced Modulation of ETTIN Activity Orchestrates Gene Expression in Arabidopsis. Plant Cell 29 (8):1864-1882

Simonini S, Deb J, Moubayidin L, Stephenson P, Valluru M, Freire-Rios A, Sorefan K, Weijers D, Friml J, Ostergaard L (2016) A noncanonical auxin-sensing mechanism is required for organ morphogenesis in Arabidopsis. Genes Dev 30 (20):2286-2296

Slewinski TL, Zhang C, Turgeon R (2013) Structural and functional heterogeneity in phloem loading and transport. Front Plant Sci 4:244

Smith RA, Schuetz M, Roach M, Mansfield SD, Ellis B, Samuels L (2013) Neighboring parenchyma cells contribute to Arabidopsis xylem lignification, while lignification of interfascicular fibers is cell autonomous. Plant Cell 25 (10):3988-3999

Smith SM, Li J (2014) Signalling and responses to strigolactones and karrikins. Curr Opin Plant Biol 21:23-29

Somers DE, Fujiwara S (2009) Thinking outside the F-box: novel ligands for novel receptors. Trends in plant science 14 (4):206-213

Somorjai IM, Lohmann JU, Holstein TW, Zhao Z (2012) Stem cells: a view from the roots. Biotechnol J 7 (6):704-722

Song J, Perreault J-P, Topisirovic I, Richard S (2016) RNA G-quadruplexes and their potential regulatory roles in translation. Translation 4 (2):e1244031

Soundappan I, Bennett T, Morffy N, Liang Y, Stanga JP, Abbas A, Leyser O, Nelson DC (2015) SMAX1-LIKE/D53 family members enable distinct MAX2-dependent responses to strigolactones and karrikins in Arabidopsis. Plant Cell 27 (11):3143-3159

Sozzani R, Iyer-Pascuzzi A (2014) Postembryonic control of root meristem growth and development. Curr Opin Plant Biol 17:7-12

Stadler R, Wright KM, Lauterbach C, Amon G, Gahrtz M, Feuerstein A, Oparka KJ, Sauer N (2005) Expression of GFP-fusions in Arabidopsis companion cells reveals non-specific protein trafficking into sieve elements and identifies a novel post-phloem domain in roots. The Plant journal : for cell and molecular biology 41 (2):319-331

Stahl Y, Wink RH, Ingram GC, Simon R (2009) A signaling module controlling the stem cell niche in Arabidopsis root meristems. Current biology : CB 19 (11):909-914

Stanga JP, Morffy N, Nelson DC (2016) Functional redundancy in the control of seedling growth by the karrikin signaling pathway. Planta 243 (6):1397-1406

Stanga JP, Smith SM, Briggs WR, Nelson DC (2013) SUPPRESSOR OF MORE AXILLARY GROWTH2 1 controls seed germination and seedling development in Arabidopsis. Plant physiology 163 (1):318-330

Steeve TA, Sussex IM (1989) Patterns in Plant Development. 2 edn. Cambridge University Press, Cambridge

Steudle E (2001) The Cohesion-Tension Mechanism and the Acquisition of Water by Plant Roots. Annu Rev Plant Physiol Plant Mol Biol 52:847-875

Stirnberg P, van De Sande K, Leyser HM (2002) MAX1 and MAX2 control shoot lateral branching in Arabidopsis. Development (Cambridge, England) 129 (5):1131-1141

Strabala TJ, O'Donnell P J, Smit AM, Ampomah-Dwamena C, Martin EJ, Netzler N, Nieuwenhuizen NJ, Quinn BD, Foote HC, Hudson KR (2006) Gain-of-function phenotypes of many CLAVATA3/ESR genes, including four new family members, correlate with tandem variations in the conserved CLAVATA3/ESR domain. Plant physiology 140 (4):1331-1344

Suer S, Agustí J, Sanchez P, Schwarz M, Greb T (2011) WOX4 Imparts Auxin Responsiveness to Cambium Cells in Arabidopsis. Plant Cell 23 (9):3247-3259

Sun H, Tao J, Gu P, Xu G, Zhang Y (2016) The role of strigolactones in root development. Plant signaling & behavior 11 (1):e1110662

Sun L, Shi L, Li W, Yu W, Liang J, Zhang H, Yang X, Wang Y, Li R, Yao X, Yi X, Shang Y (2009) JFK, a Kelch domain-containing F-box protein, links the SCF complex to p53 regulation. Proceedings of the National Academy of Sciences of the United States of America 106 (25):10195-10200

Sussex IM (1989) Developmental programming of the shoot meristem. Cell 56 (2):225-229

Suzuki N, Rivero RM, Shulaev V, Blumwald E, Mittler R (2014) Abiotic and biotic stress combinations. New Phytol 203 (1):32-43

Szemenyei H, Hannon M, Long JA (2008) TOPLESS mediates auxin-dependent transcriptional repression during Arabidopsis embryogenesis. Science 319 (5868):1384-1386

Tamaru H (2010) Confining euchromatin/heterochromatin territory: jumonji crosses the line. Genes Dev 24 (14):1465-1478

Tan X, Calderon-Villalobos LI, Sharon M, Zheng C, Robinson CV, Estelle M, Zheng N (2007) Mechanism of auxin perception by the TIR1 ubiquitin ligase. Nature 446 (7136):640-645

ten Hove CA, Lu KJ, Weijers D (2015) Building a plant: cell fate specification in the early Arabidopsis embryo. Development (Cambridge, England) 142 (3):420-430

Thomas CL, Schmidt D, Bayer EM, Dreos R, Maule AJ (2009) Arabidopsis plant homeodomain finger proteins operate downstream of auxin accumulation in specifying the vasculature and primary root meristem. The Plant journal : for cell and molecular biology 59 (3):426-436

Tian H, Baxter IR, Lahner B, Reinders A, Salt DE, Ward JM (2010) Arabidopsis NPCC6/NaKR1 is a phloem mobile metal binding protein necessary for phloem function and root meristem maintenance. Plant Cell 22 (12):3963-3979

Toh S, Holbrook-Smith D, Stogios PJ, Onopriyenko O, Lumba S, Tsuchiya Y, Savchenko A, McCourt P (2015) Structure-function analysis identifies highly sensitive strigolactone receptors in Striga. Science 350 (6257):203-207

Tonn N, Greb T (2017) Radial plant growth. Current biology : CB 27 (17):R878-R882

Truernit E, Bauby H, Belcram K, Barthelemy J, Palauqui JC (2012) OCTOPUS, a polarly localised membrane-associated protein, regulates phloem differentiation entry in Arabidopsis thaliana. Development (Cambridge, England) 139 (7):1306-1315

Truernit E, Bauby H, Dubreucq B, Grandjean O, Runions J, Barthelemy J, Palauqui JC (2008) High-resolution whole-mount imaging of three-dimensional tissue organization and gene expression enables the study of Phloem development and structure in Arabidopsis. Plant Cell 20 (6):1494-1503

Turner S, Gallois P, Brown D (2007) Tracheary element differentiation. Annual review of plant biology 58:407-433

Ueda H, Kusaba M (2015) Strigolactone Regulates Leaf Senescence in Concert with Ethylene in Arabidopsis. Plant physiology 169 (1):138-147

Ueda M, Zhang Z, Laux T (2011) Transcriptional activation of Arabidopsis axis patterning genes WOX8/9 links zygote polarity to embryo development. Developmental cell 20 (2):264-270

Umehara M, Cao M, Akiyama K, Akatsu T, Seto Y, Hanada A, Li W, Takeda-Kamiya N, Morimoto Y, Yamaguchi S (2015) Structural requirements of strigolactones for shoot branching inhibition in rice and arabidopsis. Plant & cell physiology 56 (6):1059-1072

Umehara M, Hanada A, Yoshida S, Akiyama K, Arite T, Takeda-Kamiya N, Magome H, Kamiya Y, Shirasu K, Yoneyama K, Kyozuka J, Yamaguchi S (2008) Inhibition of shoot branching by new terpenoid plant hormones. Nature 455 (7210):195-200

Ursache R, Andersen TG, Marhavy P, Geldner N (2018) A protocol for combining fluorescent proteins with histological stains for diverse cell wall components. The Plant journal : for cell and molecular biology 93 (2):399-412

van den Berg C, Willemsen V, Hage W, Weisbeek P, Scheres B (1995) Cell fate in the Arabidopsis root meristem determined by directional signalling. Nature 378:62

van den Berg C, Willemsen V, Hendriks G, Weisbeek P, Scheres B (1997) Short-range control of cell differentiation in the Arabidopsis root meristem. Nature 390 (6657):287-289

Vaten A, Dettmer J, Wu S, Stierhof YD, Miyashima S, Yadav SR, Roberts CJ, Campilho A, Bulone V, Lichtenberger R, Lehesranta S, Mahonen AP, Kim JY, Jokitalo E, Sauer N, Scheres B, Nakajima K, Carlsbecker A, Gallagher KL, Helariutta Y (2011) Callose biosynthesis regulates symplastic trafficking during root development. Developmental cell 21 (6):1144-1155

Vegh A, Incze N, Fabian A, Huo H, Bradford KJ, Balazs E, Soos V (2017) Comprehensive Analysis of DWARF14-LIKE2 (DLK2) Reveals Its Functional Divergence from Strigolactone-Related Paralogs. Front Plant Sci 8:1641

Voinnet O, Rivas S, Mestre P, Baulcombe D (2003) An enhanced transient expression system in plants based on suppression of gene silencing by the p19 protein of tomato bushy stunt virus. The Plant journal : for cell and molecular biology 33 (5):949-956

Voss TC, Hager GL (2014) Dynamic regulation of transcriptional states by chromatin and transcription factors. Nat Rev Genet 15 (2):69-81

Voxeur A, Hofte H (2016) Cell wall integrity signaling in plants: "To grow or not to grow that's the question". Glycobiology 26 (9):950-960

Waldie T, McCulloch H, Leyser O (2014) Strigolactones and the control of plant development: lessons from shoot branching. The Plant journal : for cell and molecular biology 79 (4):607-622

Wallner E (2014) Characterizing the role of SMXL5 in vascular development of Arabidopsis thaliana. University of Vienna, Vienna

Wallner ES, Lopez-Salmeron V, Belevich I, Poschet G, Jung I, Grunwald K, Sevilem I, Jokitalo E, Hell R, Helariutta Y, Agusti J, Lebovka I, Greb T (2017) Strigolactone- and Karrikin-Independent SMXL Proteins Are Central Regulators of Phloem Formation. Current biology : CB 27 (8):1241-1247

Wallner ES, Lopez-Salmeron V, Greb T (2016) Strigolactone versus gibberellin signaling: reemerging concepts? Planta 243 (6):1339-1350

Wang H-Z, Dixon RA (2012) On–Off Switches for Secondary Cell Wall Biosynthesis. Molecular plant 5 (2):297-303

Wang L, Wang B, Jiang L, Liu X, Li X, Lu Z, Meng X, Wang Y, Smith SM, Li J (2015) Strigolactone signaling in Arabidopsis regulates shoot development by targeting D53-Like SMXL repressor proteins for ubiquitination and degradation. Plant Cell 27 (11):3128-3142

Wang Y, Patel DJ (1993) Solution structure of a parallel-stranded G-quadruplex DNA. J Mol Biol 234 (4):1171-1183

Waters MT, Gutjahr C, Bennett T, Nelson DC (2017) Strigolactone Signaling and Evolution. Annual review of plant biology 68:291-322

Waters MT, Nelson DC, Scaffidi A, Flematti GR, Sun YK, Dixon KW, Smith SM (2012) Specialisation within the DWARF14 protein family confers distinct responses to karrikins and strigolactones in Arabidopsis. Development (Cambridge, England) 139 (7):1285-1295

Waters MT, Scaffidi A, Flematti GR, Smith SM (2013) The origins and mechanisms of karrikin signalling. Curr Opin Plant Biol 16 (5):667-673

Waters MT, Scaffidi A, Sun YK, Flematti GR, Smith SM (2014) The karrikin response system of Arabidopsis. The Plant journal : for cell and molecular biology 79 (4):623-631

Waters MT, Smith SM (2013) KAI2- and MAX2-mediated responses to karrikins and strigolactones are largely independent of HY5 in Arabidopsis seedlings. Molecular plant 6 (1):63-75

Weller B, Zourelidou M, Frank L, Barbosa IC, Fastner A, Richter S, Jurgens G, Hammes UZ, Schwechheimer C (2017) Dynamic PIN-FORMED auxin efflux carrier phosphorylation at the plasma membrane controls auxin efflux-dependent growth. Proceedings of the National Academy of Sciences of the United States of America 114 (5):E887-E896

Wendrich JR, Weijers D (2013) The Arabidopsis embryo as a miniature morphogenesis model. New Phytol 199 (1):14-25

Williams L, Carles CC, Osmont KS, Fletcher JC (2005) A database analysis method identifies an endogenous trans-acting short-interfering RNA that targets the Arabidopsis ARF2, ARF3, and ARF4 genes. Proceedings of the National Academy of Sciences of the United States of America 102 (27):9703-9708

Wolf S, Hematy K, Hofte H (2012) Growth control and cell wall signaling in plants. Annual review of plant biology 63:381-407

Wolfe AL, Singh K, Zhong Y, Drewe P, Rajasekhar VK, Sanghvi VR, Mavrakis KJ, Jiang M, Roderick JE, Van der Meulen J, Schatz JH, Rodrigo CM, Zhao C, Rondou P, de Stanchina E, Teruya-Feldstein J, Kelliher MA, Speleman F, Porco JA, Jr., Pelletier J, Ratsch G, Wendel HG (2014) RNA G-quadruplexes cause eIF4A-dependent oncogene translation in cancer. Nature 513 (7516):65-70

Wu YY, Hou BH, Lee WC, Lu SH, Yang CJ, Vaucheret H, Chen HM (2017) DCL2- and RDR6-dependent transitive silencing of SMXL4 and SMXL5 in Arabidopsis dcl4 mutants causes defective phloem transport and carbohydrate over-accumulation. The Plant journal : for cell and molecular biology 90 (6):1064-1078

Wysocka J, Swigut T, Xiao H, Milne TA, Kwon SY, Landry J, Kauer M, Tackett AJ, Chait BT, Badenhorst P, Wu C, Allis CD (2006) A PHD finger of NURF couples histone H3 lysine 4 trimethylation with chromatin remodelling. Nature 442 (7098):86-90

Xie B, Wang X, Zhu M, Zhang Z, Hong Z (2011) CalS7 encodes a callose synthase responsible for callose deposition in the phloem. The Plant journal : for cell and molecular biology 65 (1):1-14

Xie X (2016) Structural diversity of strigolactones and their distribution in the plant kingdom. Journal of Pesticide Science 41 (4):175-180

Xie X, Yoneyama K (2010) The strigolactone story. Annu Rev Phytopathol 48:93-117

Xie Z, Allen E, Wilken A, Carrington JC (2005) DICER-LIKE 4 functions in trans-acting small interfering RNA biogenesis and vegetative phase change in Arabidopsis thaliana. Proceedings of the National Academy of Sciences of the United States of America 102 (36):12984-12989

Xiong Y, McCormack M, Li L, Hall Q, Xiang C, Sheen J (2013) Glucose-TOR signalling reprograms the transcriptome and activates meristems. Nature 496 (7444):181-186

Yang T, Zhang L, Hao H, Zhang P, Zhu H, Cheng W, Wang Y, Wang X, Wang C (2015) Nuclear-localized AtHSPR links abscisic acid-dependent salt tolerance and antioxidant defense in Arabidopsis. The Plant journal : for cell and molecular biology 84 (6):1274-1294

Yang T, Zhang P, Wang C (2016) AtHSPR may function in salt-induced cell death and ER stress in Arabidopsis. Plant signaling & behavior 11 (7):e1197462

Yao R, Li J, Xie D (2018) Recent advances in molecular basis for strigolactone action. Sci China Life Sci 61 (3):277-284

Ye ZH, Freshour G, Hahn MG, Burk DH, Zhong R (2002) Vascular development in Arabidopsis. International Review of Cytology 220:225-256

Yoneyama K, Mori N, Sato T, Yoda A, Xie X, Okamoto M, Iwanaga M, Ohnishi T, Nishiwaki H, Asami T, Yokota T, Akiyama K, Yoneyama K, Nomura T (2018) Conversion of carlactone to carlactonoic acid is a conserved function of MAX1 homologs in strigolactone biosynthesis. New Phytol

Yoneyama K, Xie X, Sekimoto H, Takeuchi Y, Ogasawara S, Akiyama K, Hayashi H, Yoneyama K (2008) Strigolactones, host recognition signals for root parasitic plants and arbuscular mycorrhizal fungi, from Fabaceae plants. New Phytol 179 (2):484-494

Yoshida S, Barbier de Reuille P, Lane B, Bassel GW, Prusinkiewicz P, Smith RS, Weijers D (2014) Genetic control of plant development by overriding a geometric division rule. Developmental cell 29 (1):75-87

Yoshikawa M (2013) Biogenesis of trans-acting siRNAs, endogenous secondary siRNAs in plants. Genes Genet Syst 88 (2):77-84

Yoshikawa M, Peragine A, Park MY, Poethig RS (2005) A pathway for the biogenesis of trans-acting siRNAs in Arabidopsis. Genes Dev 19 (18):2164-2175

Zhang H, Lin X, Han Z, Wang J, Qu LJ, Chai J (2016) SERK Family Receptor-like Kinases Function as Co-receptors with PXY for Plant Vascular Development. Molecular plant 9 (10):1406-1414

Zhang L, Yang T, Li X, Hao H, Xu S, Cheng W, Sun Y, Wang C (2014a) Cloning and characterization of a novel Athspr promoter specifically active in vascular tissue. Plant physiology and biochemistry : PPB / Societe francaise de physiologie vegetale 78:88-96

Zhang LY, Peng YB, Pelleschi-Travier S, Fan Y, Lu YF, Lu YM, Gao XP, Shen YY, Delrot S, Zhang DP (2004) Evidence for apoplasmic phloem unloading in developing apple fruit. Plant physiology 135 (1):574-586

Zhang Y, van Dijk AD, Scaffidi A, Flematti GR, Hofmann M, Charnikhova T, Verstappen F, Hepworth J, van der Krol S, Leyser O, Smith SM, Zwanenburg B, Al-Babili S, Ruyter-Spira C, Bouwmeester HJ (2014b) Rice cytochrome P450 MAX1 homologs catalyze distinct steps in strigolactone biosynthesis. Nat Chem Biol 10 (12):1028-1033

Zhang Y, Wang P, Shao W, Zhu JK, Dong J (2015) The BASL polarity protein controls a MAPK signaling feedback loop in asymmetric cell division. Developmental cell 33 (2):136-149

Zhang Z, Laux T (2011) The asymmetric division of the Arabidopsis zygote: from cell polarity to an embryo axis. Sex Plant Reprod 24 (2):161-169

Zhao LH, Zhou XE, Yi W, Wu Z, Liu Y, Kang Y, Hou L, de Waal PW, Li S, Jiang Y, Scaffidi A, Flematti GR, Smith SM, Lam VQ, Griffin PR, Wang Y, Li J, Melcher K, Xu HE (2015) Destabilization of strigolactone receptor DWARF14 by binding of ligand and E3-ligase signaling effector DWARF3. Cell research 25 (11):1219-1236

Zhou F, Lin Q, Zhu L, Ren Y, Zhou K, Shabek N, Wu F, Mao H, Dong W, Gan L, Ma W, Gao H, Chen J, Yang C, Wang D, Tan J, Zhang X, Guo X, Wang J, Jiang L, Liu X, Chen W, Chu J, Yan C, Ueno K, Ito S, Asami T, Cheng Z, Lei C, Zhai H, Wu C, Wang H, Zheng N, Wan J (2013) D14-SCF(D3)-dependent degradation of D53 regulates strigolactone signalling. Nature 504 (7480):406-410

Zourelidou M, Absmanner B, Weller B, Barbosa ICR, Willige BC, Fastner A, Streit V, Port S, Colcombet J, van Bentem SD, Hirt H, Kuster B, Schulze WX, Hammes UZ, Schwechheimer C (2014) Auxin efflux by PIN-FORMED proteins is activated by two different protein kinases, D6 PROTEIN KINASE and PINOID. Elife 3

Zwanenburg B, Pospisil T (2013) Structure and activity of strigolactones: new plant hormones with a rich future. Molecular plant 6 (1):38-62

Zwanenburg B, Pospisil T, Cavar Zeljkovic S (2016) Strigolactones: new plant hormones in action. Planta 243 (6):1311-1326

Zwanenburg B, Zeljkovic SC, Pospisil T (2015) Synthesis of strigolactones, a strategic account. Pest Manag Sci